

BIBLIOGRAPHY

Edited by

Z. KOPAL

University of Manchester, England

M. MOUTSOULAS

University of Athens, Greece

and

F. B. WARANIUS

Lunar and Planetary Institute, Houston, Texas, U.S.A.

(Articles entered into the data base at the Lunar and Planetary Institute Library, November 1982 through January 1983)

1. Motion of the Moon and Dynamics of the Earth-Moon System: Shape and Gravity Field of the Moon

Brumberg, V. A. and Ivanova, T. V. (Inst. for Theoretical Astronomy, 191187 Leningrad, USSR): 'New Approach to Determining Planetary Perturbations in Lunar Theory', *Celest. Mech.* **26**, 77-81 (1982)

The technique of the general planetary theory has been proposed for constructing a theory of motion of the Moon. This method enables us to elaborate the consistent theory of motion of the principal planets and the Moon, which is of particular importance for determining planetary perturbations in lunar motion. As an initial approximation for lunar motion, an intermediate orbit generalizing the Hill's variational curve has been built. This orbit includes all solar and planetary inequalities independent of eccentricities and inclinations of the Moon, Sun and planets. In calculating this orbit, the motion of the principal planets in quasi-periodic intermediate orbits has been taken into account. This solution was produced with the aid of the Universal Poissonian Processor (UPP) elaborated in the Institute for Theoretical Astronomy (Leningrad).

Cappallo, R. J. and Eckhardt, D. H. (Dept. of Earth and Planetary Sciences, MIT, Cambridge, MA 02139): 'A Comparison of Numeric and Semi-Analytic Lunar Libration Models', *Celest. Mech.* **26**, 125-127 (1982)

Cappallo, R. J., King, R. W., Counselman, C. C. III., and Shapiro, I. I. (Dept. of Earth and Planetary Sciences, MIT, Cambridge, MA 02139): 'Evidence for Lunar Librations Near Resonance', *Celest. Mech.* **26**, 145 (1982)

The Moon's rotation has been modeled by numerical integration of Euler's equations of rigid-body rotation, with modifications for elasticity and dissipation. The free parameters in the model have been adjusted to best fit, in a weighted-least-squares sense, eight years of laser range observations of the retroreflectors on the lunar surface. The postfit rms range residual was 27 cm. The numerical rotation ephemeris was compared with a semi-analytical theory of D. H. Eckhardt, which was generated using the same values for the physical constants, but in which the homogeneous solution was constrained to be zero. The differences were displayed graphically in reference frames chosen to depict the three modes of free oscillation: libration in longitude, precession, and wobble. There exist relatively minor discrepancies of several tenths of an arcsecond which are not characteristic of the expected form of the free oscillations, and which can be attributed to errors in one or both of the models. On the other hand, the dominant signatures have amplitudes of several seconds of arc and cannot be distinguished

¹*The Moon and the Planets* **29** (1983) 237.

from free oscillations. However, considering the estimate of Cappallo *et al.* for the lunar $Q = 23$, and Peale's expressions for the characteristic damping times for free oscillations, it is difficult to accept the identity of these large motions as free oscillation. Instead, we suggest the possibility that the differences are due to small forcing terms omitted from the analytic theory for the lunar orbit, which are very near to resonance, and thus magnified enormously in the rotational response.

Chapront, J. and Chapront-Touzé, M. (Service de Mécanique Céleste du Bureau des Longitudes, Equipe de Recherche Associée au CNRS, Paris, France): 'Planetary Perturbations of the Moon in ELP 2000', *Celest. Mech.* **26**, 83–94 (1982)

A new solution for the planetary perturbations of the Moon is being built in the frame of ELP 2000, using Bretagnon's planetary theories, and achieved at the first order. It contains the two actions commonly distinguished: direct and indirect. The internal precision of computation is 2×10^{-6} arcsec. First-order planetary perturbations, in the direct case (Venus and Mars), have been compared to Standaert's solution. The major discrepancy reaches 70 cm in the longitude of Venus. Perturbations of the second order with respect to planetary masses, have been undertaken and illustrations are given. Finally, new values for the perigee and node motions are proposed.

Chapront-Touzé M. (Service de Mécanique Céleste du Bureau de Longitudes, Equipe de Recherche Associée au CNRS, Paris, France): 'The ELP Solution for the Main Problem of the Moon and Some Applications', *Celest. Mech.* **26**, 63–69 (1982)

First derivatives of the ELP 2000 solution of the main problem have been obtained. They are used for computation of the lunar motion perturbations due to the Earth's oblateness and to secular terms in the solar eccentricity and perigee.

Chapront-Touzé, M. (Service de Mécanique Céleste du Bureau des Longitudes, Equipe de Recherche Associée au CNRS, Paris, France): 'Progress in the Analytical Theories for the Orbital Motion of the Moon', *Celest. Mech.* **26**, 53–62 (1982)

For the last 15 years, an important effort has been done by several authors to produce new and precise analytical solutions for the Moon's orbital motion. This construction is still in a very growing phase. Achieved works are described and compared. Some indications are given about what remains to be done.

Eckhardt, D. H. (Air Force Geophysical Lab., Hanscom Air Force Base, MA 01731): 'Semi-Analytic Model of the Moon's Rotation', *Celest. Mech.* **26**, 129 (1982)

A comprehensive semi-analytic model of the Moon's rotation has been developed and libration tables have been compiled which are suitable for the analysis of lunar laser ranging measurements. In the model, the Moon is considered to be rigid, elastic (using a potential disturbance Love number) or anelastic (using a complex Love number), and its gravity potential is represented through its fourth degree harmonics. The Moon is assumed to move about the Earth according to the Analytic Lunar Ephemeris (ALE of Deprit, Henrard and Rom, and it is torqued by the Earth and Sun. The ALE is supplemented by the additive and planetary perturbations of the improved Lunar Ephemeris (ILE); modified for the Earth figure perturbations according to Van Flandern, and with some corrections to resolve minor inconsistencies. The direct effects of the Earth figure and the rotation of the ecliptic are also included in the model.

To derive the main libration theory from the ALE, the Euler dynamical equations are solved iteratively using a digital computer to perform all the semi-analytic mathematical manipulations required. The libration perturbations are solved by the computer in two iterations, taking into account cross terms between the main theory and the perturbations. The overall libration model is estimated to be accurate to 0'010; this is the truncation level of the tabulated libration series.

Henrard, J. (Dept. of Mathematics, Facultés Universitaires de Namur, B-5000 Namur, Belgium): 'Perturbations by the Oblateness of Earth and Moon', *Celest. Mech.* **26**, 95 (1982).

A complete reevaluation of the effects upon the motion of the Moon due to the oblateness of the Earth and the Moon has been computed. It is based upon the semi-analytical solution of the main problem (SALE) described in previous papers. The characteristic of this solution is a high accuracy of the nominal solution (at least $0''.001$) and mostly a high accuracy of the partial derivatives (up to the order 4) with respect to the integration constants. For the perturbation due to the oblateness of the Earth, the contributions of J_2 , J_3 and J_4 have been considered. The perturbations by J_2 have been computed up to order 2 whose contribution is not neglectible ($0''.001\ 14 \sin(F - \xi) + \dots$ in longitude). The contribution of J_4 is very marginal ($0''.000\ 01 \sin(F - \xi)$ in longitude).

For the perturbation due to the oblateness of the Moon, the contributions of the second harmonics and of two terms of the third harmonics have been considered. The effects of the physical libration of the Moon is neglectible.

Comparison with previous theories (Hill, ALE, ILE) shows large discrepancies of the order of $0''.01$. The accuracy of our results is confirmed by the new solution of Chapront-Touzé.

Kubo, Y. (Hydrographic Dept., Tsukiji, Chuo-Ku, Tokyo, Japan): 'Perturbations by the Oblateness of the Earth and by the Planets in the Motion of the Moon', *Celest. Mech.* **26**, 97–112 (1982)

Perturbations in the motion of the Moon are computed for the effect by the oblateness of the Earth and for the indirect effect of planets. Based on Delaunay's analytical solution of the main problem, the computations are performed by a method of Fourier series operation. The effect of the oblateness of the Earth is obtained to the second order, partly adopting an analytical evaluation. Both in longitude and latitude are found a few terms whose coefficient differs from the current lunar ephemeris based on Brown's theory by about $0''.01$. While, concerning the indirect effect of planets, several periodic terms in the current ephemeris seem to have errors reaching $0''.05$.

As for the secular variations of ω and Ω due to the figure of the Earth and the indirect effect of planets, the newly-computed values agree within $1''/\text{cy}$ with Brown's results reduced to the same values of the parameters. Further, the accelerations in the mean longitude, $\dot{\omega}$ and $\dot{\Omega}$ caused by the secular changes in the eccentricity of the Earth's orbit e' and in the obliquity of the ecliptic ϵ are obtained. The comparison with Brown shows an agreement within $0''.3/\text{cy}^2$ for the former cause and $0''.02/\text{cy}^2$ for the latter. An error is found in the argument of the principal term for the perturbations due to the ecliptic motion in the current ephemeris.

Moons, M. (Dept. of Mathematics, Facultés Universitaires de Namur, B-5000 Namur, Belgium): 'Physical Libration of the Moon', *Celest. Mech.* **26**, 131–142 (1982)

The aim of this paper is to present a semi-analytical theory of the libration of the Moon obtained by the application of the Lie transform method to the Hamiltonian of the problem: free rotation of a rigid Moon around its center of mass plus perturbations due to Earth and Sun. The different contributions to the Hamiltonian are kept separate in order to be easily recognized in the final solution. The variations of the constants of inertia are taken into account. The motion of the center of mass is described by the solution proposed by Chapront-Touzé. The Hamiltonian is brought into a well suited form and the generators of the different transformations are applied to the usual libration parameters p_1 , p_2 , and τ . These series are computed with a precision of $0''.001$ and comparisons are made with the results obtained previously by Eckhardt and by Migus.

Oesterwinter, C. (Naval Surface Weapons Center, Dahlgren Lab., VA 23691): 'Orbit and Rotation of the Moon by Numerical Integration', *Celest. Mech.* **26**, 143 (1982)

The Dahlgren Solar System Program has been augmented to allow computation of the librational motion of the Moon. The model considers the torques exerted by Earth and Sun on the triaxial gravity field of the Moon. All current computer runs are using a gravity field through degree and order three. Also modeled are the effects of the librating lunar field on the motion of Moon and Earth. The Euler angles describing the spatial orientation of the Moon are obtained simultaneously by numerical integration. They are compared to Euler angles provided by the Jet Propulsion Laboratory which in turn were fitted to laser range data.

Schmidt, D. S. (Dept. of Mathematical Sciences, Univ. of Cincinnati, Cincinnati, OH 45221): 'The Main Problem of Lunar Theory Solved by the Method of Brown', *Celest. Mech.* **26**, 75 (1982).

Brown's method for solving the main problem of lunar theory has been adapted for the computation by machine. The computations are carried out with the help of an algebraic processor called POLY-PAK, which can manipulate power series in several real or complex variables. Brown's result have been recovered and refined first and the solution, in Cartesian coordinates to the sixth order, has been compared to the work of Eckert. The solution has then been expanded to include most terms through order nine. This order is necessary to get an accuracy of 0.000 01" for the terms in longitude and latitude and of 0.000 001" for the terms in the sine parallax. A preliminary comparison with the theories of Chapront and Henrard indicates that the solution has an accuracy which is close to the one desired.

The next step in developing a complete lunar theory requires the computation of the partial derivatives of the solution with respect to the primary parameters. Since Brown's method gives a semi-analytical solution only the derivative with respect to n , the mean motion of the Moon, is difficult to compute. It is possible to find this derivative with the one quadrature from the other derivatives if one takes into account that the Jacobian has to be a symplectic matrix when a canonical set of primary parameters is used.

The mean motions of the perigee and node often exhibit the largest discrepancies among the different theories. Therefore it is not too surprising that also their derivatives show significant differences. It is hoped by providing another independent computation of the derivatives by a different method their accuracy can be improved.

Standaert, D. (Dept. of Mathematics, Facultés, Universitaires de Namur, B-5000 Namur, Belgium): 'Comments About the Direct Perturbations of Venus and Mars on the Moon's Motion', *Celest. Mech.* **26**, 113–119 (1982)

In a previous paper we have described an algorithm to compute the direct perturbation of the planets on the Moon's motion. A short summary of this algorithm is presented in Section 2 of this paper. Our first results permit us to present some complements and comments about these computations.

The algorithm is based upon the Lie transform method and is implemented using Chapront's ELP as solution of the main problem with the partial derivatives of Henrard's Semi-Analytical Lunar Ephemeris (SALE), and Bretagnon's mean Keplerian orbit.

An analysis of truncation errors in intermediate results is presented including the resonance effects. The final accuracy of the solution is intended to be about 0''0005 for terms of period up to 2000 yr in the case of Venus and up to 5000 yr in the case of Mars.

The effects of second-order terms in the masses are investigated. Only those depending upon the second derivatives of the mean motions are found to be significant to the given accuracy and are included.

Waldrop, M. M.: 'The Origin of the Moon', *Science* **216**, 606–607 (1982)

The problem of the origin of the Moon is briefly discussed.

Webb, D. J. (Inst. of Oceanographic Sciences, Wormley, Godalming GU8 5UB): 'Tides and the Evolution of the Earth-Moon System', *Geophys. J. Roy. Astron. Soc.* **70**, 261–271 (1982)

A model of the tides in a hemispherical ocean is used to investigate the effect of changes in the Earth's rotation rate on the power dissipated by the ocean tides. The results obtained are then used in an idealized astronomical model to investigate how they affect the history of the Earth-Moon system.

Using the tidal model it is found that at rotation rates higher than that of the present Earth, the power dissipated by the semi-diurnal tides in the ocean drops off rapidly as a result of the increased tidal frequency. Thus if the Earth's rotation rate is doubled from its present value, then the rate of energy dissipation in the ocean is reduced to approximately one-third of its present value and the tidal torque is reduced by a factor of about 6.

The present value for secular acceleration of the Moon, calculated from the results of the tidal

model is -30.5 arcsec century $^{-2}$. Using this value in the astronomical model, which has the Moon and Sun in circular orbits above the equator, and assuming that the tidal torque is independent of the tidal frequency, the Gerstenkorn event is predicted to have occurred 1.3×10^9 yr ago.

When the astronomical model is run with a torque determined at all times from the tidal model, the reduction in the energy dissipated early in the history of the system, leads to a Gerstenkorn date of 5.3×10^9 yr ago. However, dissipation within the solid earth is found to be important early in the history of the system and when this effect is included it gives a date for the Gerstenkorn event of 3.9×10^9 yr ago.

Morse, S. A. (Dept. of Geology and Geography, Univ. of Massachusetts, Amherst, MA 01003): 'Adcumulus Growth of Anorthosite at the Base of the Lunar Crust', Proceedings of the Thirteenth Lunar and Planetary Science Conference, Part 1, *J. Geophys. Res.* **87**, Suppl A10-A18, November 15, 1982 (1982)

Unzoned plagioclase crystals imply isothermal adcumulus solidification and cannot result from reactive equilibrium crystallization in dry magma. Extraction of latent heat upward through lunar crust result only in chilled or cotectic mesocumulate rocks, not anorthosite or adcumulates. Adcumulus growth of anorthosite requires exchange of refractory for incompatible components between the site of crystal growth and nearby fresh magma, and the extraction of calories from growing crystals to the flowing, supercooled magma. Supercooling can be acquired at remote sites like upwellings and then be carried by convective flow beneath crust which is accreting plagioclase by flotation or *in situ* nucleation and growth. If transport distances are larger than the scale of rockbergs, cotectic norites and troctolites may result. Impact-induced upwellings tend to promote growth of buoyant rather than mafic crust, hence impacts are not solely destructive.

Nakamura, Y., Latham, G. V. and Dorman, H. J. (Univ. of Texas, Inst. for Geophysics, Galveston, Marine Geophysics Lab., TX 77550-2768): 'Apollo Lunar Seismic Experiment' - Final Summary, Proceedings of the Thirteenth Lunar and Planetary Science Conference, Part 1, *J. Geophys. Res.* **87**, Suppl. A117-A123, November 15, 1982 (1982).

Processing and initial analysis of the entire set of Apollo lunar seismic data collected continuously from 1969 through 1977 have now been completed. Recent results include: (1) better defined deep moonquake locations, which appear to be bounded rather sharply between about 800 km and 1000 km depths with concentrations near both boundaries; and (2) middle mantle (~ 500 to 1000 km depth) seismic velocities of $V_p = 8.3 \pm 0.4$ km s $^{-1}$ and $V_s = 4.6 \pm 0.2$ km s $^{-1}$, which are significantly higher than previous estimates and represent an increase of velocities from the upper mantle as opposed to a decrease in previous estimates.

2. Physical Structure of the Moon; Thermal and Stress History of the Moon

Chen, H.-H., Oelano, J. W. and Lindsley, D. H. (Dept. of Earth and Space Sciences, State Univ. of New York, Stony Brook, NY 11794): 'Chemistry and Phase Relations of VLT Volcanic Glasses from Apollo 14 and Apollo 17', Proceedings of the Thirteenth Lunar and Planetary Science Conference, Part 1, *J. Geophys. Res.* **87**, Suppl. A171-A181, November 15, 1982 (1982)

The VLT (very low titanium) volcanic glasses from Apollo 14 and Apollo 17 have been analysed for the major elements and trace Ni. These glasses display compositional trends that may not result entirely from olivine fractionation. The phase relations have been determined experimentally. Olivine is the liquidus phase in the pressure interval from 0 to ~ 18 kbar. Pigeonite is the liquidus phase from ~ 18 kbar to ≥ 22 kbar. If these VLT volcanic glasses are samples of primary melts that had been in chemical equilibrium with olivine and low-Ca pyroxene in their source regions, then these liquids were derived from depths of 360-380 km within the Moon.

Delano, J. W., Lindsley, D. H., Ma, M.-S. and Schmitt, R. A. (Dept. of Earth and Space Sciences, State Univ. of New York, Stony Brook, NY 11794): 'The Apollo 15 Yellow Impact Glasses: Chemistry, Petrology, and Exotic Origin', Proceedings of the Thirteenth Lunar and Planetary Science Conference, Part 1, *J. Geophys. Res.* 87, Suppl. A159-A170, November 15, 1982 (1982)

The Apollo 15 yellow impact glasses are characterized by moderate TiO_2 (~ 4.8%) and high abundances of the large ion lithophile elements (e.g., K, P, Hf, Th, REE). Since the chemistry of these glasses cannot be duplicated by any combination of local components presently known to occur at the Apollo 15 landing site, these yellow glasses seem to be exotic to that area. Chemical and petrologic constraints suggest that these samples were produced by impact melting of an immature mare regolith developed upon an unusual variety of mare basalt. We speculate that the target basalts were the youngest lava flows known to exist on the Moon (i.e., Eratosthenian-age lavas in Oceanus Procellarum and Mare Imbrium). Specific tests are proposed for evaluating this provocative hypothesis.

Devine, J. M., McKay, D. S. and Papike, J. J. (Dept. of Earth and Space Sciences, State Univ. of New York at Stony Brook, Stony Brook, NY 11794): 'Lunar Regolith: Petrology of the < 10 Micron Fraction', Proceedings of the Thirteenth Lunar and Planetary Science Conference, Part 1, *J. Geophys. Res.* 87, Suppl. A260-A268, November 15, 1982 (1982).

It has been known for some time that the part of the lunar regolith smaller than 10 micrometers (< 10 μm) is chemically distinct from the bulk soil. Specifically, it is enriched in Al, Ca, Na, K, light rare-earth elements, and Th, and depleted in Mg, Fe, Mn, and Sc. Three models have been proposed to explain those systematics. The Exotic Component model holds that a fine-grained, KREEPy exotic component was distributed on a global scale, perhaps by the Imbrian impact. In the Simple Comminution model, the < 10 μm chemical systematics are due to differential comminution processes with fine-grained melt-rock mesostasis and feldspar concentrating in this fraction. The Soil Mixing model states that the chemical systematics are due to mixing of compositionally distinct soils that have different grain-size distributions. To determine which model is correct, modal petrographic data were obtained by scanning transmission electron microscopy with energy dispersive X-ray analysis for the < 10 μm fractions of four Apollo soils: 10084, 14163, 15271, and 64501. Modal results are consistent with chemical data regarding feldspathic and KREEP enrichments in the finest fraction. Soil glass contents, crystalline silica, and plagioclase/mafic mineral ratios are greater in the < 10 μm fraction than in the coarser fractions for all soils. Grain-size distributions are inconsistent with a fine-grained exotic component derived from distant sources. Comminution of local lithologies, vertical mixing, and local lateral transport controls the < 10 μm soil composition.

Houck, K. J. (Dept. of Geology, Indiana Univ., Bloomington, IN 47405): 'Petrologic Variations in Apollo 16 Surface Soils', Proceedings of the Thirteenth Lunar and Planetary Science Conference, Part 1, *J. Geophys. Res.* 87, Suppl. A197-A209, November 15, 1982 (1982)

Detailed modal analyses of fifteen surface soils were compared with rake and rock sample data to provide information about source rocks, maturation history, and intrasite variations in Apollo 16 regolith. Triangular plots of source rock components [defined as anorthosites, crystalline (melt) matrix breccias, and metamorphosed breccias] show that, with the possible exception of soils 64501 and 68501, Apollo 16 soils have similar source rocks that are well homogenized throughout the site. Modal abundance variations in submillimeter size fractions tend to reflect those of rake and rock samples. Maturity plots in agglutinate-monomineralic fragment-lithic and crystalline breccia space show Apollo 16 soils to be generally mature except for those collected from trenches (61221 and 61241) and from locations near North Ray Crater (stations 11 and 13). Data produced by other workers is combined with data from this study and used to divide the Apollo 16 site into three soil petrographic provinces. Central site soils are mature, well homogenized, and enriched in glass, but patches of immature and/or inhomogenous material are also present. They are probably the most typical Cayley Plains materials present at the site. North Ray soils are immature to submature, containing North Ray ejecta in the form of feldspathic fragmental breccia and plagioclase. South Ray soils are mature, but contain small amounts of fresh impact melts and plagioclase, possibly from breakdown of block South Ray ejecta. South Ray and North Ray ejecta differ in composition and physical properties, supporting the

hypothesis that the South Ray event evacuated Cayley material while the North Ray event excavated Descartes material.

Houck, K. J. (Dept. of Geology, Indiana Univ., Bloomington, IN 47405): 'Modal Petrology of Six Soils from Apollo 16 Double Drive Tube Core 64002', Proceedings of the Thirteenth Lunar and Planetary Science Conference, Part 1, *J. Geophys. Res.* 87, Suppl. A210-A220, November 15, 1982 (1982)

Detailed petrographic data were collected from six size fractions for six samples from Apollo 16 drive tube section 64002. Soils from the core were found to have similar source rocks (defined as anorthosites, impact melts, and metamorphosed breccia) to Apollo 16 surface soils and core 60009. Two slightly differing sets of source rocks, one with a metamorphose breccia to crystalline matrix breccia ratio of ~2:3 and the other with a ratio of ~1:1, were defined for the upper and lower sections of the core, respectively. Analysis of modal data shows that the upper three and the lowermost core soils are mature and have similar maturation histories, whereas the two middle soils are submature and have maturation histories similar to each other but differing from the upper and lowermost soils. In core 64002 soils, mixing has dominated over reworking. Mixing components are thought to be two mature soils distinguished by differing source rocks, and an immature plagioclase-rich soil. The plagioclase-rich soil is most prominent in the submature section of the core, and appears to correlate with larger clasts of chalky, friable breccia. The friable breccias and the immature plagioclase-rich soil are tentatively associated with the Descartes Formation. Supplementation of petrographic data with ^{53}Mn , ferromagnetic resonance (FMR), and core dissection data allows division of the core into three zones. The upper mature zone is fairly homogenous and was recently deposited in a short span of time. The middle submature zone is less homogenous, more plagioclase rich, and may be an ejecta deposit. The lower zone, though mature and homogenous, has the same source rocks as the middle zone.

Korotev, R. L. (Dept. of Earth and Planetary Sciences, Washington Univ., St. Louis, MO 73130): 'Comparative Geochemistry of Apollo 16 Surface Soils and Samples from Cores 64002 and 60002 Through 60007', Proceedings of the Thirteenth Lunar and Planetary Science Conference, Part 1, *J. Geophys. Res.* 87, Suppl. A269-A278 November 15, 1982 (1982)

New data are presented for the concentrations of 23 to 27 elements in nine Apollo 16 surface soil samples, two subsplits each of 12 splits of core 60002-7, and one subsplit each of 10 splits of drive tube 64002. The surface soils are generally similar to other surface soils collected at their respective stations. All ten 64002 samples are similar to each other and to the station 4 surface soils and distinctly different from soils at other stations. High iron concentrations previously reported for these same subsplits of 60002-7 result primarily from meteoritic metal. One sample from each core is contaminated by stainless steel. The recently proposed ferroan anorthositic norites are required to explain the soil compositions. A yet uncharacterized component with high concentrations of Na, Sr, and Eu is also needed.

Laul, J. C., Papike, J. J. and Simon, S. B. (Radiological Sciences Dept., Battelle, Pacific Northwest Labs., Richland, WA 99352): 'The Apollo 14 Regolith: Chemistry of Cores 14210/14211 and 14220 and Soils 14141, 14148, 14149', Proceedings of the Thirteenth Lunar and Planetary Science Conference, Part 1, *J. Geophys. Res.* 87, Suppl. A247-A259, November 15, 1982 (1982)

Chemical data for 31 major, minor, and trace elements were obtained by instrumental neutron activation analysis (INAA) for bulk and size fractions of drive tubes 14210/11 (39 cm) and 14220 (16.5 cm) and soils 14141, 14148, and 14149. Both cores are KREEPy and homogeneous in chemical composition. The meteoritic components varies from 3 to 7% in both cores. The heterogeneous Ni profiles suggest little in situ mixing of the cores since their emplacements. The bulk soils on the average contain 20% low-K-Fra Mauro basalt (LKF) (62295), 10 to 15% mare basalt (14072), 6% anorthosite-noritetroctolite (ANT) and 59% high-K KREEP. There are no significant intrasite chemical variations at the Apollo 14 site. Among the grain sizes, the coarse 1000-90, 90-20, and 20-10 μm fractions are similar in chemistry, but quite different from the < 10 μm fine fractions. The < 10 μm fine fractions comprise 5 to 15% of the bulk soils and are consistently more feldspathic and enriched in incompatible (LIL)

elements relative to the coarse fractions. In the mature soils, agglutinates dominate the chemistry of the coarser fractions, and the similarity of LIL contents between the 1000–90 μm fractions and the < 10 μm fine fractions strongly suggests that agglutinates are derived from the fine fraction, which supports the F^3 model of Papike *et al.* Relative to the bulk soil, the < 10 μm fine fraction is enriched in Al_2O_3 , CaO , Na_2O , K_2O , Ba, Sr, La(REE), Eu, and Th and depleted in MgO , FeO , Mn, and Sc. The observed varying degrees of enrichments and depletions can largely be explained by simple comminution of mesostasis and feldspar and their preferential incorporation into the finest fraction. Lateral mixing over short distances, simple comminution, and vertical mixing of the regolith are the dominant soil-forming processes.

Longhi, J. (Dept. of Geology and Geophysics, Yale Univ., New Haven, CT 06511): 'Effects of Fractional Crystallization and Cumulus Processes on Mineral Composition Trends of Some Lunar and Terrestrial Rock Series', Proceedings of the Thirteenth Lunar and Planetary Science Conference, Part 1, *J. Geophys. Res.* 87, Suppl. A54–A64, November 15, 1982 (1982)

A plot of Mg of mafic minerals versus An of plagioclase in cumulate rocks from various lunar and terrestrial rock series shows each series to have a distinct curvilinear trend. The slopes of these trends vary from nearly vertical in the case of lunar anorthosites and Mg-norites to nearly horizontal in the case of gabbros from the mid-Atlantic ridge. Calculations based upon known major element partitioning between mafic minerals, plagioclase and subalkaline basaltic liquids indicate that fractional crystallization coupled with cotectic accumulation of mafic minerals and plagioclase will produce mineral composition trends on the Mg versus An diagram with slopes > 1 for cases where $\text{An} \gtrsim \text{Mg}$. Furthermore, fractional crystallization of basaltic magmas with alkali concentrations approaching zero will produce near vertical Mg versus An trends. Therefore, the steep slopes of the lunar rock series are consistent with relatively simple fractionation processes. The relatively flat slope of mineral compositions from gabbros collected from the mid-Atlantic ridge at 26°N is inconsistent with simple fractionation processes, and calculations show that periodic refilling of a fractionating magma chamber with picritic magma cannot simply explain this flat slope either.

Nagle, J. S. (Northrop Services, Inc., Lunar Curatorial Lab., Houston, TX 77234): 'Subcrater Lithification of Polymict Regolith Breccias', Proceedings of the Thirteenth Lunar and Planetary Science Conference, Part 1, *J. Geophys. Res.* 87, Suppl. A131–A146, November 15, 1982 (1982)

Crater bottom structures show a consistent orientation in lunar cores. They have dust-free vesicular schlieren glass at the top, which grades downward to mafic arenite – a concentration of densely packed mafic mineral grains in a dark glass matrix. Next in the succession is a coarse-grained, polymict, compact and lineated breccia that has a nonporous brown glass matrix; it grades downward into a fine-grained, polymict lineated breccia that has a microporous glass matrix that is laden with fine fragments. All polymict regolith breccias formed by subcrater lithification shown evidence of compaction (> 2 contacts/grain in thin section), directional movement (linear fabric in at least some places) and rapid cooling (glassy matrix but no reaction rims or obvious annealed grain margins). In contrast, suevitic polymict regolith breccias, which are lithified by heating, are not compacted (< 2 contacts/grain in thin section, highly porous matrix), show evidence of rolling (radial-arcuate lapillar structures instead of linear fabric) and show sintered grain margins and/or reaction rims on mineral grains. The presence of relatively large fragments of shock-resistant minerals in the upper parts of the crater bottom structure, with other minerals being not clearly visible, suggests that fines and minerals easily damaged by shock are selectively fused to form the glass matrix.

Ostertag, R. and Stoffler, D. (Institut für Mineralogie, Universität Münster, D-4400 Münster, Germany): 'Thermal Annealing of Experimentally Shocked Feldspar Crystals', Proceedings of the Thirteenth Lunar and Planetary Science Conference, Part 1, *J. Geophys. Res.* 87, Suppl. A457–A464, November 15, 1982 (1982)

Single crystals of sanidine, orthoclase, microcline, oligoclase, and labradorite, as well as polycrystalline bytownite, were shocked experimentally to peak pressures as high as 45 GPa and subsequently annealed under dry conditions for various times at 800°C, 900°C, and 1000°C. These experiments

reveal that alkali feldspars do not change their Al, Si-distribution due to shock alone, but when subjected to shock pressures > 22 GPa and then annealed, microcline and orthoclase rapidly transform to sanidine, displaying a highly disordered Al, Si-distribution. High diffusivity of K, Na, and Ca was observed in a labradorite sample shocked to 26 GPa. Subsequent annealing may thus disturb chemical, structural, and isotopic characteristics of shocked minerals and rocks more easily than of unshocked specimens. This is of considerable importance for the interpretation of isotopic age data of impact breccias. Recrystallization textures of annealed diaplectic plagioclase glasses are very distinctive and may be used as a relative measure of the shock pressure experienced by the samples.

Ryder, G. and Blair, E. (Lunar Curatorial Lab., Northrop Services Inc., Houston, TX 77234): 'KREEP Glass and the Exotic Provenance and Formation of Polymict Breccia 66055', Proceedings of the Thirteenth Lunar and Planetary Science Conference, Part 1, *J. Geophys. Res.* **87**, Suppl. A147-A158, November 15, 1982 (1982)

Polymict breccia 66055 from the Apollo site is unique in that it contains abundant brown KREEP glass (0.3–0.4% K₂O) and related brown glassy breccias which have fluid forms. During assembly it consisted of hot and cold debris which flowed together. Most of the rock consists of clasts of poikiloblastic breccia (granulitic impactite) and mesostasis-rich impact melt (VHA basalt), both of which pre-date the assembly of 66055. In contrast, the KREEP glass was created in the impact which produced the rock. KREEP compositions are sparse among glasses in soils and other breccias at the Apollo 16 site, and the rock would not have formed locally; it must be exotic. Terrains in which 66055 might have formed exist to the west of the landing site. Suitable igneous target materials for the KREEP glass have not positively been identified in 66055, so the petrogenesis of Apollo 16 KREEP remains enigmatic, although the presence of a 'granitic' glass fragment embedded in KREEP glass suggests that it is igneous. A local volcanic origin is more consistent with the spatial relationships, as deduced from orbital geochemical data, than is a basin ejecta deposit.

Simon, S. B., Papike, J. J. and Laul, J. C. (Inst. for the Study of Mineral Deposits, South Dakota School of Mines and Tech., Rapid City, SD 57701): 'The Apollo 14 Regolith: Petrology of Cores 14210/14211 and 14220 and Soils 14141, 14148, and 14149', Proceedings of the Thirteenth Lunar and Planetary Science Conference, Part 1, *J. Geophys. Res.* **87**, Suppl. A232–A246, November 15, 1982 (1982)

New modal data are presented for continuous polished thin sections from double drive tube 14210/14211, and single drive tube 14220, and for polished grain mounts of four soils from the double drive tube, one from the single drive tube, and the soils 14148 (trench top), 14149 (trench bottom), and 14141 (Cone Crater). Modal data show that the Cone Crater soil is immature, whereas the 'smooth plains' soil are mature and rich in agglutinates and breccias. Neither core exhibits any major variations with depth. Microprobe analyses of mineral and glass fragments are consistent with derivation of the soils predominantly from the local rocks, with ~ 5–11% exotic mare component indicated by the modal data. About 4% of the glasses are SiO₂- and K₂O-rich granitic glasses which are comminuted mesostasis from the local melt rocks. The soils are depleted in feldspar relative to the source rocks. The preferred explanation for this depletion is that feldspar is concentrated in the < 10 μm fines and is consumed in the formation of agglutinates, regolith breccias, and feldspathic glass.

Stone, C. D., Taylor, L. A., McKay, D. S. and Morris, R. V. (Dept of Geological Sciences, Univ. of Tennessee, Knoxville, TN 37996): 'Ferromagnetic Resonance Intensity: A Rapid Method for determining Lunar Glass Bead Origin', Proceedings of the Thirteenth Lunar and Planetary Science Conference, Part 1, *J. Geophys. Res.* **87**, Suppl. A182–A196 November 15, 1982 (1982)

Ferromagnetic resonance intensity (I_g) was tested as a criterion for use as a nondestructive, reliable, and rapid screening method for distinguishing volcanic from impact glass spherules in the lunar soils. This method relies on the absence or presence of single-domain Fe formed during impact melting by auto-reduction of Fe²⁺ in the melt. Extensive scanning electron microscope (SEM) inspection of individual glass bead surfaces provided reliable evidence of the mode of glass genesis. Ferromagnetic resonance intensity was tested against the 'type' Apollo 15 and Apollo 17 volcanics. Additional

volcanics were also found during the course of the study. Ninety-four percent of the volcanic glasses had I_s values less than one, implying the absence of single-domain Fe. Seventy-five percent of impact glasses had elevated I_s values. The remaining impact beads had I_s values less than one. These samples lack single-domain Fe and could represent impact melts of bedrock with little or no regolith contribution. The ability to discriminate bedrock-derived impact melts as opposed to impact melts partially or completely derived from regolith, and the primary discrimination of volcanic glasses from impact glasses, suggests the FMR technique can be important in determining the origin of lunar glass spheres.

Takeda, H., Mori, H. and Miyamoto, M. (Mineralogical Inst., Univ. of Tokyo, Hongo, Tokyo 113, Japan): 'Comparison of Thermal History of Orthopyroxenes Between Lunar Norites 78236, 72255, And Diogenites', Proceedings of the Thirteenth Lunar and Planetary Science Conference, Part 1, *J. Geophys. Res.* 87, Suppl. A124-A130, November 15, 1982 (1982)

Orthopyroxene crystals from lunar norite 78236 and Civet Cat clast 72255 were compared with those of two diogenites, Johnstown and Ibbenbüren. Their exsolution and deformation textures were studied by analytical transmission electron microscope (ATEM) in addition to single crystal X-ray diffraction and electron microprobe techniques. 72255 pyroxenes contain clinobronzite lamellae similar to those in Johnstown, which were interpreted to have formed by stress-induced transformation by shock events. The X-ray and TEM observation of the orthopyroxene ($\text{En}_{76}\text{Fs}_{21}\text{Wo}_3$) in 78236 shows no augite exsolution with (100) in common. Abundant Guinier-Preston zones, with several unit-cells wide, are present. The textures in conjunction with the thermal history proposed by chronologic data suggest that 78236 experienced slow cooling deep in the crust above 1000°C, cooled rapidly due to excavation by an impact event, then then cooled slowly again at moderate temperature. This history is similar to that proposed for Johnstown. Computer simulation on the development of the (100) augite lamellae in 72255 and Ibbenbüren suggests a deep origin in the crust.

Von Gunten, H. R., Wegmüller, F. and Krehenbühl, U., (Anorganisch Chemisches Institut, Universität Bern, CH-300 Bern 9, Switzerland): 'Low Temperature Volatilization on the Moon', Proceedings of the Thirteenth Lunar and Planetary Science Conference, Part 1, *J. Geophys. Res.* 87, Suppl. A279-A282, November 15, 1982 (1982)

The concentrations of volatile elements in grain-size separated agglutinate and mineral fractions of samples 76240 (permanently shadowed) and 76260 were compared in heating experiments. The surface concentrations of Hg were found to be considerably higher in the shadowed sample. For the rest of the investigated elements only small or insignificant differences in the concentrations were observed between the two samples which differ in the storage temperature during the last 10^4 y. The difference in the concentrations of Hg must be the result of the shadowing. Based on the present investigation and on our earlier heating experiments, it can be concluded that Hg and Cd are mobilized by solar heating of the uppermost lunar soil and are trapped in cold places on the Moon. This low-temperature volatilization leads to a redistribution of volatiles (e.g., Hg and Cd) on the lunar surface.

3. Morphology of the Lunar Surface: Origin and Stratigraphy of Lunar Formations: Mapping of the Moon

Hale, W. S. and Grieve, R. A. F. (Dept. of Geological Sciences, Brown Univ., Providence, RI 02912): 'Volumetric Analysis of Complex Lunar Craters: Implications for Basin Ring Formation', Proceedings of the Thirteenth Lunar and Planetary Science Conference, Part 1, *J. Geophys. Res.* 87, Suppl. A65-A76, November 15, 1982 (1982)

The transition in hypervelocity impact structures from complex craters to basins is defined by a transition in uplifted central features from peaks to peak rings. Volumetric and morphologic analyses of the central peaks in complex lunar craters are combined with subsurface data from terrestrial complex impact structures in an effort to characterize the crater to basin transition. Central peak volumes in lunar craters with rim diameters (D_{rc}) < 51 km follow a power-law relationship to apparent crater volume. In craters with D_{rc} > 80 km, central peak volume is relatively reduced and a second power-law

relationship is defined. The relative reduction in peak volume in craters with $D_{rc} > 80$ km is associated with a relative decrease in peak height, and is accompanied by the development of a concentric zone of enhanced floor roughening. Studies of terrestrial complex impact structures suggest that the amount of uplifted material, as judged from its depth of origin, continues to increase with increasing rim diameter. This suggests that a redistribution of uplifted material away from a centralized peak may occur in the larger craters. The volumetric and morphologic changes described occur over a rim diameter range of 51–80 km, far below the previously proposed range for the crater to basin transition ($D_{rc} = 140$ –175 km). Evidence is presented to support a crater to basin transition beginning at $D_{rc} = 51$ –80 km, characterized by a relative reduction in central peak volume and the development of rings of floor roughening, which are suggested to be precursors of peak ring development.

Moutsoulas, M. and Preka, P. (Univ. of Athens, Greece): 'Morphological Characteristics of Lunar Craters with Moderate Depth/Diameter Ratio. II (0.12 < $D/D < 0.15$)', *The Moon and the Planets* 27, 111–130 (1982)

The morphological characteristics of craters, the depth/diameter ratio of which is between 0.12 and 0.15, are discussed. Many small secondary craters belong to that class – results of low velocity impacts – as well as young craters created by low angle impacts. Revised values for the craters' selenographic coordinates are also presented.

Walker, A. S. and El-Baz, F. (Center for Earth and Planetary Studies, National Air and Space Museum, Smithsonian Institution, Washington, DC 20560): 'Analysis of Crater Distributions in Mare Units on the Lunar Far Side', *The Moon and the Planets* 27, 91–106 (1982)

Mare material is asymmetrically distributed on the Moon. The Earth-facing hemisphere, where the crust is believed to be 26 km thinner than on the farside, contains substantially more basaltic mare material in three farside craters, Aitken (0.59 km), Isaev (1.0 km), and Tsiolkovskiy (1.75 km). We also studied crater frequency distribution in five farside mare units (Aitken, Isaev, Lacus Solitudinis, Langemak, and Tsiolkovskiy) and one light plains unit (in Mendeleev). Nearly 10 000 farside craters were counted. Analysis of the crater frequency on the light plains unit gives an age of 4.3 billion yr. Crater frequency distributions on the mare units indicate ages of 3.7 and 3.8 billion yr, suggesting that the units are distributed over a narrow time period of approximately 100 million yr. Returned lunar samples from nearside maria give dates as young as 3.1 billion yr. The results of this study suggest that mare basalt emplacement on the far side ceased before it did on the near side.

4. Chemical Composition of the Moon: Lunar Petrology, Mineralogy, and Crystallography

Bernatowics, T. J., Kramer, F. E., Podosek, F. A. and Honda, M. (McDonnell Center for the Space Sciences, Washington Univ., St. Louis, MO 63130): 'Adsorption and Excess Fission Xe: Adsorption of Xe on Vacuum Crushed Minerals', Proceedings of the Thirteenth Lunar and Planetary Science Conference, Part 1, *J. Geophys. Res.* 87, Suppl. A465–A476, November 15, 1982 (1982)

We report the results of Xe adsorption studies at low partial pressures of Xe ($\sim 2 \times 10^{-13}$ atm) for a terrestrial labradorite and lunar anorthosite 15415 which were crushed under high vacuum. The creation of fresh surfaces resulted in a distribution of surface adsorption potentials, with the most energetic, but least abundant, fractions of the surface dominating adsorption behaviour at lower temperatures. Atmospheric exposure tends to eliminate the most energetic surface fractions. For sample 15415, surfaces with an adsorption potential as great as 13.7 kcal/mole were created, but these constituted only about 10^{-6} of the surface area. Observation of the adsorption behavior of this sample over a period of days revealed the gradual disappearance of the most energetic fractions of the surface, probably because of site competition effects caused by sorption of active gases in our high vacuum manifold. Our results consist of values of the Henry constants of Xe adsorption at various temperatures. We have used extrapolations based upon these data to evaluate the possible role of adsorption in the excess fission Xe effect observed in lunar highland gas-rich breccias, for a model in which excess fission

Xe is concentrated by adsorption while diffusing through the regolith. Our experimental results, and estimations of the sorptive properties of the in situ regolith based on the time scale of lunar surface Rn emanations, indicate that adsorption falls about five orders of magnitude short of accounting for the effect. We also infer that the adsorption characteristics of our vacuum-crushed lunar sample are reasonable analogs to those of in situ lunar soil, so that the failure of adsorption to account for excess fission Xe cannot be attributed to significant differences in sorptive behavior of these materials.

Bibring, J. P., Langevin, Y. and Rocard, F. (Laboratoire René-Bernas, 91406 Orsay, France): 'Synthesis of Molecules by Irradiation in Silicates', Proceedings of the Thirteenth Lunar and Planetary Science Conference, Part 1, *J. Geophys. Res.* **87**, Suppl. A446-A450, November 15, 1982 (1982)

We have studied the molecular synthesis induced by the implantation of C and H ions in SiO₂ by *in situ* infrared spectroscopy. We have observed the infrared CO and CO₂ bands; the relative concentrations of CO and CO₂ depend on the C and H fluences; the bands have characteristics different from those of the corresponding gaseous species. This enables us to identify unambiguously CO₂ synthesized by solar wind irradiation in lunar fines.

Binder, A. B. (Institut für Mineralogie, Universität Münster, 4400 Münster, West Germany): 'The Mare Basalt Magma Source Region and Mare basalt Magma Genesis', Proceedings of the Thirteenth Lunar and Planetary Science Conference, Part 1, *J. Geophys. Res.* **87**, Suppl. A37-A53, November 15, 1982 (1982)

Given the available data, we find that the wide range of mare basaltic material characteristics can be explained by a model in which: (1) The mare basalt magma source region lies between the crust-mantle boundary and a maximum depth of 200 km and consists of a relatively uniform peridotite containing 73-80% olivine, 11-14% pyroxene, 4-8% plagioclase, 0.2-9% ilmenite and 1-1.5% chromite. (2) The source region consists of two or more density-graded rhythmic bands, whose compositions grade from that of the very low TiO₂ magma source regions (0.2% ilmenite) to that of the very high TiO₂ magma source regions (9% ilmenite). These density-graded bands are proposed to have formed as co-crystallizing olivine, pyroxene, plagioclase, ilmenite, and chromite settled out of a convecting magma (which was also parental to the crust) in which these crystals were suspended. Since the settling rates of the different minerals were governed by Stoke's law, the heavier minerals settled out more rapidly and therefore earlier than the lighter minerals. Thus the crystal assemblages deposited nearest the descending side of each convection cell were enriched in heavy ilmenite and chromite with respect to lighter olivine and pyroxene and very much lighter plagioclase. The reverse being the case for those units deposited near the ascending sides of the convection cells. Simultaneously with this density controlled settling of the crystals, the heating of the magma at the bottom of the convection cells resulted in the partial remelting of significant amounts of suspended, but settling plagioclase, ilmenite, and pyroxene. This partial remelting process was also partially responsible for the decrease in the ilmenite content (from 9 to 0.2%) between the very high TiO₂ and the very low TiO₂ source regions and caused the plagioclases and pyroxenes in the former source regions to be more sodic and clinopyroxene richer, respectively, than in the latter. (3) During the mare basalt epoch, radiogenic induced remelting of various parts of the density-graded bands led to the formation of the initial mare basalt magmas. The viscosity of melting systems, which decreases rapidly at about 30 ± 5% partial melting, appears to have limited the degree of partial melting of the source region to about 30 ± 2%. (4) These ~30% partial melts rose to the crust-mantle boundary where they pooled in magma storage chambers. The magmas remained in these chambers for different lengths of time, cooled to different degrees, and lost 0 to ~30% olivine or ~30% olivine plus 0 to ~20% pyroxene by fractional crystallization. Those magmas which remained in the chambers for very short times and lost no, or essentially no olivine before eruption were the parental magmas of the pyroclastic glass units. Those magmas which lost increasing amounts of olivine ± pyroxene were the parental magmas of the Apollo 12 and 15 magmas, the Apollo 11 and 17 magmas, and the Luna 16 and 24 magmas, respectively. This fractional crystallization phase in the genesis of the magmas explains both the pattern of the mare basalt magmas in the pseudo-quaternary phase diagrams and the decrease in the siderophile contents of the magmas as a function of their degree of fractionation. (5) The magma storage chambers, being located

at the crust-mantle boundary, were located in the zone where urKREEP formed during the initial differentiation of the Moon. Due to the low melting point of KREEP compared with the initially high temperatures of the magmas, residuals of the urKREEP layer were assimilated by the cooling magmas. Since the urKREEP materials underwent varying degrees of fractional melting early in lunar history, these urKREEP residuals had varying degrees of light REE depletion. Thus the assimilation of up to a few percent of these residuals caused the magmas to have differing Eu and light REE depletion patterns, as well as a wide range in their REE abundances. (6) The fractional crystallization and urKREEP residual assimilation phase of mare basalt magma genesis ended with the eruption of the magmas onto the lunar surface.

Bagard, D. O., Morris, R. V., Johnson, P. and Lauer, H. V. Jr. (NASA/Johnson Space Center, Houston, TX 77058): 'The Apennine Front Core 15007/8: Irradiational and Depositional History', Proceedings of the Thirteenth Lunar and Planetary Science Conference, Part 1, *J. Geophys. Res.* 87, Suppl. A221-A231, November 15, 1982 (1982).

Ferromagnetic resonance (FMR), magnetic, and noble gas measurements were made on soils from the Apennine Front core 15007/8 as part of a multidisciplinary study. Values of the I_s/FeO surface exposure (maturity) index and FeO concentrations are reported for 0.5 cm depth intervals; noble gas and FMR data are reported for 13 soils and 2 clasts selected from various depths in the ~57-cm-long core. These data, along with mineralogical and stratigraphic data reported by others, indicate four major core units whose contacts are at ~18, 49, and 55 cm. An *in situ* reworking zone at the top of the core is not indicated by the I_s/FeO data, and the cosmogenic gas data show that the core soils have experienced multistage exposure to cosmic rays. The 0-18 cm unit has values of cosmogenic $^{131}Xe/^{126}Xe$ that are higher than underlying soil and are indicative of irradiation at average depths > 50 cm; thus this unit cannot have a simple irradiational relationship to soil beneath it. This unit is probably the ejecta from the crater on whose rim the core was collected. The 18-49 cm unit is characterized by relatively constant values of I_s/FeO and abundances of cosmogenic gases and most likely represents a soil zone well mixed, possibly by downslope movement during the precrater era. I_s/FeO drops by about 30 units at the 49-cm contact. The two units below it are correspondingly more immature than overlying soil and, in addition, contain soils with either high concentrations of green glass or relatively low FeO contents. The significant heterogenetics in these two units indicate they have not been involved in the mixing layer which is presumed to occur due to downslope soil movement. Comparison of the 15007/8 core to other cores suggests that soils on slopes tend to be mixed and not contain units with long *in situ* irradiation profiles. Such cores are less likely to contain old or exotic soil layers.

5. Electromagnetic Properties of the Moon

Hood, L. L., Herbert, F. and Sonett, C. P. (Lunar and Planetary Lab., Univ. of Arizona, Tucson, AZ 85721): 'Further Efforts to Limit Lunar Internal Temperatures from Electrical Conductivity Determinations', Proceedings of the Thirteenth Lunar and Planetary Science Conference, Part 1, *J. Geophys. Res.* 87, Suppl. A109-A116, November 15, 1982 (1982).

A Monte-Carlo procedure is used to generate a representative set of eighteen electrical conductivity profiles that are consistent with previously published lunar transfer function data in the frequency range 10^{-5} to 10^{-3} Hz. The electrical conductivity is most strongly constrained by these data in the approximate depth range 450 to 1350 km. Published laboratory electrical conductivity versus temperature data (extrapolated to higher and lower temperatures) are applied to convert the eighteen electrical conductivity profiles into temperature profiles for a series of radially homogeneous olivine-pyroxene mixtures ranging from 100% olivine [(Mg)/(Mg + Fe) = 0.91] to 100% aluminous orthopyroxene (6.8 wt% Al_2O_3). The 100% olivine composition yields selenotherms that approach the Ringwood-Essene solidus at depths near 500 km while the addition of aluminous orthopyroxene (either 1.9 or 6.8 wt Al_2O_3) in concentrations exceeding 15-30 vol% leads to cooler selenotherms that approach the solidus only at depths greater than about 1000 km. The shape of the temperature-depth profiles is not found to be strongly sensitive to the olivine/pyroxene ratio if the assumption of radial homogeneity is valid at depths greater than 450-500 km.

On the basis of independent geophysical constraints (low seismic shear wave attenuation in the upper mantle, maintenance of mascon anisostasy over 3–4 b.y., locations of the deep moonquake foci), the profile envelopes for compositions containing more than 15–30 vol% aluminous orthopyroxene are considered to be most probable. A comparison of the latter with present day selenotherms calculated according to thermal history models indicates the greatest consistency with the model of Toksöz *et al.* which assumed initial partial melting and differentiation to a depth of 500 km and significant radial heat transport by subsolidus convection only during the first few b.y. of lunar history.

PLANETS

Arlot, J. -E. (Service de Mécanique Céleste du Bureau des Longitudes, Equipe de Recherche Associée au CNRS, Paris, France): 'The Determination of the Center of Gravity of a Planet from Photographic Plates', *Celest. Mech.* **26**, 199–205 (1982)

The difficulty of the determination of the center of gravity of a planet depends on the fact that it has usually a large apparent diameter. On a photographic plate, the size of the image of a planet depends on the exposure time and, mainly, on the focal length. Moreover the phase angle (Sun–Planet–Earth) makes the image of the planet dissymmetric and the surface features – when existing – make its brightness not uniform.

For a planet the position of the satellites of which is well known (for example, Jupiter), tests for the determination of the center of gravity have been made using different methods. These methods need a micro-densitometric analysis of the plates and allow a better accuracy for the position of the center of gravity of the planet (referred to near stars) than the classical methods using manual measuring machines.

Barbosa, D. D. (Inst. of Geophysics and Planetary Physics, Univ. of California, Los Angeles, CA 90024): 'Low-Level VLF and LF Radio Emissions Observed at Earth and Jupiter', *Rev. Geophys. Space Phys.* **20**, 316–334 (1982)

This paper examines the current state of knowledge of VLF and LF radio wave emissions in the magnetosphere. Specifically, the properties of the low-level noise commonly referred to as continuum radiation are reviewed with emphasis on the capabilities of the noise to diagnose local and remote plasma parameters. The relationship of the radiation to ≥ 1 -mV/m electrostatic upper hybrid emissions is critically assessed. There is a fair amount of indirect observational evidence to suggest that upper hybrid noise is associated with the generation of the VLF–LF radiation, and proposed theoretical mechanisms lean toward this interpretation also. However, no definitive association has been established to date. The theoretical luminosities of several mechanisms, which include synchrotron radiation, linear mode conversion of upper hybrid waves, and nonlinear scattering of upper hybrid waves off plasma density irregularities, are estimated. The wave-wave scattering hypothesis is adjudged to be a viable mechanism if the presence of low-frequency waves as a scattering agent can be established either theoretically or observationally. The alternative mechanisms are considered to be too weak as potential sources, but efficiency-saving modifications may make the linear mode conversion hypothesis more competitive. Recommendations for future studies on this subject are given.

Belton, M. J. S. (Kitt Peak National Observatory, P.O. Box 26732, Tucson, AZ 85726-6732): 'An Interpretation of the Near-Ultraviolet Absorption Spectrum of SO₂: Implications for Venus, Io, and Laboratory Measurements', *Icarus* **52**, 149–165 (1982)

The character of the line spectrum of SO₂ between 2000 and 3200 Å is described, and a crude band model for its absorption characteristics longward of 2280 Å is formulated. The model predicts planetary spectra that are substantially different from those predicted using a continuum model (Beer's law) for SO₂ absorption, the latter model being widely used to interpret the IUE spectrum of Io and ground-based and Pioneer orbiter spectra of Venus. As a result, the SO₂ scale height and mixing ratio

in the Venus stratosphere could be substantially different from the values that have been previously supposed, thereby changing the range of acceptable photochemical models. Also, it is found that the absence of the signature of SO_2 vapour absorption in Io's spectrum can be treated as a physically reasonable *lower* limit to the mean column abundance of SO_2 on the satellite as well as an upper limit. Thus a substantial SO_2 atmosphere may yet be found on Io. Laboratory measurements to establish accurate parameters for the band model are urgently required.

Bretagnon, P. (Service de Mécanique Céleste du Bureau des Longitudes, Equipe de Recherche Associée au CNRS, Paris, France): 'Theory of the Inner Planets', *Celest. Mech.* **26**, 161–167 (1982) (in French)

In the construction of planetary theories for the whole of the solar system undertaken at the Bureau des Longitudes, the aim is to obtain the precision of: for the inner planets 0''001 over several centuries; for the outer planets 0'01 over one century, 0'1 over 1000 years. To get these precisions one must compute the perturbations at least to the 3rd order of the masses for the inner planets and to the 6th order of the masses for the outer planets.

We have used an iterative method which has given the perturbations up to the 6th order of the masses for the outer planets and a method working order after order with respect to the masses. Through the latter, we have built the perturbations up to the 3rd order with respect to the masses for all the planets.

In the mean longitudes the precision now obtained is of 0''0005 for Mercury, 0''0030 for Venus and the Earth and 0''0047 for Mars.

For Mercury, the obtained precision is about 130 meters. One has therefore to introduce, besides the advance of the perihelium due to relativity, the periodic relativistic corrections, whose amplitude is over 3000 meters for that planet.

We have completed our theory of the Earth–Moon barycenter by the relativistic effects, as well as by the perturbations due to the Moon. As a whole, our solution is about 100 times better than that of Newcomb. Our solution for the variables q and p of the Earth shows that the equinox is moved by a periodic motion of 0'04 amplitude and with a period of 883 year – a thing not considered generally.

The precision of our solution for the mean longitude of Mars is 0''0047, which means a real progress over the theory of Clemence. We have indeed noticed many arguments missing in that theory we last mentioned. For the years to come we intend to replace the theories of Le Verrier by these solutions in the ephemerides published by the Bureau des Longitudes. Beforehand we are going to improve the constants of integration by a comparison to numerical integrations or directly to observation.

Encrenaz, T. and Combes, M. (Observatoire de Meudon, 92190 Meudon, France): 'On the C/H and D/H Ratios in the Atmospheres of Jupiter and Saturn', *Icarus* **52**, 54–61 (1982)

Using a method defined in a previous paper, we reestimated the C/H ratio in the atmospheres of Jupiter and Saturn by the measurements of the weak visible CH_4 bands, the CH_4 $3\nu_3$ band, and the (3–0) and (4–0) quadrupole bands of H_2 . In the case of Jupiter we conclude that the C/H ratio is enriched by a factor ranging from 1.7 to 3.6 relative to the solar value. In the case of Saturn, our derived C/H value ranges from 1.2 to 3.2 times the solar value. The Jovian D/H ratio derived from this study is $1.2 \times 10^{-5} < \text{D/H} < 3.1 \times 10^{-5}$. The value derived for the D/H ratio on Saturn is not precise enough to be conclusive.

Ingresoll, A. P. and Pollard, D. (California Inst. of Tech., Pasadena, CA 91125): 'Motion in the Interiors and Atmospheres of Jupiter and Saturn: Scale Analysis, Anelastic Equations, Barotropic Stability Criterion', *Icarus* **52**, 62–80 (1982)

If Jupiter's and Saturn's fluid interiors were inviscid and adiabatic, any steady zonal motion would take the form of differentially rotating cylinders concentric about the planetary axis of rotation. B. A. Smith *et al.* showed that Saturn's observed zonal wind profile extends a significant distance below cloud base. Further extension into the interior occurs if the values of the eddy viscosity and superadiabaticity are small. We estimate these values using a scaling analysis of deep convection and reduces the effective eddy viscosity. Viscous dissipation of zonal mean kinetic energy is then within

the bounds set by the internal heat source. The differential rotation increases the superadiabaticity, but not so much as to eliminate the cylindrical structure of the flow. Very large departures from adiabaticity, necessary for decoupling the atmosphere and interior, do not occur. Using our scaling analysis we develop the anelastic equations that describe motions in Jupiter's and Saturn's interiors. A simple problem is solved, that of an adiabatic fluid with a steady zonal wind varying as a function of cylindrical radius. Low zonal wavenumber perturbations are two dimensional (independent of the axial coordinate) and obey a modified adiabatic stability equation. The parameter analogous to β is negative and is three to four times larger than the β for thin atmospheres. Jupiter's and Saturn's observed zonal wind profiles are close to marginal stability according to this deep sphere criterion, but are several times, supercritical according to the thin atmosphere criterion.

Kovalevsky, J. (Cerga, Grasse, France): 'Hipparcos and the Dynamics of the Solar System', *Celest. Mech.* **26**, 213-220 (1982)

The HIPPARCOS program may contribute to dynamical astronomy in two different ways: by determining the positions of some bodies of the solar system or by improving the positions of the reference stars with respect to which observations of members of the solar system are made.

It is shown that only minor planets may be observed validly by HIPPARCOS but these observations alone cannot contribute significantly to the determination of a reference frame. However, they can be useful for the improvement of orbits and as a complement to a major observational effort in preparation of a new determination of dynamical system of reference.

HIPPARCOS will provide a new global reference frame and improved proper motions of stars. This may be used to rediscuss earlier observations and provide corrections to the theory of motion of the Moon and planets. Such corrections may be rather large and their possible effect is indicated for several cases. Furthermore, the celestial reference system of HIPPARCOS will allow to avoid, in future observations, many of the presently existing biases.

Kwok, J. H. and Nacozy, P. E. (Jet Propulsion Lab., Pasadena, CA 91109): 'Periodic Orbits of the Elliptic Restricted Problem for the Sun-Jupiter-Saturn System', *Celest. Mech.* **27**, 27-38 (1982)

A systematic approach to generate periodic orbits in the elliptic restricted problem of three bodies is introduced. The approach is based on (numerical) continuation from periodic orbits of the first and second kind in the circular restricted problem to periodic orbits in the elliptic restricted problem are found by this approach. The mass ratio of the primaries of these orbits is equal to that of the Sun-Jupiter system. The sidereal mean motions between the infinitesimal body and the smaller primary are in a 2:5 resonance, so as to approximate the Sun-Jupiter-Saturn system. The linear stability of these periodic orbits are studied as functions of the eccentricities of the primaries and of the infinitesimal body. The results show that both stable and unstable periodic orbits exist in the elliptic restricted problem that are close to the actual Sun-Jupiter-Saturn system. However, the periodic orbit closest to the actual Sun-Jupiter-Saturn system is (linearly) stable.

Lange, M. A. and Ahrens, T. J. (Seismological Lab., California Inst. of Tech., Pasadena, CA 91125): 'Impact Induced Dehydration of Serpentine and the Evolution of Planetary Atmospheres', Proceedings of the Thirteenth Lunar and Planetary Science Conference, Part 1, *J. Geophys. Res.* **87**, Suppl. A451-A456, November 15, 1982 (1982)

Shock recovery experiments in the 25 to 45 GPa range on antigorite serpentine determine the amount of shock-induced loss of structural water as a function of shock pressure. Infrared absorption spectra of shock recovered samples demonstrate systematic changes in the amount of structural water and molecular, surface adsorbed water. These yield qualitative estimates of shock-induced water loss and demonstrate that a portion of the shock released structural water is reabsorbed on interfacial grain surfaces. Determination of the post-shock water content of the shocked samples relates shock-induced water loss and shock pressure. Based on the present results and theoretical predictions, we conclude that shock pressures of from 20 to ~60 GPa induce incipient to complete water loss, respectively. This result agrees closely with theoretical estimates for total dehydration. The dehydration interval and the activation energies for dehydration in shocked samples decrease systematically with increasing shock

pressure as experience by the sample. We believe the present experiments are applicable to describing dehydration processes of serpentine-like minerals in the accretional environment of the terrestrial planets. We conclude that complete loss of structural water in serpentine could have occurred from accretional impacts of $\sim 3 \text{ km s}^{-1}$ when earth and Venus have grown to about 50% of their final size. Accreting planetesimals, impacting Mars, never reached velocities sufficient for complete dehydration of serpentine. Our results support a model in which an impact generated atmosphere/hydrosphere forms while the earth is accreting.

Lupo, N. J. (Dept. of Earth and Planetary Sciences, MIT, Cambridge, MA 02139): 'Mass-Radius Relationships in Icy Satellites after Voyager', *Icarus* **52**, 40-53 (1982)

Using improved data for the masses and radii of the satellites of Jupiter and Saturn, models accounting for self-compression effects are presented for the interiors of Europa, Ganymede, Callisto, Rhea, and Titan. For the differentiated models, two different possible scenarios for heat transport are treated, as well as two different compositions for the silicate component. Undifferentiated models are also treated. In each case, the models of Ganymede, Callisto, and Titan show noticeable similarities. It is found that estimates of the ice-rock ratio are dependent upon the assumptions made about the heat transport mechanisms, the rock composition, and on the distribution of rock and ice in the satellite's interior.

Richardson, D. L. (Dept. of Aerospace Engineering, Univ. of Cincinnati, Cincinnati, OH 45221): 'A Third-Order Intermediate Orbit for Planetary Theory', *Celest. Mech.* **26**, 187-195 (1982)

By use of a new canonical transformation procedure, a third-order intermediary for planetary motion is developed. The intermediary contains all contributions that arise from the assumption of circular, coplanar orbits for the disturbing masses. The results are expressible in terms of elliptic integrals of the first, second, and third kinds.

Seidelmann, P. K. (U.S. Naval Observatory, Washington, DC 20390): 'Orbital Motion of the Planets, Theoretical and Observational', *Celest. Mech.* **26**, 149-160 (1982)

A review is presented of the progress that has taken place since 1976 in our knowledge of the orbital motion of the planets. Analytical theories, numerical integrations, intercomparisons of theories and ephemerides, observational data, the fundamental constants for the theories and the calculation of ephemerides are all discussed separately. In addition, the prospects for future developments in each area are also discussed.

The challenge is to make the theoretical calculations an order or magnitude more accurate than the observational data, and then to improve our methods of observation so that the ephemerides need to be improved again. It is only by this means that our knowledge of the orbital motion of the planets will be improved.

Standish, E. M. Jr. (Jet Propulsion Lab., Pasadena, CA 91109): 'The JPL Planetary Ephemerides', *Celest. Mech.* **26**, 181-186 (1982)

In the early 1960's when the U.S. program for planetary exploration was getting underway, the task of navigating the spacecraft to the planets was undertaken at the Jet Propulsion Laboratory (JPL) in Pasadena, California. An integral part of the navigation process is the knowledge of precise planetary positions and motions. It was realized at that time that the existing planetary ephemerides were not accurate enough to support the navigational needs, and so JPL initiated a program to develop planetary ephemerides of the highest possible accuracy by using all relevant observational data. The program still exists today at JPL, and the resultant ephemerides continue to be improved as newer and more accurate observational data become available. In the past few years, the JPL ephemerides have been sent throughout the world and are being used for various purposes.

This paper discusses the JPL ephemerides, concentrating on what the ephemerides represent and which facets are well-determined. It also presents numerical estimates of these elements, mentions the expected progress in the future and discusses possible uses for the ephemerides themselves.

Van Flandern, T. C. (U.S. Naval Observatory, Washington, DC 20390): 'Application of a New Algebraic Manipulator Theory', *Celest. Mech.* **26**, 197 (1982)

We have developed a new algebraic manipulator at the Naval Observatory, for application to lunar and planetary theories. The manipulator is quite general in that it is written in IBM FORTRAN IV language, but otherwise is independent of the bit and word structure of any particular computer. If the user desires, the number of polynomial and trigonometric arguments may be varied without limit. The math and order subroutines use an efficient one-to-one core mapping process. A higher level set of operation codes to simplify programming is built in. For example, the problem $h = [(ab)/(cd)]^{1/2}$, where a, b, c, d are series, is computed by the statement: CALL EXPR (H, '*', A, B, '*', C, D, 'DV', \$1, \$2, 'R', \$3, '=').

Applications to planetary theory are already developed with enough accuracy for analytical partial derivatives. Special problems encountered in the analytical theory of Pluto will be described, since Pluto represents a 'worst case' situation in planetary theory. The manipulation had to be performed with a nonsingular element set. Operations had to be reordered to improved convergence, and a 3-to-2 resonance with Neptune had to be assumed. Even then, the analytical partial derivatives for Pluto had to be developed with nearly four significant figures because of the relatively short arc of observations and the consequent difficulty of separating unknowns.

Wood, B. J. and Holloway, J. R. (Depts. of Chemistry and Geology, Arizona State Univ., Tempe, AZ 85287): 'Theoretical Prediction of Phase Relationships in Planetary Mantles', Proceedings of the thirteenth Lunar and Planetary Science Conference, Part 1, *J. Geophys. Res.* **87**, Suppl. A19-A30, November 15, 1982 (1982)

Calorimetric and phase equilibrium data have been used to establish an internally consistent thermodynamic data base for the silico-undersaturated part of the system $\text{Na}_2\text{O}-\text{FeO}-\text{CaO}-\text{MgO}-\text{Al}_2\text{O}_3-\text{SiO}_2$. This data base has been used to calculate the stability fields of assemblages involving the phases: olivine (ol), orthopyroxene (opx), clinopyroxene (cpx), spinel (sp), plagioclase (plag) and garnet (gt) at high pressures and temperatures. In the six-component system all these phases are solid solutions; their mixing properties were also obtained from phase equilibrium and calorimetric data. In the model system $\text{CaO}-\text{MgO}-\text{Al}_2\text{O}_3-\text{SiO}_2$ (CMAS), the stable assemblages are ol-opx-cpx-plag at pressures less than 8 kb at 1300°C and less than 6 kb at 900°C. Above these pressures, spinel replaces plagioclase, until pressures of 16 kb at 1300°C and 14 kb at 900°C are reached. At higher pressures, garnet lherzolite (ol + opx + cpx + gt) is stable. Stable phase assemblages have also been calculated for sodium and iron-bearing compositions postulated as possible Martian Mantles. The McGetchin-Smyth composition would not contain orthopyroxene and a low-pressure assemblage of plag + ol + cpx + sp would be replaced by gt + ol + cpx + sp at pressures above 13 kb. In contrast, the Morgan-Anders composition has stability fields of plagioclase lherzolite ($P < 8$ kb) and garnet lherzolite ($P > 8$ kb) and a small field of spinel lherzolite at about 6 kb at temperatures below 900°C.

1. Jupiter

Biancale, R., Ferraz-Mello, S., and Tsuchida, M. (Departamento de Astronomia, Universidade de Sao Paulo, Sao Paulo, Brazil): 'Comparison of Sampson-Lieske Theory of the Galilean Satellites of Jupiter With Observations', *Celest. Mech.* **26**, 225-228 (1982)

The aim of the present work is to compare photographic observations of the Galilean satellites of Jupiter with the theory developed by Sampson at the beginning of the century and corrected and implemented recently by Lieske.

The comparisons between the observed and computed values give differences in geocentric angular distances of the order of 0.08 for modern observations (1968 to 1977) and of the order of 0.14 for older ones (1913 to 1928).

These results lead to the suggestion that important long period defects still exist in the theory of Sampson-Lieske. This is not surprising, due to the difficulties of the computation of the long-period inequalities in mean longitudes, even in a first-order theory.

Brown, B. C. (Computer Sciences Corp., Houston, TX 77058): 'Secular and Long Period Effects in the Orbits of the Galilean Satellites', *Celest. Mech.* **26**, 229 (1982)

This paper presents some results of an investigation into the secular and long period behavior of the orbits of the Galilean satellites. A set of non-singular elements is used in the investigation since the eccentricities and inclinations are very small. A Jovicentric coordinate system is used, with Jupiter's equatorial plane as the reference plane. In this investigation Kamel's extension of Deprit's form of the Lie transform perturbation method to non-Hamiltonian systems has been used extensively. Using Kamel's perturbation method, all explicitly periodic terms in the differential equations governing the long period behavior of the orbital elements have been removed. In this way the differential equations for the secular behavior have been generated to third order in the small parameters of the system. The resulting equations for the secular effects have been solved by successive approximations, convergence having been reached in three iterations. By inverting the perturbation method, expressions for the long period behavior of the elements have been generated to second order. The expressions for the secular and long period behavior of the elements and several numerical examples are presented. Particular attention is drawn to the fact that the coefficients of the free oscillation terms in the expressions for the long period behavior are different from the coefficients of the corresponding terms in the expressions for the secular behavior. For this reason particular care must be taken when defining what is meant by the 'free eccentricity' and 'free inclination'.

Duriez, L. (Laboratoire d'Astronomie, L. Impasse de l'Observatoire, 59000 Lille, France): 'General Planetary Theory Extended to the Case of Resonance and Application to the Galilean Satellite System of Jupiter', *Celest. Mech.* **26**, 231-255 (1982) (in French).

We consider a system of planets defined by a given distribution of mean motions and masses: we represent the osculating elliptic elements of their heliocentric orbits by quasi-periodic functions of time, through a method adapted to the commensurability case: these functions are the sum of the general solution of a critical system, expressed in long-period terms, and of a particular solution. As in the B. Brown's method (applied to the galilean satellites), the critical system contains the secular terms, the long-period terms (great inequalities), and the resonant terms: the particular solution consists of short-period terms only, whose amplitude is an explicit function of the solution of the critical system.

If all the long-period terms in the critical system are harmonic of one fundamental term, we can perform a simple change of variables which transforms the critical system in an autonomous one, and thus we reduce the resolution to an eigenvalue problem. Applying that to the galilean satellites of Jupiter and neglecting the solar perturbations, we obtain a differential system with constant coefficients, whose linear part concerns all the variables (including the major-axes and the mean longitudes) and gives, as a first approximation, the great inequalities, the free oscillations and the libration: nevertheless this solution agrees already with known results, but should be improved by taking into account the non-linear parts and the solar terms in a new approximation.

Eberhart, J.: 'Did Voyager 2 Sense Jupiter at Saturn?', *Science News* **121**, 247 (1982)

The study of Jupiter's magnetic field with the Pioneer 10 spacecraft is reported, and the possibility of a Jovian component in Saturn's continuum radiation is discussed.

Gautier, D., Bezaud, B., Marten, A., Baluteau, J. P., Scott, N., Chedin, A., Kunde, V., and Hanel, R. (Laboratoire d'Astronomie Infrarouge, Observatoire de Paris-Meudon, France): 'The C/H Ratio in Jupiter From the Voyager Infrared Investigation', *Astrophys. J.* **257**, 901-912 (1982)

From a selection of *Voyager* IRIS spectra corresponding to the cloud-free areas of Jupiter, we have determined the CH_4/H_2 volume ratio in the atmosphere of this planet as equal to $(1.95 \pm 0.22) \times 10^{-3}$ which corresponds to 2.07 ± 0.24 times the solar value of Lambert ($\text{C}/\text{H} = 4.7 \times 10^{-4}$). Estimate of errors includes both instrument noise and systematic uncertainties. Implications of this result on the formation and evolution of Jupiter are discussed.

Golombek, M. P. (Lunar and Planetary Inst., 3303 NASA Road 1, Houston, TX 77058): 'Constraints on the Expansion of Ganymede and the Thickness of the Lithosphere', Proceedings of the Thirteenth Lunar and Planetary Science Conference, Part 1, *J. Geophys. Res.* **87**, Suppl. A77-A83, November 15, 1982 (1982)

Grooves and furrows have been interpreted as grabens resulting from extension of Ganymede's lithosphere. Geologically reasonable estimates of the dip (90° - 60°) and displacement (less than 1 km to a few hundred meters) of faults bounding grooves on Ganymede allow calculation of the extension and surface area increase (0.04-2%) required for the formation of all grooved terrain. The implied radius increase is thus limited between 0.02 and 1%; 1% planetary expansion is the maximum possible since formation of the grooved terrain began. Similar estimates for faults bounding furrows, the oldest preserved tectonic features on Ganymede, indicate a maximum surface area increase of $\sim 0.5\%$ for the best developed furrow system, which is located in Galileo Regio. If equivalent furrow systems existed on all of the cratered terrain, then a maximum of $\sim 0.5\%$ increase in surface area of Ganymede is possible after the formation of the lithosphere and prior to the formation of grooved terrain. Faults bounding simple graben originate at a subsurface mechanical discontinuity and propagate upwards, resulting in grabens with similar widths and similar spacings between members of a set. The depth to this mechanical discontinuity for furrows and grooves on Ganymede must give at least a minimum lithosphere thickness, because it is impossible for faults to originate and propagate upwards from a point below the lithosphere. Therefore the minimum lithosphere thickness on Ganymede is 5 km and 9 km (in Marius and Galileo Regiones, respectively) at the time of furrow formation and 4 km at the time of groove formation.

Hinson, D. P. and Tyler, G. L. (Center for Radar Astronomy, Stanford Univ., CA 94305): 'Spatial Irregularities in Jupiter's Upper Ionosphere Observed by Voyager Radio Occultations', *J. Geophys. Res.* **87**, 5275-5289 (1982)

Dual frequency radio occultation experiments carried out with Voyagers 1 and 2 provided data on the spatial irregularities in Jupiter's ionosphere at four different locations. Sample spectra of weak fluctuations in amplitude and phase of the 3.6-cm and 13-cm wavelength radio signals can be interpreted by using the theory for scattering from an anisotropic power law phase screen. Least squares solutions for ionospheric parameters derived from the observed fluctuation spectra yielded estimates of (1) the axial ratio, (2) angular orientation of the anisotropic irregularities, (3) the power law exponent of the spatial spectrum of irregularities, and (4) the magnitude of the spatial variations in electron density. Equipment limitations and the method of analysis constrain the observations to irregularities of approximate size 1-200 km. No evidence of the inner or outer scale of the irregularities was found. For length scales in the range given, the three-dimensional spatial spectrum obeys a power law with exponent varying from -3.0 to -3.7, and the root mean square fractional variations in electron density are 1-15%. All observed irregularities appear to be anisotropic with axial ratios between 2:1 and 10:1. Ionospheric parameters vary with altitude and latitude. We conclude that the measured angular orientation of the anisotropic irregularities indicates magnetic field direction and may provide a basis for refining Jovian magnetic field models.

Lieske, J. H. (Astronomisches Rechen-Institut, Mönchhofstrasse 12-14, D-6900 Heidelberg, FRG): 'Early Eclipses of the Galilean Satellites', *Celest. Mech.* **26**, 257-263 (1982)

A brief summary of the development of the theory of motion of the Galilean satellites is presented. Over 7700 eclipse observations have been collected and reduced using the Ephemeris E-2. They are of great potential in improving the ephemerides of the satellites and can yield important information on the evolution of the Galilean system.

Lunine, J. I. and Stevenson, D. J. (Div. of Geological and Planetary Sciences, California Inst. of Tech., Pasadena, CA 91125): 'Formation of the Galilean Satellites in a Gaseous Nebula', *Icarus* **52**, 14-39 (1982)

A model for Galilean satellite formation was analyzed in which the satellites accrete in the presence of a dense, gaseous disk-shaped nebula and rapidly form optically thick, gravitationally bound primordial atmospheres. Upper-bound temperatures expected during accretion lead to partially differentiated structures for both Ganymede and Callisto, although with Ganymede much more differentiated than Callisto. When allowance is made for the aerodynamic breaking of infalling planetesimal fragments, lower surface temperatures results, and the amount of partial differentiation of Callisto is small, possibly approaching zero for a narrow size distribution of infalling planetesimals. The model is chosen to be consistent with the observed densities of the Galilean satellites and our current understanding of Jupiter formation. The retention of ices more volatile than H_2O is considered but not modeled in detail. A nominal nebula of ~ 0.1 Jupiter masses is constructed by consideration of likely surface density profiles and existing Jupiter collapse calculations. This nebula is optically thick (even if grain opacity is ignored) in both radial and vertical directions and has a temperature profile $T \sim 3600 (R_J/R)$, where R_J is Jupiter's radius and R is the radial distance in the disk midplane. Satellites accrete very rapidly (dynamical time scales being 10^2 – 10^4 years) and their optically thick gaseous envelopes are unable to eliminate the heat of accretion by radiation. Water-saturated, convective, adiabatic envelopes form, through which planetesimals fall, break up, and partially disseminate their mass. The resulting satellite surface temperatures during accretion are calculated. Possible implications of these models for the subsequent evolution of Ganymede and Callisto are explored and it is suggested that the extensive differentiation undergone by Ganymede may provide the right environment for subsequent resurfacing, whereas the relative lack of extensive differentiation for Callisto may explain the inferred absence of endogenic tectonism.

Morgan, J. S. and Pilcher, C. B. (Inst. for Astronomy, Univ. of Hawaii, Honolulu, HI 96822): 'Plasma Characteristics of the Io Torus', *Astrophys. J.* **253**, 406–421 (1982)

We have obtained simultaneous low spectral resolution ($\Delta\lambda \approx 1.5$ – 3 \AA) measurements of the following seven forbidden emission lines of the Jovian plasma torus: [S II] $\lambda\lambda 4069, 4076$; [S II] $\lambda\lambda 6716, 6731$; [S III] $\lambda 3722$; [O II] $\lambda\lambda 3726, 3729$. Significant changes in the characteristics of these emissions occur on a time scale of days. The previously reported relative maximum in the brightness of the red [S II] lines at magnetic longitudes near that of the north magnetic pole (the active sector) is evident in the new data. Variations in the [O II] emission with magnetic longitude are also apparent. The [O II] emission is more extensive in magnetic latitude than the [S II] emission. This is the expected result of the mass difference between these ions if they have a common temperature. The [S II] and [O II] lines yield independent and consistent values for the average electron density. Variations about this average are larger than the measurement uncertainties. A few unusual spectra in which the blue but not the red [S II] lines are present indicate the existence of transient conditions of high plasma density ($n_e \gtrsim 10^4$ – 10^5 cm^{-3}) and low electron temperature ($T_e < 1 \times 10^4 \text{ K}$).

Orton, G. S., Appleby, J. F., and Martonchik, J.3V. (Earth and Space Sciences Div., Jet Propulsion Lab., California Inst. of Tech., 4800 Oak Grove Drive, Pasadena, CA 91109): 'The Effect of Ammonia Ice on the Outgoing Thermal Radiance From the Atmosphere of Jupiter', *Icarus* **52**, 94–116 (1982)

We examine the effects of NH_3 ice particle clouds in the atmosphere of Jupiter on outgoing thermal radiances. The cloud models are characterized by a number density at the cloud base, by the ratio of the scale height of the vertical distribution of particles (H_p) to the gas scale height (H_g), and by an effective particle radius. NH_3 ice particle-scattering properties are scaled from laboratory measurements. The number density for the various particle radius and scale height models is inferred from the observed disk average radiance at 246 cm^{-1} , and preliminary lower limits on particle sizes are inferred from the lack of apparent NH_3 absorption features in the observed spectral radiances as well as the observed minimum flux near 2100 cm^{-1} . We find lower limits on the particle size of $3 \mu\text{m}$ if $H_p/H_g = 0.15$, or $10 \mu\text{m}$ if $H_p/H_g = 0.50$ or 0.05 . NH_3 ice particles are relatively dark near the far-infrared and $8.5\text{-}\mu\text{m}$ atmospheric windows, and the outgoing thermal radiances are not very sensitive to various assumptions about the particle-scattering function as opposed to radiances at $5 \mu\text{m}$, where particles are relatively brighter. We examined observations in these three different spectral window regions which

provide, in principle, complementary constraints on cloud parameters. Characterization of the cloud scale height is difficult, but a promising approach is the examination of radiances and their center-to-limb variation in spectral regions where there is significant opacity provided by gases of known vertical distribution. A blackbody cloud top model can reduce systematic errors due to clouds in temperature sounding to the level of 1 K or less. The NH_3 clouds provide a substantial influence on the internal infrared flux field near the 600-mbar level.

Orton, G. S., Aumann, H. H., Martonchik, J. V., and Appleby, J. F. (Earth and Space Sciences Div., Jet Propulsion Lab., California Inst. of Tech., Pasadena, CA 91109): 'Airborne Spectroscopy of Jupiter in the 100- to 300-CM-1 Region: Global Properties of Ammonia Gas and Ice Haze', *Icarus* **52**, 81-93 (1982)

A spectrum of the disk of Jupiter was obtained in January 1978 from the Kuiper Airborne Observatory, covering the 100- to 300- cm^{-1} spectral range at a resolution corresponding to 1.65 cm^{-1} . Although taken more than a year before the Voyager 1 Jupiter encounter, this spectrum serves to extend the Voyager IRIS experiment coverage down from its lower limit of 200 cm^{-1} . Analysis of the spectrum provides information on global mean properties of ammonia gas and an ammonia ice haze. A vertical distribution indistinguishable from saturation equilibrium, with a sharp depletion near the temperature minimum, matches the observed shape of the rotational line absorption best. Constraints on the total optical thickness of the ammonia ice haze can be made, but other properties, such as particle size or vertical scale height, cannot be distinguished clearly from our data in this spectral region. Nevertheless, all models of the haze produce a "continuum" thermal emission between the NH_3 line manifolds which is much lower than that produced by the H_2 collision-induced dipole opacity.

Squyres, S. W. and Veverka, J. (NASA Ames Research Center, Moffet Field, CA 94035): 'Color Photometry of Surface Features on Ganymede and Callisto', *Icarus* **52**, 117-125 (1982)

Voyager imaging data demonstrate that the scattering properties ("phase curves") of all major terrain types on Ganymede and Callisto are not significantly wavelength dependent between 0.4 and 0.6 μm . Our data suggest that the phase curves may be slightly steeper at the shorter wavelengths, consistent with the trend of telescopic observations near opposition. However, the differences are small and entirely within the uncertainties of our analysis. Our result indicates that the phase integrals (0.8 for Ganymede and 0.6 for Callisto) derived by S. W. Squyres and J. Veverka from the abundant Voyager clear filter observations are reliable measures of the radiometric phase integrals. The corresponding values of the Bond albedo turn out to be 0.35 for Ganymede and 0.11 for Callisto.

Vu. D. T. (Service de Mécanique Céleste du Bureau des Longitudes Equipe de Recherche Associée du CNRS 070808, 77, Avenue Denfert-Rochereau, 75014 Paris, France): 'Détermination of the Semi-Major Axes of the Galilean Satellites of Jupiter', *Celest. Mech.* **26**, 265-270 (1982) (in French)

In non-resonant cases, a constant part coming from the perturbations can be easily separated from the observed mean motion, which can be called the perturbed part. Another part created by resonance must be separated from the observed mean motion in the case of the first three Galilean satellites. The determination of it gives better value of the semi-major axis.

In this investigation, the analytical process is chosen to avoid a mixture of orders in successive expansions and integrations.

The main terms entering in the computation of the libration are the great inequalities of the first three satellites. Each of them is introduced in the development by its eight components: while in Sampson's theory only the great inequality of Satellite 2 is given by two components.

The equations of motion used in this work are derived from Sagnier's theory.

2. Mars

Blasius, K. R., Vetrone, A. V., Lewis, B. H., and Martin, M. D. (Planetary Science Inst., Science Applications, Inc., 283 S Lake, Pasadena, CA 91101): 'Viking Orbiter Stereo Imaging Catalog', NASA CR-3501, NASW-3208. February 1982. Pp. 404 (1982)

The extremely long missions of the two Viking Orbiter spacecraft produced a wealth of photos of surface features. Many of these photos can be used to form stereo images allowing the Earth-bound student of Mars to examine a subject in 3-D. This catalog is a technical guide to the use of stereo coverage within the complex Viking imaging data set. This second edition of the catalog supercedes the first edition published in June 1980 as NASA CR-3277.

Cragin, B. L., Hanson, W. B., and Sanatani, S. L. (Univ. of Texas at Dallas, Center For Space Sciences, Richardson, TX 75080): 'The Solar Wind Interaction With Mars as Seen by the Viking Retarding Potential Analyzers', *J. Geophys. Res.* 87, 4395-4404 (1982)

In addition to the published retarding potential analyzer (RPA) data that were taken in the Martian ionosphere, there exist many Viking RPA measurements of low-energy (< 75 eV) electron fluxes out to 16 000 km above the Mars surface. Both energy spectra and periods of continuous monitoring of the total flux above 15 eV are available. The mean electron current at energies greater than 15 eV increases monotonically by nearly 2 orders of magnitude from about 9000 km down to 700 km on Viking 1, but no clear signature of the bow shock is seen. The total wave power in the 2-s measurement intervals for this current does, however, show a broad peak near 1000-km altitude. The preshock variations in the low-energy electron fluxes can be related to whistler mode oscillations in the solar wind plasma. It is concluded that there may be a highly turbulent shock structure that masks a clear signature of the bow shock in the time-averaged data. The interaction model that is consistent with the bow shock at 1700 km, coupled with the ionosphere measurements, indicates that Mars is likely to have a permanent magnetic field adequate to stand off the solar wind during the Viking 1 entry.

Dobrovolskis, A. R. (Jet Propulsion Lab., 183-501, California Inst. of Tech., Pasadena, CA 91109): 'Internal Stresses in Phobos and Other Triaxial Bodies', *Icarus* 52, 136-148 (1982)

The unusual dynamical behavior of Phobos, its strange appearance, and its mysterious network of grooves all make it an intriguing object. Geophysical studies, though, have been hampered by the lack of suitable theories applicable to nonspherical bodies. In this paper the Martian satellites are modeled as homogeneous, elastic triaxial ellipsoids subject to tidal, rotational, and self-gravitational stresses. A novel semi-analytical treatment then gives the stress and strain fields throughout their interiors. Yield phenomena and their possible surface expressions are also investigated. The results indicate that Phobos and Deimos have always been stable with respect to tidal fracture or disruption, but that Phobos will probably break up before colliding with Mars. Applications of the new formulation to other nonspherical bodies in the solar system are also discussed.

Eberhart, J.: 'Mars Album 10; Some Spectacular Final Views from the Viking 1 Orbiter', *Science News* 121, 364-366 (1982)

Images of the surface of Mars, taken by the Viking 1 orbiter in May and June 1980, are described.

Evans, N. (Jet Propulsion Lab., 4800 Oak Grove Drive, Pasadena, CA 91109): 'The Viking Mosaic Catalog' (Volume 1), NASA CR-3496, NAS7-100. March 1982, P. 668 (1982)

Evans, N. (Jet Propulsion Lab., 4800 Oak Grove Drive, Pasadena, CA 91109): 'The Viking Mosaic Catalog' (Volume 2), NASA CR-3496, NAS7-100. March 1982. P. 668 (1982)

This two-volume Catalog is a collection of more than 500 mosaics prepared from Viking Orbiter images. Accompanying each mosaic is a footprint plot, which identifies by location, picture number, and order number, each frame in the mosaic. Corner coordinates and pertinent imaging information are also included. A short text provides the camera characteristics, image format, and data processing

information necessary for using the mosaic plates as a research aide. Procedures for ordering mosaic enlargements and individual images are also provided.

Hamilton, K. (National Center for Atmospheric Research, Boulder, CO 80307): 'The Effect of Solar Tides on the General Circulation of the Martian Atmosphere', *J. Atmosph. Sci.* **39**, 481-485 (1982)

The mean flow accelerations induced by solar tides in the Martian atmosphere have been calculated using separable tidal theory together with the thermal excitations of Leovy and Zurek. The calculated accelerations are generally small in the dust-free Martian atmosphere, although they may be important in a small region near the surface. During global dust storms the tidally-induced mean flow accelerations are much larger and the tides probably play an important role in the general circulation.

Harmon, J. K., Campbell, D. B., and Ostro, S. J. (National Astronomy and Ionosphere Center, Arecibo, Puerto Rico 00613): 'Dual-Polarization Radar Observations of Mars: Tharsis and Environs', *Icarus* **52**, 171-187 (1982)

Observations of the Tharsis region of Mars with the 12.6-cm radar at Arecibo Observatory have yielded radar echoes which are highly depolarized and which are, in terms of total echo power, dominated by diffuse rather than quasi-specular backscattering. The observations were made on February 7, 8, and 9, 1980, and the subradar track extended from 77 to 126°W Longitude at 22°N Latitude. Dual-polarized reception was employed, i.e., the echo was received in the same sense of circular polarization as transmitted ("depolarized" sense) as well as in the opposite ("polarized") sense. The disk-integrated ratio of depolarized power to polarized power averages 0.37 and the ratio of diffuse power to quasi-specular power averages 3.2. The depolarized spectra are dominated by a broad "enhancement" identified primarily with echoes from the Tharsis Ridge, implying that extensive areas of Tharsis are rough on decimeter scales. The major Tharsis shield volcanoes are candidates for sources of strong depolarization, although they alone cannot account for the entire depolarization enhancement.

Jakosky, B. M. and Farmer, C. B. (Div. of Geological and Planetary Sciences, California Inst. of Tech., Pasadena, CA 91125): 'The Seasonal and Global Behavior of Water Vapor in the Mars Atmosphere: Complete Global Results of the Viking Atmospheric Water Detector Experiment', *J. Geophys. Res.* **87**, 2999-3019 (1982)

The water vapor content of the Mars atmosphere was measured from the Viking Orbiter Mars Atmospheric Water Detectors (MAWD) for a period of more than 1 Martian year, from June 1976 through April 1979. Results are presented in the form of global maps of column abundance for 24 periods throughout each Mars year. The data reduction incorporates spatial and seasonal variations in surface pressure and supplements earlier published versions of less complete data. Column abundances vary between 0 and about 100 precipitable microns (pr μm), depending on location and season, while the entire global abundance varies seasonally between an equivalent of about 1 and 2 km³ of ice. The first appearance of vapor at nonpolar latitudes as northern summer approaches and the drop in abundance at mid-latitudes as summer ends both strongly imply the existence of a seasonal reservoir for water within the regolith. There appear to be no net annual sources away from the poles that contribute significant amounts of water. However, the strong annual gradient of vapor from north to south implies a net annual flow of vapor toward the south. This southward flow may be balanced by a northward flow during the global dust storms, by transport in the form of clouds or adsorbed onto dust grains, or during other years. The perennially cold nature of the south polar residual cap, along with the relatively large summertime vapor abundances over the cap, implies a net annual condensation of vapor onto the cap. Comparison with earlier (Earth-based) observations of vapor in the south during the local summer indicates that all of the seasonal CO₂ cap may sublime away in some years to reveal the water ice cap which must lie underneath, with corresponding large southern summer vapor abundances. The global distribution of the annual average abundance of vapor correlates well with Martian topography, as might be expected for a uniform constant atmospheric mixing ratio. If this topographic effect is divided out, the resulting residual map correlates well with maps of surface albedo and thermal inertia; this correlation may be related to the control exerted by the surface and subsurface temperatures on the adsorption/desorption process and on the atmospheric temperature profile and, hence, the vapor holding capacity of the atmosphere.

Kahn, R. and Gierasch, P. (Center for Radiophysics and Space Research, Cornell Univ., Ithaca, NY 14853): 'Long Cloud Observations on Mars and Implications for Boundary Layer Characteristics over Slopes', *J. Geophys. Res.* **87**, 867-880 (1982)

Viking orbiter images of Mars show several instances of long continuous cloud formations on the slopes of Arsia and Pavonis Mons. We have searched all the images of the planet for occurrences of such formations. Only in the Tharsis region were long clouds unambiguously identified. We have measured the times and locations of occurrence, the wavelengths and when possible, the apparent velocity of motion of these clouds. We have also tabulated the wavelengths of patches of ripple clouds that are often found with the long formations. The long clouds are observed only in the early morning hours, suggesting that they are associated with drainage winds due to a cold planetary boundary layer. We develop simple mathematical models to examine various aspects of such boundary layer winds; these allow us to construct a complete and self-consistent explanation of all the observed features of the cloud formations. We use the results to characterize some physical properties of the Mars boundary layer. There is strong downslope flow in the boundary layer on the high slopes of both volcanos. In the saddle region between the peaks the flow slows and undergoes a hydraulic jump, producing the long clouds. Downstream of the jump, standing internal gravity waves can exist and are excited by flow over surface irregularities. Small variations in their observed wavelengths behind the jump may be attributed to variation in the flow speed and depth. Finally, we can account for the location of the jumps by the variation of relative strength of the boundary layer flows on the two volcanos.

Kinoshita, H. and Nakai, H. (Tokyo Astronomical Observatory, Osawa, Mitaka, Tokyo, Japan): 'Mars Theory and its Comparison With Numerical Integration', *Celest. Mech.* **26**, 169 (1982)

Clemence constructed ephemeris of Mars using Hansen's theory. His aiming accuracy was 0".01 in the geocentric position. For testing the precision, he compared his ephemeris with numerical integration from 1919 to 1954. The largest difference in orbital longitude was 0".042. We have reconstructed Clemence's theory, following his procedure as closely as possible, and compared new ephemeris with numerical integration. The largest difference in orbital longitude is 0".025 (0".042 Clemence), in latitude 0".006 (0".008 Clemence), and in radius vector 1.5×10^{-7} AU (1.9×10^{-7} Clemence).

The improvement of new ephemeris over Clemence's ephemeris is quite small, even if in any theoretical calculations we kept one more digit than Clemence did. We think the discrepancies between numerical integration and theory arise from the following causes:

- (1) errors or oversights in our work,
- (2) a lack of convergence of the planetary theory along powers of the disturbing mass,
- (3) necessity of reevaluation of perturbations with the revised elements.

As far as the third possibility is concerned, Clemence recalculated the first-order perturbation by Jupiter with the revised elements and evaluated the new perturbations for the 161 data used in the comparison with numerical integration. The largest difference in $n\delta z$ is 0".004. We think the second possibility, a lack of convergence along the mass of the disturbing planets, is the most probable origin. Bretagnon recently finished third-order theory of inner planets and obtained the accuracy of 0".005 in the orbital mean longitude of Mars over 25 years, near the fundamental epoch of his theory.

Maxwell, T. A. (Center for Earth and Planetary Studies, National Air and Space Museum, Smithsonian Institution, Washington, DC 20560): 'Orientation and Origin of Ridges in the Lunae Palus - Coprates Region of Mars', Proceedings of the Thirteenth Lunar and Planetary Science Conference, Part 1, *J. Geophys. Res.* **87**, Suppl. A97-A108, November 15, 1982 (1982)

Numerous wrinkle ridges similar in appearance to lunar mare ridges occur on volcanic plains units surrounding the Tharsis region of Mars, where they are oriented circumferential to the center of the plateau. By analogy with lunar mare ridges and form morphologic evidence such as the smooth slopes of arches, these features are interpreted to result primarily from compressional folding of the volcanic plains, although the uppermost ridge may represent faulting of the near surface materials. East of the Tharsis region, ridges are best developed in the Lunae Paulus and Coprates quadrangles, where they can be used to indicate the degree of compressional stress occurring there. Comparison of ridge

orientations in these quadrangles to a Tharsis center at 1°N, 122°W indicates that more than 60% of the total length of ridges is orthogonal to a normal from this center. Non-orthogonal ridges are seen to have general northerly orientations after removal of the Tharsis orthogonal population. Trends of graben in surrounding terrain indicate that non-orthogonal ridges are not greatly affected by regional scale structures. Comparison of the frequency of orthogonal and non-orthogonal ridges further suggests that loading due to the Tharsis plateau was effective in producing compressional features as far as 4000 km from the center of the load; additional sources for compressional stress are necessary to account for ridge systems at greater distances from the Tharsis plateau.

McCord, T. B., Clark, R. N., and Singer, R. S., (Planetary Geosciences, Hawaii Inst. of Geophysics, Univ. of Hawaii, Honolulu, HI 96822): 'Mars: Near-Infrared Spectral Reflectance of Surface Regions and Compositional Implications', *J. Geophys. Res.* 87, 3021-3032 (1982)

Reflectance spectra (0.65–2.50 μm) are presented for 11 Martian areas. The spectral resolution is $\sim 1\frac{1}{2}\%$ and the spatial resolution is 1000–2000 km. These are the first high-quality spectrophotometric data at these wavelengths for regions on the surface. Spectral features previously observed are confirmed and better defined, and a number of important spectral properties are characterized for the first time. The spectra show water ice absorptions in the 1.5- and 2.0- μm regions, which if due to surface frost, would imply the presence of 1 to 2 mg cm^{-2} H_2O . However, other studies have shown that the presence of an unprotected surface frost in late morning is unlikely. Water ice is stable at night even at the equator and might persist until late morning when the air is well undersaturated if it is intimately dispersed in weathering products, especially if clays are present. The dark region spectra indicate about 4 times less water ice than seen in bright regions. Since some bright material is present in dark regions there may be no water ice associated with the dark materials themselves. This tends to confirm that weathering products (thought to be more abundant in bright regions) are involved in the mechanism that allows temporary persistence of unstable water ice. The presence of weak 2.3- μm features in many of the spectra are consistent with the presence of hydroxylated magnesium-rich minerals such as sheet silicates (serpentine, talc, and magnesian smectites) or amphiboles (anthophyllite). The apparent absence of a 2.2- μm absorption implies that montmorillonite may not be a major component of the Martian regolith. Many of the spectra also show an apparent absorption at 1.0 μm , in the wing of the 2.0- μm Martian atmospheric CO_2 absorption, which would indicate bound molecular water. Observed dark regions have distinctive near-infrared spectral shapes, previously not well determined, which are characteristic of thin semi-transparent alteration coatings overlying dark unaltered rock. Previously observed ferrous- and ferric-iron absorptions in the 1- μm region are better defined by these new data. Clinopyroxene (augite) is definitely present, but olivine is not spectrally apparent.

Morris, E. C. (Branch of Astrogeologic Studies, U.S. Geological Survey, Flagstaff, AZ 86001): 'Aureole Deposits of the Martian Volcano Olympus Mons', *J. Geophys. Res.* 87, 1164–1178 (1982)

The aureole of grooved terrain that surrounds the large shield volcano Olympus Mons consists of several overlapping roughly circular sheets, each 0.5 to 1.5 km thick. The surfaces of these materials bear abundant curvilinear ridges and troughs 10 to 100 km long and 1 to 5 km wide, which form anastomosing patterns that vary in length and width over the aureole. The aureole is asymmetric to Olympus Mons, extending almost 1000 km northwest from the center of the volcano but only 600 km southeast. The lobate form of the deposits, the pressure ridges on their surfaces, and the deflection of aureole material around barriers indicate that the deposits were emplaced as viscous flows. High-resolution Viking orbiter pictures show the aureole material to be unstratified, and it is inferred to contain randomly distributed large dark blocks whose weathering produces dark streaks in the talus on the flanks of ridges. A pyroclastic origin is proposed for the aureole. The following sequence is suggested. At least six great pyroclastic eruptions occurred prior to the construction Olympus Mons, they formed very fluid ash flows that became viscous during late stages of emplacement, and pressure ridges formed on the surfaces of the deposits before they finally came to rest. The oldest and most extensive aureole deposit (finely grooved terrain) was considerably modified by erosion prior to being partly covered by later eruptions. A positive gravity anomaly over the Olympus Mons area may define the site of a near-surface magma chamber that was the source of the pyroclastic eruptions.

Mouginis-Mark, P. J., Zisk, S. H., and Downs, G. S. (Dept. of Geological Sciences, Brown Univ., Providence, RI 02912): 'Ancient and Modern Slopes in the Tharsis Region of Mars', *Nature* 297, 546-550 (1982)

The directions of lava flows in the Tharsis region of Mars are used to identify regional palaeo-slopes, vent areas and local topography. A comparison is made between these flow directions and the present day radar-measured topography; good agreement between these data sets indicates that little intra-regional tectonic deformation has occurred following the emplacement of the preserved lavas.

Niimi, Y. (Tokyo Astronomical Observatory, Tokyo, Japan): 'Motion of Mars: 1935-1976', *Celest. Mech.* 26, 179 (1982)

Meridian observations of Mars, covering the period from 1935 to 1976, are discussed based on Clemence's theory of Mars. A total of 1441 observations is referred to the FK4 system. By three times the approximation of the least squares method, two definitive sets of orbital elements, without the empirical secular term for Clemence's theory, are obtained as follows:

Elements		Solution A	Solution B
Mean sidereal motion	n	689051 ^o 06435	689051 ^o 06479
Eccentricity	e	0.09326 730	0.09326 694
Longitude of perihelion	ϖ	333 ^o 17' 56 ^o .54	333 ^o 17' 57 ^o .99
Mean longitude at the epoch	ε ₀	83 ^o 09' 04 ^o .17	83 ^o 09' 04 ^o .51
Inclination to the ecliptic	i	1 ^o 51' 02 ^o .21	1 ^o 51' 02 ^o .32
Longitude of the ascending node	Ω	48 ^o 23' 58 ^o .42	48 ^o 23' 58 ^o .39
Semi-major axis	a	1.52369 12526 AU	1.52369 12521 AU

These elements are referred to as the mean equinox and ecliptic of 1850.0 and for the epoch 1850.0 January 0, Greenwich Ephemeris Noon. Solution A is a system of solutions only for corrections to the orbital elements of Mars. Solution B is that for corrections to the orbital elements of Mars and the Earth.

The equator and equinox correction to the FK4 system are obtained for the solution B as $-0^{\circ}08$ and $+0^{\circ}042$ respectively, of which the mean epoch is 1957.7.

Even after an improvement of orbital elements, there still remain systematic trends in the residuals, which differ from each other. The residuals have a periodic term with a nearly synodic period (780 days) of Mars with the Earth. By removing the periodic term from the residuals, the systematic trends in the residuals decrease noticeably. Thus, an origin of the systematic trends is considered to be due to the phase effect.

At present, the physical meaning of this phase effect is not yet known. However, it would be considered that there are unaccounted effects, due to irradiation of illuminated limb and to Polar Caps.

Patera, E. S. and Holloway, J. R. (Dept. of Chemistry, Arizona State Univ., Tempe, AZ 85278): 'Experimental Determination of the Spinel-Garnet Boundary in a Martian Mantle Composition', Proceedings of the Thirteenth Lunar and Planetary Science Conference, Part 1, *J. Geophys. Res.* 87, Suppl. A31-A36, November 15, 1982 (1982)

The high pressure reaction orthopyroxene + clinopyroxene + spinel to garnet + olivine is applicable to the mantle of Mars. Experimental reversals of this reaction in the system CaO-MgO-FeO-Al₂O₃-SiO₂ have been made in the range 100-1200°C using the bulk composition proposed by Morgan and Anders. At 1000°C, 1100°C, and 1200°C the garnet-out equilibrium is bracketed at 10.8 ± 0.5 , 12.6 ± 0.5 , and 15.2 ± 0.5 kbars, respectively. A dP/dT slope of 14.0 bar K^{-1} at 1000°C increasing to 26.0 bar K^{-1} at 1200°C has been inferred. Depending on bulk composition, the mantle of Mars is inferred to have a phase assemblage of either olivine + clinopyroxene + orthopyroxene + garnet or olivine + clinopyroxene + garnet + spinel. In the second, the partial melts will not be buffered by olivine and orthopyroxene and will have markedly lower silica activities than those of the terrestrial mantle.

Schultz, P. H. and Lutz-Garihan, A. B. (Lunar and Planetary Inst., 3303 NASA Road 1, Houston, TX 77058): 'Grazing Impacts on Mars: a Record of Last Satellites', Proceedings of the Thirteenth Lunar and Planetary Science Conference, Part 1, *J. Geophys. Res.* **87**, Suppl. A84-A96, November 15, 1982 (1982)

Grazing impacts can be identified on the basis of the elongate shape of the resulting crater and a distinctive pattern of ejecta deposits. Over 170 such impact craters larger than 3 km are recognized on Mars, and they represent more than 5% of the total crater population of the ridged plains. In contrast, the moon exhibits only one comparable example larger than 3 km on the maria, a frequency consistent with theoretical estimates for an isotropic influx of impactors. Many Mars grazers appear to occur along great circles. The most recent examples generally impacted in an east-west direction, whereas older grazers impacted in more northerly directions. We interpret the excessive number of grazers and the common impact directions as the result of satellites whose orbits tidally decayed with time. If all orbits originally had small inclinations similar to the orbits of Phobos and Deimos as well as the most recent grazers, then the change in impact direction with time can be explained as the result of shifts in the crust due to changes in the martian moments of inertia. The locations of the projected orbital axes (orbit-pole points) on the martian surface indicate that the geographic poles of Mars originally were situated at lower latitudes. More than 95% of the mass represented by these proposed satellites impacted prior to the emplacement of the volcanic plains of Lunae Planum. The estimated combined mass of grazing impactors would form a satellite at least 225 km in diameter. These results may provide new clues for the origin of Phobos and Deimos and perhaps the angular momentum of Mars.

Scott, D. H. and Tanaka, K. L. (U.S. Geological Survey, Flagstaff, AZ 86001): 'Ignimbrites of Amazonis Planitia Region of Mars', *J. Geophys. Res.* **87**, 1179-1190 (1982)

A series of postulated ignimbrite units is mapped in the Amazonis, Memnonia, and Aeolis quadrangles of Mars. The units cover about $2.2 \times 10^6 \text{ km}^2$ within a broad but discontinuous and irregular belt trending east-west along the highland-lowland boundary. The ignimbrites overlie parts of the western and southern aureole materials of Olympus Mons but are embayed in places by the lava plains of the lowlands. Stratigraphic relations between the basalt flows from the Tharsis Montes region and the ignimbrites are not clearly defined; crater counts suggest that the younger ignimbrites postdate the lava flows. Crater counter per square kilometer for the ignimbrites range from $7.29 \pm 1.95 \times 10^{-4}$ to $6.36 \pm 2.01 \times 10^{-5}$ for craters larger than 1 km in diameter. The ignimbrite materials form thick ($\geq 100 \text{ m}$), extensive, relatively flat sheets that are smooth to grooved or gently undulating. Grooved surfaces appear to be yardangs and, in most places, are not aligned with prevailing wind directions. The seven mapped ignimbrite units are characterized by morphologic expression, stratigraphic position, and crater counts. Similarities to ignimbrites in the Pancake Range of central Nevada include (1) rounded patches of smooth, high-albedo, nonwelded material superposed on jointed, low-albedo, welded material, (2) local complementary joint sets in welded materials, and (3) thick flow sheets of great areal extent that follow but subdue underlying topography. Four major eruptive centers occur in areas where units are thickest and where a dominant, NNW-SSE structural trend is expressed locally by unit margins, elongate collapse features, and normal faulting. A minimum volume of $3.85 \times 10^6 \text{ km}^3$ for the deposits has been calculated from thickness estimates based on shadow measurements and crater rim height relations.

Simpson, R. A., Tyler, G. L., Harmon, J. K., and Peterfreund, A. R. (Center For Radar Astronomy, Stanford Univ., CA 94305): 'Radar Measurement of Small-Scale Surface Texture: Syrtis Major', *Icarus* **49**, 258-283 (1982)

Recent radar observations of Syrtis Major have shown it to be smooth and relatively homogeneous when sensed at centimeter wavelengths λ . There is a gradual decrease in surface roughness east to west across the basin, which correlates with an apparent decrease in small ($< 1 \text{ km}$ diameter) crater density. Root mean square surface slopes σ range from more than $1.5\text{--}2.0^\circ$ in the east to less than 0.5° along the western margin at $\lambda = 12.6 \text{ cm}$. The surface appears somewhat rougher at $\lambda = 3.6 \text{ cm}$: a $\sigma \propto \lambda^{-0.3}$ dependence is inferred. Radar reflectivity increases from about 5% to about 12% across Syrtis Major, being greatest near the western margin. High-resolution (8 to 20 m/pixel) Viking images suggest that an

increasing amount of resurfacing has occurred in western Syrtis Major compared with the eastern parts. The radar, infrared, and optical imaging evidence are consistent with resurfacing by geologically recent, low-viscosity lavas which were subsequently mantled by thin layers of aeolian material. Each data set may be taken as a unique source of scale-dependent information on surface materials and properties. From comparison of radar-derived surface roughness with image-derived crater density curves we conclude that processes other than cratering control the surface texture on 0.03- to 100-m surface scales.

Sjogren, W. L. and Ritke, S. J. (Jet Propulsion Lab., Pasadena, CA 91109): 'Mars: Gravity Data Analysis of the Crater Antoniadi', *Geophys. Res. Lett.* **9**, 739-742 (1982)

Topography and gravity information for this 370-km crater are analyzed to determine a depth of compensation using an Airy isostatic model. A least squares fit to the gravity profile produces an estimate of 115 km for the depth of compensation.

Thomson, A. A.: 'Exploring Mars with "Kepler"', *Spaceflight* **24**, 151-153 (1982)

The ESA proposal for a Mars orbiter is outlined.

Wu, S. S. C. and Schafer, F. J. (U.S. Geological Survey, Flagstaff, AZ 86001): 'Photogrammetry of the Viking Lander Imagery', *Photogrammetric Engineering and Remote Sensing* **48**, 803-816 (1982)

Two fixed-base facsimile cameras are installed on each of the two Viking landers now on Mars. Imagery from the cameras is composed of image elements recorded by scanning in both azimuth and vertical directions; the resulting pictures are equivalent to images on a spherical surface. We have solved the problem of photogrammetric mapping from the Viking lander photography in two ways: (1) by converting the azimuth and elevation scanning imagery to the equivalent of a frame picture by means of computerized rectification; and (2) by interfacing a high-speed, general-purpose computer to the AS-11A analytical plotter so that all computations of corrections can be performed in real time during the process of model orientation and map compilation.

A series of pre-mission tests, comparing accuracy of terrestrial maps compiled by the photographic rectification method with maps made from aerial photographs, has shown both the efficiency of the lander cameras and the validity of the rectification method. The cameras and the method have been further validated on the Martian surface by topographic maps of Viking lander sites 1 and 2 at a scale of 1:10 with a contour interval of 1 cm. Examples are presented of photographs and maps of Earth and Mars.

Wu, S. S. C., Elassal, A. A., Jordan, R., and Schafer, F. J. (U.S. Geological Survey, Flagstaff, AZ 86001): 'Photogrammetric Application of Viking Orbital Photography', *Planet. Space Sci.* **30**, 45-55 (1982)

Special techniques are described for the photogrammetric compilation of topographic maps and profiles from stereoscopic photographs taken by the two Viking Orbiter spacecraft. These techniques were developed because the extremely narrow field of view of the Viking cameras precludes compilation by conventional photogrammetric methods. The techniques adjust for internal consistency the Supplementary Experiment Data Record (SEDR - the record of spacecraft orientation when photographs were taken) and the computation of geometric orientation parameters of the stereo models. A series of contour maps of Mars is being compiled by these new methods using a wide variety of Viking Orbiter photographs, to provide the planetary research community with topographic information.

3. Mercury

Landau, R. (Univ. of Minnesota, Minneapolis, MN 55455): 'A Comment on the Insolation at Mercury', *Icarus* **52**, 202-204 (1982)

E. Van Hemelrijck and J. Vercheval presented calculations of the insolation at Mercury and Venus which neglect the finite angular size of the Sun. To determine the temperature structure in the subsurface a more accurate calculation is needed, especially at longitudes $\pm 90^\circ$ on Mercury, where the Sun takes 18 days to rise or set. These calculations are presented here.

Thomas, P. G., Masson, P., and Fleitout, L. (Laboratoire de Geophysique et Geodynamique Interne, Université Paris-Sud, 91405 Orsay, France): 'Global Volcanism and Tectonism on Mercury: Comparison with the Moon', *Earth Planet. Sci. Lett.* **58**, 95–103 (1982)

Both morphologic and tectonic studies indicate that Mercury and the Moon have quite different internal histories, despite their apparently similar morphologies. The evaluation of the volcanic surfaces indicates a decreasing volcanism on Mercury at the largest impacting time, despite short and local re-activations. On the Moon, the basaltic volcanism was increasing at the same time and continued for 1 billion years. That indicates a strongly different thermal evolution from these two planetary bodies.

A widespread graben pattern is present on the Moon, with a statistical dominance of radial or tangential orientation with respect to the Imbrium basin, thus suggesting a relation between this major basin and the expansion of the Moon.

Azimuthal studies show that the compressive structures, observed on the stereographic covered surface of Mercury are not randomly oriented, but seem radial towards the Caloris basin, thus indicating a possible influence of this largest basin on Mercurian contraction.

The qualitative and quantitative formulations of these tectonic perturbations induced by large basins will be developed in a companion paper.

4. Neptune

Hecht, J. (No Address Given): 'Does Neptune Have Rings Too?', *New Scientist* **94**, 760 (1982)

The 'discovery' of Neptune's rings is not based on sufficient information; more evidence is needed to prove their essence.

Thomsen, D. E.: 'Neptune Rings: An Occultation Story', *Science News* **121**, 403 (1982)

Additional evidence is needed to confirm the 'discovery' of Neptune's rings.

5. Pluto

Breger, M. and Cochran, W. D. (Dept. of Astronomy and McDonald Observatory, Univ. of Texas, Austin, TX 78712): 'Polarimetry of Pluto', *Icarus* **49**, 120–124 (1982)

The polarization of Pluto has been measured for a range of solar phase angles from 0.8 to 1.8°. A mean linear polarization of $0.29 \pm 0.01\%$ (error of the mean) was found. No dependence of both the amount of polarization and position angles with rotational phase or solar phase angle could be detected. The positional angles of polarization agree with calculated position angles of the defect of illumination and are therefore parallel to the scattering plane. The observed polarization cannot be explained as resulting purely from a surface material which is similar to asteroidal surfaces. A hypothesis of polarization from a thin atmosphere, in addition to the surface polarization, is advanced.

Trafton, L. (McDonald Observatory, Univ. of Texas at Austin, TX 78712): 'Comments on Pluto's Atmosphere', In *Vibrational-Rotational Spectroscopy for Planetary Atmospheres - Volume II*, NASA CP-2223, Report No. 82B0303. April 1982. Pp. 709–715 (1982)

A pure CH₄ atmosphere would rapidly escape from Pluto. For such an atmosphere, even CH₄ frosts on Pluto's surface would completely sublimate on a time scale short compared to Pluto's life. Observations of CH₄ on Pluto therefore imply that its atmosphere must also contain another gas in significant quantity.

6. Saturn

Bastin, J. A. and Smith, D. H. (Queen Mary College, Mile End Road, London E1, UK): 'Saturn's Ringlets', *The Moon and the Planets* **26**, 97–100 (1982)

This paper suggests that Saturn's magnetic field is, in part, responsible for the very fine-scale radial features, or ringlets, seen in the ring-system. The planet's dipole field interacts with slight radial variations in plasma density, and the operation of an instability segregates the magnetic flux and plasma in the ring-plane into narrow alternating zones.

We suggest that this mechanism may act by itself to give rise to the inner ringlets. At greater radial distances we believe it amplifies gravitational resonances.

Bec-Borsenberger, A. (Bureau des Longitudes, 77 Avenue Denfert-Rochereau, Paris 14, France): 'Literal Theory of the Ninth Satellite of Saturn, Phoebe', *Celest. Mech.* **26**, 271–276 (1982) (in French).

We study a theory for the ninth satellite of Saturn, Phoebe, based on the literal solution we have obtained in the main problem of the lunar theory.

These series were computed by solving, by successive approximations, the Lagrange's equations expressed in variables, functions of the elliptic elements.

We may consider the case of Phoebe simpler than a lunar case because we seek less precision ($1/10''$ geocentric) and in the Lunar case, although the eccentricity of Phoebe is stronger.

Main problem: our series are computed to the complete seventh order and a great part of the perturbations of the eighth and ninth order, where we have attributed to the small lunar parameters, the order 1 to $m_0 = n'/n_0, e_0, e', \sin(i_0/2)$, the order 2 to $\alpha_0 = (a_0/a')(M_1 - M)/(M_1 + M)$ and the order 4 to $\mu\alpha = (a_0/a')M_1 M/(M_1^2 - M^2)$.

In the case of Phoebe, μ_1 equal zero and α_0 is the ratio a_1/a' .

We study the further development of these series by using, instead of parameter m_0 , the quantity $\Delta m_0 = n'/n_0 - m_1$ where m_1 is an approached value of m_0 in order to accelerate the convergence of the series with respect to m_0 .

Comparison with a numerical integration we are adjusting a numerical integration to the observations. We have already more than 100 observations, for the period 1900–1957.

At first, we compare the series of the main problem to a numerical integration of the Keplerian problem.

Beck, R. and Koppmann, R. (Astronomical Inst., Bonn, Germany): 'Saturn's "Spokes"', *Spaceflight* **24**, 85 (1982)

Following Voyager 1's encounter with Saturn in 1980, some of the photographs of the rings showed a surprising feature: finger-like bridges crossing the B-ring which seemed to violate Kepler's laws of planetary motion. They were named "spokes" and are generally believed to have been discovered by the Voyager cameras. J. Meadows and N. Henbest reported in *New Scientist* that the spokes were not discovered by Voyager 1 but that E. M. Antoniadi "was convinced he had observed such markings" in 1896. An even older visual observation of the spokes can be found in the German journal for popular astronomy *Sivius* in 1888. A third source concerning visual observations of the spokes is contained in a colour drawing made by Lucien Rudaux at the Observatory of Donville (France) and is published in the book *Le Ciel*. These reports show that telescopic observations and drawings of Saturn were (and still are) very effective in showing details never seen on photographs, but they were forgotten for a very long time.

Berry, R.: 'A Closer Look at Saturn's Rings', *Astronomy* **10**(2) 74–79 (1982)

The observations of Saturn's rings by the two Voyager spacecraft are summarised.

Baldwell, J. (Dept. of Earth and Space Sciences, SUNY at Stony Brook, NY 11794): 'Titan on the Eve of Voyager Encounter', In *Vibrational-Rotational Spectroscopy for Planetary Atmospheres - Volume II*, NASA CP-2223, Report No. 82B0303. April 1982. Pp. 673–677 (1982)

A decade of intense scientific study of Titan is reviewed. The atmosphere is not well understood at the time of this writing, but it is confidently expected that great progress will be made by the Voyager spacecraft now en route to the Saturn System.

Carbary, J. F., Bythrow, P. F., and Mitchell, D. G. (Applied Physics Lab., Johns Hopkins Univ., Laurel, MD 20707): 'The Spokes in Saturn's Rings: A New Approach', *Geophys. Res. Lett.* **9**, 429-422 (1982)

We propose that zonal winds in Saturn's atmosphere cause superrotation of the ionosphere and by virtue of field-aligned currents generate a potential of ~ 16 kV across the B-ring. Such a potential can momentarily polarize $\sim 1-10 \mu\text{m}$ size ice particles in a radial sense and thus create the spectacular spokes. A resulting current flowing radially through the B-ring would give rise to a power of $\sim 10^7$ W, which is close to that dissipated in an SED burst.

Cesarone, R. J. (Jet Propulsion Lab., California Inst. of Tech., Pasadena, CA 91109): 'Voyager 1 Saturn Targeting Strategy', *Journal of Spacecraft and Rockets* **19**, 72-79 (1982)

The trajectory targeting strategy for the Voyager 1 Saturn encounter was designed to accommodate predicted uncertainties in Titan's ephemeris while maximizing spacecraft safety and science return. The encounter was characterized by a close Titan flyby 18 h prior to Saturn periapse. Retargeting of the nominal trajectory to account for late updates in Titan's estimated position can disperse the ascending node location, which is nominally situated at a radius of low expected particle density in Saturn's ring plane. The strategy utilized a floating Titan impact vector magnitude to minimize this dispersion. Encounter trajectory characteristics and an actual targeting history are presented.

Chenette, D. L. and Davis, L. Jr. (California Inst of Tech., Pasadena, CA 91125): 'An Analysis of the Structure of Saturn's Magnetic Field Using Charged Particle Absorption Signatures', *J. Geophys. Res.* **87**, 5267-5274 (1982)

A new technique is derived for determining the structure of Saturn's magnetic field. This technique uses the observed positions of charged particle absorption signatures due to the satellites and rings of Saturn to determine the parameters of an axially symmetric, spherical harmonic model of the magnetic field using the method of least squares. Absorption signatures observed along the Pioneer 11, Voyager 1, and Voyager 2 spacecraft trajectories are used to derive values for the orientation of the magnetic symmetry axis relative to Saturn's axis of rotation, the axial displacement of the centre of the magnetic dipole from the center of Saturn, and the magnitude of the external field component. Comparing these results with the magnetic field model parameters deduced from the analyses of magnetometer data leads us to prefer models that incorporate a northward offset of the dipole center by about $0.05 R_S$.

Cheng, A. F., Lanzerotti, L. J., and Pirronello, V., (Bell Labs., Murray Hill, NJ 07974): 'Charged Particle Sputtering of Ice Surfaces in Saturn's Magnetosphere', *J. Geophys. Res.* **87**, 4567-4570 (1982)

Following recent investigations of the Saturn system in situ by Pioneer 11 and Voyager 1 and 2 and remotely by the International Ultraviolet Explorer, we have reconsidered the sputtering of water ice surfaces by magnetospheric ions as a possible source of hydrogen atoms and heavy ions. We use results from laboratory measurements of water ice sputtering and dissociation rates as a function of ice temperature. We also use Voyager charged particle data from the low energy charged particle experiment to obtain more accurate assessments of energetic ion fluxes and loss rates. Ion phase space densities show that, if charged particle sputtering is an important physical process, it will occur predominantly in the vicinity of Saturn's E ring and the moons Dione and Tethys, not at the outer edge of the A ring as previously suggested prior to the availability of in situ data. Charged particle sputtering of ice surfaces between 4.5 and $8 R_S$, followed by the ionization of H_2O and dissociation fragments, may be an important local source of the heavy ion plasma reported in the magnetosphere by Pioneer 11. We review several existing theories for the ring atmosphere and conclude that difficulties remain with all of them.

Cochran, W. D. (McDonald Observatory, Dept. of Astronomy, Univ. of Texas, Austin, TX 78712): 'Spatially Resolved Reflectivities of Saturn: 3000–6000 Angstroms', *Astron. J.* **87**, 718–723 (1982)

Spectrophotometric observations of seven spatially resolved regions on the disk of Saturn from 3000 to 6000 Å are reported. The data have been reduced to absolute reflectivities by standard spectrophotometric techniques. The data show an asymmetry between the northern and southern hemispheres in the equivalent width of the CH₄ 5430-Å band and in the continuum reflectivity.

Connerney, J. E. P., Ness, N. F., and Acuna, M. H. (Lab. for Extraterrestrial Physics, NASA/Goddard Spaceflight Center, Greenbelt, MD 20771): 'Zonal Harmonic Model of Saturn's Magnetic Field From Voyager 1 and 2 Observations', *Nature* **298**, 44–46 (1982)

An axisymmetric octupole model of Saturn's planetary magnetic field is proposed here. This three parameter model, characterized by the Schmidt-normalized spherical harmonic coefficients $g_1^0 = 21\,535$ nT, $g_2^0 = 1642$ nT and $g_3^0 = 2743$ nT, is extremely efficient in representing the main magnetic field of Saturn and reconciling the *in situ* magnetic field observations obtained by Pioneer 11 with those obtained by the Voyager 1 and 2 spacecraft. Saturn's unique magnetic field configuration is thus not that of a simple displaced dipole but rather appears to be the axisymmetric part of a complex dynamo field. This result is consistent with Stevenson's model of the interior of Saturn, in which the differential rotation of a metallic fluid shell above the active dynamo region attenuates all non-axisymmetric components of the dynamo field.

Daigne, G., Pedersen, B. M., Kaiser, M. L., and Desch, M. D. (Observatoire de Paris, Section d'Astrophysique, 92190 Meudon, France): 'Planetary Radio Astronomy Observations During the Voyager 1 Titan Flyby', *J. Geophys. Res.* **87**, 1405–1409 (1982)

During the Voyager 1 Titan flyby, unusual radio emissions were observed by the planetary radio astronomy experiment in the 20- to 97-kHz frequency range. In this paper we show that Titan itself is not the source of the observed radio emission. Rather, we attribute the emission features to modification of the normal Saturn kilometric radiation by propagation effects in enhanced density structures within the Titan wake. Furthermore, spiky emissions observed in the magnetic wake of Titan are interpreted in terms of local electrostatic instabilities at the electron plasma frequency. From these measurements we derive a range of electron densities in the wake region, and we discuss the consistency of the results.

Daniel, R. R., Ghosh, S. K., Iyengar, K. V. K., Rengarajan, T. N., Tandon, S. N., and Verma, R. P. (Tata Inst. of Fundamental Research, Bombay 400005, India): 'Far-Infrared Brightness Temperature of Saturn's Disk and Rings', *Icarus* **49**, 205–212 (1982)

We present far-infrared observations of Saturn in the wavelength band 76–116 μm, using a balloon-borne 75-cm telescope launched on 10 December 1980 from Hyderabad, India, when *B'*, in Saturn-centric latitude of the Sun, was 4°3. Normalizing with respect to Jupiter, we find the average brightness temperature of the disk-ring system to be 90 ± 3 K. Correcting for the contribution from rings using experimental information on the brightness temperature of rings at 20 μm, we find T_D , the brightness temperature of the disk, to be 96.9 ± 3.5 K. The systematic errors and the correction for the ring contribution are small for our observations. We, therefore, make use of our estimate of T_D and earlier observations of Saturn when contribution from the rings was large and find that for wavelengths greater than 50 μm, there is a small reduction in the ring brightness temperature as compared to that at 20 μm.

Davies, J. K.: 'A Brief History of the Voyager Project; Part 6', *Spaceflight* **24**, 253–258 (1982)

The Voyager 2 encounter with Saturn is described.

Desch, M. D. (NASA/Goddard Space Flight Center, Lab. For Extraterrestrial Physics, Planetary Magnetospheres Branch, Greenbelt, MD 20771): 'Evidence for Solar Wind Control of Saturn Radio Emission', *J. Geophys. Res.* **87**, 4549-4554 (1982)

Using data collected by the Voyager 1 and 2 spacecraft in 1980 and 1981, strong evidence is presented for a direct correlation between variations in the solar wind at Saturn and the level of activity of Saturn's nonthermal radio emission. Correlation coefficients of 57-58% are reached at lag times of 0-1 days between the arrival at Saturn of high pressure solar wind streams and the onset of increased radio emission. During both 160-day analysis intervals studied, the radio emission exhibits a long-term periodicity of 25 days, identical to the periodicity seen in the solar wind at this time and consistent with the solar rotation period. The energy coupling efficiency between the solar wind and the Saturn radio emission is estimated and compared with that for the Earth.

Dollfus, A. and Brunier, S. (Observatoire de Paris, 92190 Meudon, France): 'Observation and Photometry of an Outer Ring of Saturn', *Icarus* **49**, 194-204 (1982)

A faint outer ring (E ring), which lies outside the classical rings A, B, C, and F, has been detected out to eight Saturn radii. We first observed it on November 1, 1979, and thereby confirmed the 1966 observation by Feibelman. Our plates were taken with a coronagraphic design and are specially intended for photometry. They are directly scaled in reflectance by reference to the Saturn disk which is properly attenuated. Photometry of the edge-on ring E lineament shows a strong brightness increase at small phase angles, which is compatible with scattering by particles of several microns in radius. The excess reflectivity in blue compared to the B ring implies a significant contribution of small particles in the scattering process. The E ring shows brightness and radial gradient changes, with condensations, which differ between east and west limbs are not always the same from night to night. The E ring is probably a flat structure with a condensation centered at a distance of $4R_s$, but without a simple axial symmetry. It is probably shaped by segments or lumps and may have streamerlike structures.

Drobyshevski, E. M. (A. F. Ioffe Physical-Technical Inst., USSR Academy of Sciences, Leningrad, USSR): 'On the Excess Thermal Fluxes of Titan and Saturn', *The Moon and the Planets* **26**, 33-46 (1982)

The assumption of a recent (3.5-10 thousand years ago) explosion of the electrolysis products of Titan's ices suggests a common explanation for many peculiar features of Saturn's system.

In particular, the high excess luminosity of Saturn is due, possibly, to its having accreted a part of the material lost by Titan. The accretion of this material from Saturn's rings is continuing at present.

The crucial experiment to support the possibility of a recent Titan's ices explosion would be detection of excess heat flux. At the present time it could constitute 1.5-15% of the solar radiation flux absorbed by this satellite.

Eberhart, J.: 'Mapping the Moons of Saturn; Tethys', *Science News* **121**, 106-107 (1982)

The map of Tethys drawn by Patricia M. Bridges is reproduced in its original scale (1:10,000,000).

Eberhart, J.: 'Saturn: After the Spacecraft, Some Time to Think', *Science News* **121**, 357 (1982)

Observations of Saturn, as well as of Saturn's satellites and rings, which were discussed during a meeting of specialists in Tucson, Arizona, are reported.

Eberhart, J.: 'Mapping the Moons of Saturn; Rhea', *Science News* **121**, 140-141 (1982)

The map of Rhea, drawn by Jay L. Inge, is reproduced at 1:7,000,000 scale.

Eberhart, J.: 'Mapping the Moons of Saturn; Dione', *Science News* **121**, 157-157 (1982)

The map of Dione, drawn by Patricia M. Bridges, is reproduced in its original scale (1:10,000,000).

Eberhart, J.: 'Mapping the Moons of Saturn, Part Six; Mimas', *Science News* **121**, 234–235 (1982)

The map of Mimas, drawn by Jay L. Inge, is reproduced at 1 : 3,750,000 scale.

Gurnett, D. A., Scarf, F. L., and Kurth, W. S. (Dept. of Physics and Astronomy, Univ. of Iowa, Iowa 52242): 'The Structure of Titan's Wake from Plasma Wave Observations', *J. Geophys. Res.* **87**, 1395–1403 (1982)

During the Voyager 1 flyby of Saturn's moon Titan, the plasma wave instrument detected several types of plasma wave emissions. On the inbound leg a broad region of intense low-frequency noise was detected on the side of Titan facing away from Saturn. This noise has characteristics similar to the electric field turbulence observed in the magnetosheath at the earth and the ionosheath at Venus and is believed to be generated by newly created ions that are being accelerated in the vicinity of Titan by the corotational electric field. During the pass through the induced magnetic tail of Titan, a series of upper hybrid resonance emissions were observed. The electron density profile inferred from these emissions shows three distinct peaks with densities of $\sim 40 \text{ cm}^{-3}$, the first peak corresponding to the entry into the magnetic tail, the second peak corresponding to the neutral sheet crossing from the northern to the southern tail lobe, and the third, somewhat smaller, peak corresponding to the outbound exit from the tail. Large depressions in the magnetic field strength are observed coincident with each of the density peaks. These effects indicate that a dense plume of plasma is being carried downstream of Titan by the interaction with the rapidly rotating magnetosphere of Saturn. By equating the magnetic field pressure in the tail lobe to the plasma pressure in the neutral sheet, the temperature of the plasma is estimated to be about 8600 K. This low temperature suggests that the plasma originates from the ionosphere of Titan, probably forming a plume of plasma with a θ or H cross-section extending downstream from Titan. Within the tail lobes, a second type of low-frequency electric field noise was observed, with characteristics very similar to a type of noise called broadband electrostatic noise, which is found in the earth's magnetic tail. As in the case of the earth, this noise is most intense near the outer boundary of the plasma sheet and is almost completely absent in the high-density region near the neutral sheet.

Hämeen-Anttila, K. A. (Dept. of Astronomy, Univ. of Oulu, Finland): 'Saturn's Rings and Bimodality of Keplerian Systems', *The Moon and the Planets* **26**, 171–196 (1982)

The correction terms which are introduced by non-zero size of the particles into the mechanics of Keplerian systems can be replaced by relatively simple approximations which agree with computer simulations. The theory of finite particles confirms the bimodality of collisional systems which has previously been discussed in terms of the mass-point approximation. In Saturn's rings the ringlets correspond to the 'degenerate' mode while the matter which fills the gaps is in the 'non-degenerate' state. The predicted volume density of the ringlets (the fraction of space which is occupied by the particles), ≥ 0.2 , is much higher than the conventional value which follows from the theory of mutual shadowing. Therefore, the opposition effect of Saturn's rings must originate in the particles themselves. The transition from one mode to the other which is needed to create a dense ring in a cloud of small particles follows from the growth of mass in the central body. This may be a recently-formed planet; but, more probably, the transition occurs in a loose pre-planetary disc.

Hartle, R. E., Sittler, E. C. Jr., Ogilvie, K. W., Scudder, D. D., Lazarus, A. J., and Acreya, S. K. (Lab. for Planetary Atmospheres, NASA Goddard Space Flight Center, Greenbelt, MD 20771): 'Titan's Ion Exosphere Observed from Voyager 1', *J. Geophys. Res.* **87**, 1383–1394 (1982)

Electron and ion measurements made by the Voyager 1 plasma science instrument revealed a plasma wake surrounding Titan in Saturn's rotating magnetosphere. This wake is characterized by a plasma that is more dense and cooler than the surrounding subsonic magnetospheric plasma. The density enhancement is produced by the deflection of magnetospheric plasma around Titan and the addition of exospheric ions picked up by the rotating magnetosphere. By using simple models for ion pickup in the ion exosphere outside Titan's magnetic tail and ion flow within the boundaries of the tail, the interaction between Saturn's rotating magnetosphere and Titan is shown to resemble the interaction between the solar wind and Venus. Outside the magnetic tail of Titan, pickup of H^+ formed by

ionization of the H exosphere is indicated when synthetic and observed ion spectra are matched. Close to the boundary of the tail, a reduction in plasma flow speed is found, providing evidence for mass loading by the addition of N_2^+/H_2CN^+ and N^+ to the flowing plasma. The boundary of the tail is indicated by a sharp reduction in the flux of high-energy electrons, which are removed by inelastic scattering with the atmosphere and centrifugal drift produced when the electrons traverse the magnetic field draped around Titan. Within the tail the plasma is structured as the result of spatial and/or temporal variations. The ion mass cannot be determined uniquely in the tail; however, one measurement suggests the presence of a heavy ion with a mass of order 28 amu: One candidate is H_2CN^+ , suggested as the dominant topside ion of the ionosphere, which may flow from the ionosphere into the tail.

Hill, J. R. and Mendis, D. A. (Center for Astrophysics and Space Science, Univ. of California, San Diego, La Jolla, CA 92093): 'The Isolated Non-Circular Ringlets of Saturn', *The Moon and the Planets* **26**, 217-226 (1982)

We show that the combined effect of electrodynamic and gravitational forces can account for a number of features observed by Voyagers 1 and 2 in the isolated fine dust rings of Saturn. These include (a) the appearance and disappearance of the braids in the F-ring, (b) the eccentricities of the F-ring and the ringlets within the Encke and Cassini divisions and a gap in the C-ring, and (c) the kinks in the eccentric Encke ring. They may also account for the very existence of these rings.

Holberg, J. B., Forrester, W. T., and Lissauer, J. J. (Earth and Space Sciences Inst., Univ. of Southern California, Tucson Labs., AZ 85713): 'Identification of Resonance Features Within the Rings of Saturn', *Nature* **297**, 115-120 (1982)

The Voyager 2 UV spectrometer observed a stellar occultation by the rings of Saturn, which located ring features with an accuracy of 12 km. A high-resolution (3 km) optical depth atlas of the rings shows at least nine features, including four density wave patterns, identified with satellite resonances. Analysis of these density wave patterns yields the first surface mass densities for the A ring and, together with our optical depth atlas, a total ring mass of 6.4×10^{-8} Saturn masses.

Hunt, G. E., Godfrey, D., Muller, J. -P., and Barrey, R. F. T. (Lab for Planetary Atmospheres, Dept. of Physics and Astronomy, University College London, London WC1E 6BT, UK): 'Dynamical Features in the Northern Hemisphere of Saturn from Voyager 1 Images', *Nature* **297**, 132-134 (1982)

Results of the analysis of Voyager measurements of divergence and inferred vertical velocity of convective cloud features in the northern hemisphere of Saturn are presented here. The winds in this region have been measured by tracking the cloud elements observed in sequences of images. The derived zonal winds imply that these convective features reside at the maximum of strong easterly jets centred at $41^\circ N$ planetocentric latitude and that the jet is barotropically unstable. The divergences and local dynamics of the Saturn features are found to differ from those of the jovian equatorial plumes.

Lavega, A. S. (Agrupacion Astronomica de Sabadell, Bilbao, Spain): 'Motions in Saturn's Atmosphere: Observations Before Voyager Encounters', *Icarus* **49**, 1-16 (1982)

A summary is presented of all the telescopic observations of the clouds in Saturn's atmosphere made prior to the Voyager encounters with the planet. Saturn displays a pattern of belts and zones like Jupiter, although they are practically constant in latitude and without significant changes over the last century. Some dark and white spots with diameters of about 6000 to 10 000 km have been observed, allowing us to ascertain the atmospheric rotational period. Only a strong equatorial jet can be inferred from these measurements. The most obvious features of Saturn are the great white spots (GWS) with diameters of 20 000 km or more, but only five outbursts have been detected since 1876. Corrected measurements have been obtained of the zonal velocities at different latitudes, $u(\phi)$, with variations between 430 and -14 ms^{-1} with respect to the magnetic rotation of the planet. The expansion velocities of some GWS have been measured to be $u' \sim 30$ to 100 ms^{-1} and their lifetimes, $\tau_L \sim$ from 30 to 150 days. A possible subatmospheric origin for the GWS is proposed, in which it is due to a temporary and local anisotropy in the internal heat source (a "hot spot" in the deeper atmosphere). All the

multiple features seen in both 1903 and 1933 appear to be linked to a unique system of longitudes rotating with the magnetic period.

MacLennan, C. G., Lanzerotti, L. J., Krimigis, S. M., Lepping, R. P., and Ness, N. F. (Bell Labs., Murray Hill, New Jersey 07974): 'Effects of Titan on Trapped Particles in Saturn's Magnetosphere', *J. Geophys. Res.* **87**, 1411-1418 (1982)

The close fly-by of the Voyager 1 spacecraft to the Saturnian satellite Titan provided an opportunity for the low energy charged particle (LECP) experiment to investigate the influences of Titan on the magnetosphere energetic particle distributions. Magnetic field data from the magnetometer (MAG) experiment are used with angular distribution data from LECP to study the changes in the pitch angle distributions of ions ($40 < E_i < 220$ keV), and electrons ($26 < E_e < 61$ keV). Before and after the Titan encounter the ions are observed to exhibit a bulk motion in the direction expected of corotation of the particles with the planetary magnetic field. The magnetosphere corotation velocity outside the influence of Titan is deduced to be ~ 100 to 150 km s⁻¹, less than the ~ 200 km s⁻¹ expected for rigid corotation. Titan appears to disrupt the corotation motion of the ions: the fluxes of ions in the corotation direction are appreciably diminished in intensity, while those observed in the equatorial plane perpendicular to this direction are relatively unaffected. The resulting distribution and trajectory modeling conclusions suggest that the convection electric field is effectively absent in the wake of Titan. Before and after the Titan encounter the electrons are observed to exhibit pitch angle distributions peaked at $\sim 90^\circ$, representative of trapped particles. The presence of Titan produces a reduction in the fluxes of the electrons and flatter distributions with pitch angle.

Marouf, E. A. and Tyler, G. L. (Center for Radar Astronomy, Stanford Univ., CA 94305): 'Microwave Edge Diffraction by Features in Saturn's Rings: Observation with Voyager 1, *Science* **217**, 243-245 (1982)

Classical edge diffraction patterns are formed at centimeter wavelengths by several features of Saturn's rings. These patterns were discovered in 3.6- and 13-centimeter radio signals from Voyager 1 during occultation by the rings. The observed shapes are in agreement with theoretical patterns computed for screens of perfectly abrupt edges having large but finite opacity. Comparison with models in which the opacity at the edge tapers to zero from a finite value sets a new bound of less than about 200 meters on the microwave edge thickness. Certain features of the data suggest a smaller upper bound of about 130 meters on the edge thickness.

Marouf, E. A., Tyler, G. L., and Eshleman, V. R., (Center for Radar Astronomy, Stanford Univ., CA 94305): 'Theory of Radio Occultation by Saturn's Rings', *Icarus* **49**, 161-193 (1982)

The radio occultation technique is developed here as a new method for the study of the physical properties of planetary ring systems. Particular reference is made to geometrical and system characteristics of the Voyager dual-wavelength (13 and 3.6 cm) experiment at Saturn. The rings are studied based on the perturbations they introduce in the spectrum of coherent sinusoidal radio signals transmitted *through* the rings from a spacecraft in the vicinity of the planet to Earth. Two separate signal components are identified in a perturbed spectrum: a sinusoidal component that remains coherent with the incident signal but is reduced in intensity and possibly changed in phase, and a Doppler-broadened incoherent component whose spectral shape and strength are determined by the occultation geometry and the radial variation of the near-forward radar cross section of illuminated ringlets. Both components are derived in terms of the physical ring properties starting from a conventional radar formulation of the problem of single scattering on ensembles of discrete scatterers, which is then generalized to include near-forward multiple scattering. The latter is accomplished through special solutions of the equation of transfer for particles that are larger than the wavelength. When the occultation geometry is optimized, contributions of an individual ringlet to a perturbed spectrum can be identified with radial resolution on the order of a few kilometers for the coherent components and a few hundred kilometers for the incoherent one, thus permitting high-resolution reconstruction of the radial profile of the optical depth, as well as reconstruction of the radar cross section of resolved ringlets. Simultaneous estimates of the optical depth and radar cross section of a ringlet at 3.6 cm- λ allow

separation of its aerial density and particle size, if the particles are of known material and form a narrow size distribution with radii greater than several tens of centimeters. This separation is also achieved for radii $\lesssim 10$ cm from differential effects on the coherent signal parameters at 3.6- and 13-cm wavelengths. For the more general case of a broad size distribution modeled by a power law, the absence of differential effects on the coherent signal binds the minimum size to be $\gtrsim 10$ cm. In this case, the radius inferred from an estimate of the radar cross section represents an equivalent radius, which is strongly controlled by the maximum size of the distribution provided that the power index is in the range 3 to 4. On the other hand, detection of differential coherent signal extinction determines an upper bound on the minimum size and a lower bound on the power index, assuming water-ice particles. These bounds, together with an inferred equivalent size, constrain the size distribution at both its small and large ends.

Michel, F. C. (Dept. of Space Physics and Astronomy, Rice Univ., Houston, TX 77125): 'Viscous Origin of Saturn's Ring Structure', *Astrophys. Lett.* **22**, 101-102 (1982)

We propose that Saturn's disk is subdivided into numerous fine ringlets as a direct result of internal disk viscosity. The viscosity automatically leads to separation of ringlets at the edge of an initially uniform disk, leading to the decomposition of the disk into ringlets and the consequent removal of viscosity as an important evolutionary factor.

Ness, N. F., Acuna, M. H., and Behannon, K. W. (Lab. for Extraterrestrial Physics, NASA Goddard Space Flight Center, Greenbelt, MD 20771): 'The Induced Magnetosphere of Titan', *J. Geophys. Res.* **87**, 1369-1381 (1982)

The Voyager 1 spacecraft had a close encounter (miss distance = 6970 km) with Titan (diameter = 5140 km) on November 12, 1980, while this large satellite was located within the Saturnian magnetosphere at a local solar time of 1330. No clear evidence was found for any intrinsic magnetic field nor for the development of a bow shock wave as the corotating Saturnian magnetoplasma convected past Titan. However, a strong electrodynamic interaction was evidenced with the observation of a very well developed, induced bipolar magnetic tail. Three thin current carrying regions were crossed, corresponding to the inbound and outbound tail magnetopause and an imbedded tail neutral sheet. An asymmetry in the tail axis orientation of 20° with respect to the corotation direction was observed. Also seen was an asymmetry in the structure of the two tail lobes. This interaction is unique among those in the solar system observed to date, being intermediate in the characteristic Mach numbers, both sonic and Alfvénic, when compared with Titan (or Venus) in the solar wind or Io in the Jovian magnetosphere. This paper presents the results of the analysis of the magnetic field data, which suggest an interpretation qualitatively described by the draping of the Saturnian magnetic field around the ionosphere of Titan.

Osterbrock, D. E. (Lick Observatory, Mount Hamilton, CA 95140): 'Keeler's Gap in Saturn's A Ring', *Sky Telesc.* **64**, 123-126 (1982)

It is inappropriate on grounds of history, scientific accuracy, and professional usage, to term the narrow gap, found by Keeler in 1888, the 'Encke division'.

Porco, C. A. and Danielson, G. E. (Div. of Geological and Planetary Sciences, California Inst. of Tech., Pasadena, CA 91125): 'The Periodic Variation of Spokes in Saturn's Rings', *Astron. J.* **87**, 826-833 (1982)

The discovery of a periodic variation in spoke activity in Saturn's rings from the analysis of *Voyager* images is reported. A Fourier power spectrum was computed using a data set generated by quantifying spoke activity observed on the morning (western) half of the rings in *Voyager* images spanning 5.5 days (~ 12 Saturn rotation). A peak $\sim 14\sigma$ above the noise in the frequency domain was found at a period of 621 ± 22 min. Within the formal error, this value is consistent with the 639.4-min rotation period of Saturn's magnetic field. Maximum spoke activity is most likely to be observed on the morning half of the rings when a particular magnetic field sector coincides with this area. This magnetic

sector contains the region which is aligned with local noon at the time of the emission of the SKR (Saturn Kilometric Radiation). These results suggest that the fundamental period of spoke variation is that of Saturn's magnetic field, and that spoke activity is associated with the region of the field which gives rise to the SKR. Passage of this region through Saturn's shadow may play a significant role in the creation and/or rejuvenation of spokes.

Salo, H. and Lukkari, J. (Dept. of Astronomy, Univ. of Oulu, Finland): 'Self-Gravitation in Saturn's Rings', *The Moon and the Planets* **27**, 5-12 (1982)

In a ring-shaped collisional system self-gravitation reduces the equilibrium values of the geometric and optical thickness. In Saturn's rings both effects are appreciable. The previously found discrepancy between the calculated profile and the observed profile of the rings is chiefly caused by the omission of self-gravitation.

Scattergood, T. (NASA/Ames Research Center, Moffett Field, CA 85721): 'Organic Chemistry on Titan's Atmosphere', In *Vibrational-Rotational Spectroscopy for Planetary Atmospheres - Volume II*, NASA CP-2223, Report No. 82B0303. April 1982. Pp. 679-697 (1982)

Laboratory photochemical simulations and other types of chemical simulations carried out at NASA-Ames are discussed. The discussion includes in particular:

- (1) The chemistry of methane, which is the major known constituent on Titan's atmosphere, I will stress what we can learn from photochemistry and particle irradiation (that is, what happens when high energy protons and electrons fall into a methane-dominated atmosphere);
- (2) The composition of dust that comprises the haze layer; and
- (3) Isotope fractionation in planetary atmospheres.

Sicardy, B., Lecacheux, J., Laques, P., Despiau, R., and Auge, A. (Dasop, Observatoire de Paris, F-92190 Meudon, France): 'Apparent Thickness and Scattering Properties of Saturn's Rings from March 1980 Observations', *Astron. Astrophys.* **108**, 296-305 (1982)

Ground-based observations of Saturn at the times of the transits of the Sun and the Earth through the plane of Saturn's rings are presented. The reduction of the electronographic plates indicate that, when observed and lit at low tilt angle ($\lesssim 0.5^\circ$), the rings are not well described as an homogeneous scattering layer. The analysis of the plates taken on the night of the Earth's transit (March 12th) shows that a residual flux remains in the edge-on configuration. This residual flux gives an equivalent thickness of the ring system:

$$z_0 = 1.1_{-0.2}^{+0.2} \text{ km.}$$

The non-homogeneous behaviour of the rings, the residual flux, as well as a transitory asymmetry of brightness between the rings ansae may be interpreted as a result of a wide size-distribution of particles in the rings, up to diameters of a few kilometers.

Smith, G. R., Strobel, D. F., Broadfoot, A. L., Sandel, B. R., Shemansky, D. E., and Holberg, J. R. (Earth and Space Sciences Inst., Univ. of Southern California, Tucson Labs., AZ 85713): 'Titan's Upper Atmosphere: Composition and Temperature from the EUV Solar Occultation Results', *J. Geophys. Res.* **87**, 1351-1359 (1982)

The temperature and composition of the upper atmosphere of Titan have been inferred by observing an occultation of the sun by Titan, using the Voyager 1 ultraviolet spectrometer. The temperature is 176 ± 20 K near the evening terminator and 196 ± 20 K near the morning terminator. The major constituent is N_2 with a density of $2.7 \pm 0.2 \times 10^8 \text{ cm}^{-3}$ at 3840 km. The mixing ratio of CH_4 is $8 \pm 3\%$ at a radial distance of 3700 km near the evening terminator where $[CH_4] \simeq 1.2 \times 10^8 \text{ cm}^{-3}$. On the morning terminator the $[CH_4] \simeq 1.2 \times 10^8 \text{ cm}^{-3}$ level is about 20 km lower in the atmosphere. The acetylene mixing ratio above 3400 km is measured at the 1 to 2% level. Below 3300 km it decreases to between 0.1 and 0.3%. A layer of absorbing molecules, possibly polymers, is present at both morning and evening terminators. Near the evening terminator the layer is located between 3350 and 3600 km. Near the morning terminator it is located about 100 km lower in the atmosphere. A simple

photochemical model suggests that the homopause is located at 3500 ± 70 km with an eddy diffusion coefficient of $1_{-0.7}^{+2.0} \times 10^8 \text{ cm}^2 \text{ s}^{-1}$, which decreases to $\sim 10^3 \text{ cm}^2 \text{ s}^{-1}$ in the lower stratosphere as $[\text{N}_2]^{-2/3}$.

Strobel, D. F. and Shemansky, D. E. (Naval Research Lab., Washington, DC 20375): 'EUV Emission from Titan's Upper Atmosphere: Voyager 1 Encounter', *J. Geophys. Res.* **87**, 1361–1368 (1982)

Analysis of Titan's EUV emission spectra obtained at the Voyager 1 encounter demonstrates that electron impact on N_2 above 3600 km accounts for the bulk of the observed emission short of Lyman α . In conjunction with the UVS solar occultation data it is concluded that N_2 is the major component of Titan's upper atmosphere, with upper limit mixing ratios at 3900 km on NeI, ArI, CO, H_2 , and HI of 0.01, 0.06, 0.05, 0.06, and 0.1, respectively. Magnetospheric electrons interact with Titan's sunlit hemisphere to produce a power dissipation rate of $\approx 2 \times 10^9$ W in the exosphere and $\approx 3 \times 10^9$ W below the exobase, with optical signatures from numerous N_2 bands, NI, and NII multiplets. The N_2 c'_s (0–0) Rydberg band at 958 Å acts as an optical probe of Titan's exosphere because of transmission losses caused by fluorescence and predissociation. Magnetospheric electron precipitation produces an average dayside electron density of $\approx 3 \times 10^3 \text{ cm}^{-3}$ between 3600 and 4000 km, the region of bright limb emission. When Titan is within Saturn's magnetosphere, magnetospheric electron impact dissociation of N_2 generates an N atom escape rate of $\approx 3 \times 10^{26} \text{ s}^{-1}$ from Titan's exosphere. A nonthermal H atom escape rate of $\approx 2 \times 10^{26} \text{ s}^{-1}$ is estimated from magnetospheric electron impact ionization of N_2 followed by reactions with CH_4 and H_2 and recombination to produce hot H atoms.

Thomsen, M. F., Goertz, C. K., Northrop, T. G., and Hill, J. R. (Univ. of California, Los Alamos National Lab., NM 87545): 'On the Nature of Particles in Saturn's Spokes', *Geophys. Res. Lett.* **9**, 423–426 (1982)

An observed deviation of the angular velocity of spoke features from the Keplerian value can yield the charge to mass ratio of spoke particles. Published observations of spoke motion are consistent with q/m in the neighborhood of -10 coul kg^{-1} . Since a lower limit on q is one electronic charge, this value yields a lower limit to the size of spoke particles of about $10^{-2} \mu\text{m}$. The criteria for electrostatically ejecting small particles from larger parent bodies indicate an upper limit of about 10^3 m for the parent bodies. Stability of the grains against electrostatic disruption or field emission yields an upper limit of $\sim 3 \mu\text{m}$ for the spoke particle size and leads to the conclusion that the spoke particles must consist of material which is stronger than loose dust balls.

Wolf, D. A. and Neubauer, F. M. (Institut für Geophysik und Meteorologie, Technische Universität Braunschweig, 3300 Braunschweig, FRG): 'Titan's Highly Variable Plasma Environment', *J. Geophys. Res.* **87**, 881–885 (1982)

Titan's plasma environment is variable due to two different causes. The variability of the solar wind has the consequence that Titan may be located in the outer magnetosphere, the magnetosheath, or the interplanetary medium around noon Saturnian local time. Additionally, there are local time variations in Saturn's magnetosphere. We have calculated the location of the stagnation point of Saturn's magnetosphere $r_{st} = 16-26 R_s$ assuming a terrestrial type magnetosphere. Typical plasma parameters along the orbit of Titan are shown for high solar wind pressure. The magnetoplasma incident on Titan will be generally be subsonic, subalfvénic in the tail, transsonic, transalfvénic in the outer magnetosphere, and subsonic, superalfvénic in the magnetosheath. During crossings of the Saturnian magnetopause or bow shock by Titan we expect abrupt changes of the flow direction and stagnation pressure and rapid associated changes in Titan's uppermost atmosphere.

7. Uranus

Eberhart, J.: 'Sizing up the Satellites of Uranus', *Science News* **121**, 404 (1982)

Measurements of the diameters of satellites of Uranus, with the NASA Infrared Telescope at Mauna Kea, are reported.

Encrenaz, Th. and Combes, M. (Observatoire de Meudon, 92190 Meudon, France): 'On the D/C Ratio in the Atmosphere of Uranus', *Icarus* **49**, 27-34 (1982)

A method for deriving mixing ratios in the outer planets, mostly independent of scattering processes, is applied to Uranus. It is shown that scattering processes play a major role in the line formation in the atmospheres of Uranus and Neptune; consequently, abundance ratios derived from a reflecting-layer model can be questionable. Using our method, we derive for Uranus $D/C < 6 \times 10^{-3}$ which is significantly smaller than our result on Jupiter. The simplest explanation implies a C/H enrichment by at least a factor of 6 relative to the solar value.

Matthews, K., Neugebauer, G., and Nicholson, P. D. (Palomar Observatory, California Inst. of Tech., 320-47, Pasadena, CA 91125): 'Maps of the Rings of Uranus at a Wavelength of 2.2 Microns', *Icarus* **52**, 126-135 (1982)

Maps of the ring system of Uranus, as seen in reflected sunlight at a wavelength of $2.2 \mu\text{m}$, are presented for May 1978 and July 1979. Large azimuthal brightness variations revealed by these maps are consistent with the variable width established for the ϵ ring from occultation studies and support the existing elliptical model for this ring. An upper limit of ~ 0.010 is placed on the normal optical depth of any broad (~ 5000 km wide) axisymmetric ring component. There exists, however, an unexplained east-west asymmetry in the May 1978 map. In addition, multiaperture broadband infrared photometry of Uranus is reported, from which the geometric albedo of the planet at wavelengths of 1.25, 1.65, and $2.2 \mu\text{m}$ and the geometric albedo of the rings at $2.2 \mu\text{m}$ are derived.

Nicholson, P. D., Matthews, K., and Goldreich, P. (Mount Stromlo and Siding Spring Observatories, Research School of Physical Sciences, Australian National Univ., Canberra, Australia): 'Radial Widths, Optical Depths, and Eccentricities of the Uranian Rings', *Astron. J.* **87**, 433-447 (1982)

Observations of the stellar occultation by the Uranian rings of 15/16 August 1980 are used to estimate radial widths and normal optical depths for segments of rings 6, 5, 4, α , β , η , γ , and δ . Synthetic occultation profiles are generated to match the observed light curves. A review of published data confirms the existence of width-radius relations for rings α and β , and indicates that the optical depths of these two rings vary inversely with their radial widths. Masses are obtained for rings α and β , on the assumption that differential precession is prevented by their self-gravity. A quantitative comparison of seven ϵ -ring occultation profiles obtained over a period of 3.4 yr reveals a consistent structure, which may reflect the presence of unresolved gaps and subrings. Elliptical models for rings 6, 5, 4, α , β , and ϵ are presented for comparison with the results of previous studies, particularly that of Elliot *et al.*

Noel, F. and Barros, S. (Dept. of Astronomy, Univ. of Chile and European Southern Observatory): 'Observations of Uranus Made With the Danjon Astrolabe of Santiago, Chile, During 1979', *Astron. Astrophys. Suppl.* **47**, 481-482 (1982)

This paper gives the results of the observations of Uranus made with the Danjon Astrolabe of Santiago, Chile, during 1979. The residuals in zenith distance of the planet, the number of the fundamental stars group to which the residuals are referred as well as its weight are given among other pertinent data.

8. Venus

Adelman, S. J.: 'Terraforming Venus', *Spaceflight* **24**, 50-53 (1982)

We affect our local climate by changing the amount of dust and pollutants in the atmosphere, and the worldwide climate by raising the carbon dioxide level of the atmosphere. If such inadvertent activities can cause these effects, then deliberate acts might be able to substantially change the atmosphere of other major bodies of the Solar System. Within the past few years, several planetologists have begun to suggest how to terraform or to transform other members of the Solar System into Earth-like worlds. When there is sufficient energy to bring these changes about, our descendants may well undertake such activities.

Amery, G. W. (183 Church Road, Earley, Reading, RG6 1HN): 'The Lunar Occultation of Venus, 1980 October 5', *J. Brit. Astron. Assoc.* **93**, 132–134 (1982)

Observations by amateur astronomers in England of the occultation of Venus on October 5, 1980, are reported.

Aumann, H. H., Martonchik, J. V., and Orton, G. S. (Earth and Space Sciences Div., Jet Propulsion Lab., California Inst. of Tech., Pasadena, CA 91109): 'Airborne Spectroscopy and Spacecraft Radiometry of Venus in the Far Infrared', *Icarus* **49**, 227–243 (1982)

In March 1979, the spectrum of Venus was recorded in the far infrared from the G. P. Kuiper Airborne Observatory when the planet subtended a phase angle of 62° . The brightness temperature was observed to be 275 K near 110 cm^{-1} , dropping to 230 K near 270 cm^{-1} . Radiance calculations using temperature and cloud structure formation from the Pioneer Venus mission and including gaseous absorption by the collision-induced dipole of CO_2 , yield results consistently brighter than the observations. Supplementing the spectral data, Pioneer Venus OIR data at similar phase angles provide the constraint that any additional infrared opacity must be contained in the upper cloud, below approximately 40 mbars. The addition of a haze of submicron-size droplets of hydrated H_2SO_4 to the Pioneer-measured upper cloud structure serves to reconcile the model spectrum and the observations, but cloud microphysics strongly indicates that such a high particle density haze ($N \approx 1.6 \times 10^7\text{ cm}^{-3}$) is implausible. The atmospheric environment is reviewed with regard to the far-infrared opacity and possible particle distribution modifications are discussed. We conclude that the most likely possibility for supplementing the far-infrared opacity is a population of large particles ($\bar{r} \geq 1\ \mu\text{m}$) in the upper cloud with number densities less than $1\text{ particle cm}^{-3}$ which has remained undetected by *in situ* measurements.

Barsukov, V. L., Volkov, V. P., and Khodakovsky, I. L. (Vernadsky Inst. of Geochemistry and Analytical Chemistry, USSR Academy of Sciences, Moscow, USSR): 'The Crust of Venus: Theoretical Models of Chemical and Mineral Composition', Proceedings of the Thirteenth Lunar and Planetary Science Conference, Part 1, *J. Geophys. Res.* **87**, Suppl. A3–A9, November 15, 1982 (1982)

Physico-chemical modeling of the atmospheric-lithospheric interaction on Venus is presented. The thermodynamic assessment is carried out in terms of Venera 11 and 12 and Pioneer Venus measurements and the dynamic atmospheric structure. The subcloud atmosphere is interpreted to be a zone of nonequilibrium chemical conditions while the near-surface layer is presumed to be an equilibrium zone due to catalytic effects and low wind velocities. The mineral assemblages of the 'weathering crust' are calculated. The pyrite-anhydrite-magnetite assemblage is suggested as the buffering system resulting in reducing conditions ($P_{\text{O}_2} \approx 10^{-21}\text{ atm}$). The existence of hydration is problematic and is thermodynamically conceivable only for the sulfur enrichment of primary rocks (about 2 wt.%). The carbonate minerals are suggested to be unstable.

Bazilevski, A. T., Bobina, N. N., Shashkina, V. P., Shkuratov, Yu. G., Kornienko, Yu. V., Usikov, A. Ya., and Stankevich, D. G. (V. I. Vernadsky Inst. of Geochemistry and Analytical Chemistry, USSR Academy of Sciences, Moscow, USSR): 'On Geological Processes on Venus: Analysis of the Relationship Between Altitude and Degree of Surface Roughness', *The Moon and the Planets* **27**, 63–89 (1982)

Aiming to study the relationship between Venus surface heights and surface roughness, the Pioneer Venus surface altitude map and map of r.m.s. slope in m-dkm scale have been analysed for the Beta and Ishtar regions using a system of digital image processing. To integrate the data obtained, the results of geomorphological analysis of Venera 9 and 10 TV panoramas as well as gamma-spectrometric and photometric measurements were used. The analysis gives proof that Venera 9 and 10 landing sites represent geologic-morphologic situations typical of Venus, thus enabling the results of observations made at landing sites to be extended to large provinces. Apparently this conclusion is also applicable to the Venera 8 landing site. No strong relationship exists between the roughness of the

surface and its altitude or the amount of a regional slope; neither for the Beta nor for the Ishtar region. A weak direct correlation observable for roughness-altitude pairs for the Beta region and roughness-altitude, roughness-slope pairs for the Ishtar region are quite obviously a consequence of regional roughness control, i.e. of an overall character of geological structure. On Venus the factors contributing to higher surface roughness on the m-dkm scale are, obviously, mostly volcanic and tectonic in their nature whilst those responsible for smoothing-out of the surface are chiefly exogenic. The rate of exogenic transformation of the Cytherean surface may be fairly high. On Venus, similarly as on the Earth, active tectono-magmatic processes have possibly taken place in recent geological epochs. One of the places where they are manifest is an extensive zone running from north to south across the Beta, Phoebe and Themis highlands. Within its limits occur both the process of basaltic shield-type volcanism and areal basalt effusions at low hypsometric levels accounting for the formation of lowland plains at the expense of ancient rolling plains. The basalts of the shield volcano Beta show some differences in composition compared to those of areal effusions at low hypsometric levels. The overall character of Cytherean tectonics in the recent geologic epoch is apparently block-type with a predominance of vertical movements. Against the background of the sinking of some of the block the other ones are rising and, possibly, such "compensation upheavals" have been responsible for the formation of the Ishtar region.

Beatty, J. K.: 'Report From a Torrid Planet', *Sky Telesc.* **63**, 452-453 (1982)

Preliminary results of the Venera 13 and 14 missions, presented at the 13th Lunar and Planetary Science Conference, are reported.

Beer, R. (Jet Propulsion Lab., California Inst. of Tech., Pasadena, CA 91109): 'The Spectroscopy of Venus', In *Vibrational-Rotational Spectroscopy for Planetary Atmospheres - Volume I* NASA CP-2223, Report No. 82B0303. April 1982. Pp. 271-276 (1982)

Venus has not been an especially active field for spectroscopy in the past ten years for two possible reasons: first, the almost total domination of the spectrum by CO₂ (including almost every conceivable isotopic combination) makes the search for other species very difficult, and the CO₂ bands themselves have been deeply analyzed by L. D. Gray Young and her colleagues; second, the knowledge that no wavelengths short of the microwave penetrate through the Venus cloud decks (or even very deeply into them) means that, at best, UV, visible and IR remote sensing can investigate only the middle and upper atmosphere, and even there quantitative analysis is vastly complicated by the intense multiple scattering.

Brace, L. H., Theis, R. F., and Hoegy, W. R. (NASA/Goddard Space Flight Center, Greenbelt, MD 20771): 'Plasma Clouds Above the Ionopause of Venus and Their Implications', *Planet. Space Sci.* **30**, 29-37 (1982)

Early Pioneer Venus orbiter measurements by the Electron Temperature Probe (QETP) have revealed wavelike structures at the ionopause and clouds of plasma above the ionopause, features which may represent ionospheric plasma at different stages in its removal by solar wind-ionosphere interaction processes. Continuing operation of the orbiter through three Venus years has now provided enough additional examples of these features to permit their morphologies to be examined in some detail. The global distribution of the clouds suggests that they originate at the dayside ionopause as wavelike structures which may become detached and swept downstream in the ionosheath flow. Alternatively the clouds may actually be attached streamers analogous to cometary structure. Estimates of the total ion escape rate from Venus by the process yields values up to 7×10^{26} ions s⁻¹, based on their measured transit times, their probability of occurrence, their statistical distribution and their average electron density. Preliminary analysis shows that such an escape flux could be supplied by the upward diffusion limited flow of O⁺ from the entire dayside ionosphere. Observed distortions of dayside ionosphere height profiles suggest that such flows may be present much of the time. If such an escape flux were to continue over the entire lifetime of Venus, the effects upon the evolution of its primitive atmosphere may have been significant.

Brass, G. W. and Harrison, C. G. A. (Rosenstiel School of Marine and Atmospheric Science, Univ. of Miami, 4600 Rickenbacker Causeway, Miami, FL 33149): 'On the Possibility of Plate Tectonics on Venus', *Icarus* **49**, 86–96 (1982)

Several arguments have been put forward suggesting that Venus has no plate tectonics. We examine some of these arguments and suggest that because conditions on the surface of Venus are very different from those on Earth, the arguments should be reconsidered. We show that in the absence of an ocean, the differential hypsographic curve of Earth would probably have only one mode, like that for Venus. We show that the atmosphere of Venus is quite capable of erosion, provided that near-surface velocities are about 1 m s^{-1} or more, and that therefore the "oceanic" areas on Venus, should they exist, are probably covered with some thickness of sediment. If sedimentation on Venus is at all rapid, it is likely that subduction zones could be filled up and made unrecognizable topographically. Because Venus does not have an ocean, and because its surface temperature is much greater than that on Earth, ridge crests on Venus have a much smaller topographic expression than those on Earth. If significant sedimentation occurs they would be completely unrecognizable topographically.

Burgess, E. (No Address Given): 'Venus: The Twin That Went Wrong', *New Scientist* **94**, 786–789 (1982)

Why is Venus so similar to Earth in some ways, but so different in others? And could there ever have been life on the planet shrouded in cloud? Results from recent Russian and American missions have given scientists new insights into these questions and the building of the Solar System.

Campbell, P.: 'After Pioneer – Good Science, Bad News', *Nature* **296**, 13–14 (1982)

The possibly important sources of infrared opacity in the Venusian atmosphere are identified. The mixing ratios of various atmospheric constituents are shown. CO_2 , which is the major atmospheric constituent comprising about 97 percent of the atmosphere, is the dominant infrared opacity source. Not shown is N_2 which comprises about 3 percent of the atmosphere. The mixing ratio of water vapor varies considerably with altitude but falls in the range of about 20 to 200 parts per million (ppm). The mixing ratio of SO_2 falls in the range of 100–200 ppm. This number is about 5000 times larger than estimates obtained earlier via earth-based observations. The abundance of some of the other minor constituents is also shown. While these constituents are not important in the mid-infrared their importance for the opacity beyond 20 microns has not been established. Other minor constituents such as CO and HCl may not play a role in the greenhouse effect.

Cloutier, P. A. and Russell, C. T. (Dept. of Space Physics and Astronomy, Rice Univ., Houston, TX 77001): 'The Solar Wind Interaction', *Nature* **296**, 20 (1982)

Croft, T. A. (SRI International, Menlo Park, CA 94025): 'Strong Refraction Near the Venus Surface: Effects Observed by Descent Probes', *Radio Science* **17**, 1587–1597 (1982)

The high-pressure atmosphere of Venus causes strong downward refraction of radio rays, with consequences that were evident in the telemetry signals from Pioneer Venus probes. As the probes descended, the strength of the direct signal to the earth gradually diminished because of the combined actions of absorption and refractive defocusing. Both phenomena became increasingly pronounced as penetration proceeded. Like occultation recordings of signal strength, these records too can be analyzed to yield a profile of atmospheric temperature versus altitude. During the final 30 km of descent, there was in addition to the direct signal a second measured component that traveled to the surface of Venus and from there scattered toward the earth. The strong atmospheric refraction played a key role leading to the strengthening (and hence the detectability) of these echoes. Surprisingly, it is found that such surface-reflected signals provide a good indication of the horizontal winds existing at each altitude during the descent of the probes. Since the refraction is roughly the same in the visible band as it is at radio frequencies, there was some speculation that refractive effects might be visible in the images of the surface returned by the Soviet landers. No such effects were apparent. I demonstrate that the absence is attributable to limited visibility.

Deming, D., Espenak, F., Jennings, D., Kostjuk, T., and Mumma, M. (Infrared and Radio Astronomy Branch, NASA, Goddard Space Flight Center, Greenbelt, MD 20771): 'Evidence for High-Altitude Haze Thickening on the Dark Side of Venus From 10-Micron Heterodyne Spectroscopy of CO₂', *Icarus* **49**, 35-48 (1982)

The 10.86- μm $P(44)$ and 10.33- μm $R(8)$ lines of $^{12}\text{C}^{16}\text{O}_2$ were observed on Venus with an infrared heterodyne spectrometer. The spectral resolution equals the Doppler half-width and the line profiles are fully resolved. The $P(44)$ line was observed in June 1979 on the day side of the planet. The $P(44)$ line core appears in absorption; the nonthermal core emission, which is present at low J values, is negligible at $J = 44$. Modeling of the line profile indicates that a discrete, optically thick, cloud deck occurs at 45 mbar pressure, in essential agreement with current understanding of the Venusian cloud structure. The 10.33- μm $R(8)$ line was observed in April 1980 at a variety of positions on the day side, and at a single position on the night side. The strong nonthermal core emission which appears on the day side for this line is not present on the night side, where the line core appears in absorption. This behavior is consistent with a solar radiative pump as an excitation mechanism for the nonthermal emission. Modeling of the $R(8)$ night-side profile indicates that substantial high-altitude haze occurs above the cloud tops, in the region from 15 to 35 mbar pressure. Comparing the modeling for the $R(8)$ line to the $P(44)$ line we find that the variation in the mass of the high-altitude haze was greater than a factor of 2.

Donahue, T. M., Hoffman, J. H., Hodges, R. R. Jr., and Watson, A. J. (Dept. of Atmospheric and Oceanic Science, Univ. of Michigan, Ann Arbor 48109): 'Venus Was Wet: A Measurement of the Ratio of Deuterium to Hydrogen', *Science* **216**, 630-633 (1982)

The deuterium-hydrogen abundance ratio in the Venus atmosphere was measured while the inlets to the Pioneer Venus large probe mass spectrometer were coated with sulfuric acid from Venus' clouds. The ratio is $(1.6 \pm 0.2) \times 10^{-2}$. The hundredfold enrichment of deuterium means that at least 0.3 percent of a terrestrial ocean was outgassed on Venus, but is consistent with a much greater production.

Eberhart, J.: 'Venus Volcanism: The Lightning Link', *Science News* **121**, 309 (1982)

Volcanic eruptions might be the cause of lightning observed in the atmosphere of Venus.

Eberhart, J.: 'Soviet Landing Promises a Colorful Venus', *Science News* **121**, 148 (1982)

Preliminary results for the Venera 13 and 14 missions are reported.

Eberhart, J.: 'Eyes on Venus: A New Dimension', *Science News* **121**, 248-249 (1982)

A brief account of the Venera 13 and 14 observations of the surface of Venus is presented.

Eberhart, J.: 'Venus: Another Sign of a Wet Past', *Science News* **121**, 295 (1982)

Measurements of the deuterium to hydrogen ratio in the atmosphere of Venus lead to the conclusion that water might have existed on Venus at the early stages of its history.

Elson, L. S. (Jet Propulsion Lab., California Inst. of Tech., Pasadena, CA 91109): 'Dynamics of the Atmosphere', *Nature* **296**, 17 (1982)

Henbest, N.: '127 Minutes under Venus's Orange Skies', *New Scientist* **93**, 623-624 (1982)

A brief description of the Venera 13 and 14 missions is presented.

Intriligator, D. S. (Carmel Research Center, P.O. Box 1732, Santa Monica, CA 90406): 'Observations of a Mass Addition to the Shocked Solar Wind of the Venusian Ionosheath', *Geophys. Res. Lett.* **9**, 727-730 (1982)

Analyzed are the proton and heavy ion populations observed by the Pioneer Venus Orbiter plasma analyzer in the region downstream ($11.5 R_p$) of Venus. The ion energy per unit charge (E/Q) ratios for

protons and heavy ions are consistent with the identification of oxygen (O^+) as a prevalent constituent of the heavy ions. The speeds of the heavy ions and protons are often comparable with the number densities of the heavy ions being 1% of those of the protons. The azimuthal flow angles for the heavy ions and the protons are similar and the polar flow angles of both are usually within $\pm 7\frac{1}{2}^\circ$ of the ecliptic plane. The apparent intermittent nature of the heavy ion fluxes may be an indication that erosion of the ionosphere is taking place over a limited spatial range and that the orbit of the Pioneer Venus spacecraft is such that it does not intercept the "layers" of heavy ions in a continuous manner. The efficiency of the erosion process may be time variable, e.g., dependent on external ionsheath flow conditions, the state of the ionosphere. Evidence is found of a shear layer, the presence of oxygen ions of varying speeds or of other ionospheric constituents. The heavy ion observations are consistent with a viscous interaction and several other processes that have been suggested as giving rise to the removal and acceleration of ionospheric ions. The analyses reported here may be relevant to an understanding of the plasma interactions associated with comets and Mars and perhaps even with the subsonic interaction at Io and at Titan.

Kahn, R. (Center for Radiophysics and Space Research, Cornell Univ., Ithaca, NY 14853): 'Deducing the Age of the Dense Venus Atmosphere', *Icarus* 49, 71-85 (1982)

We show how crater size-density counts may be used to help constrain the history of the Venus atmosphere, based on the predictions of simple but reasonable models for crater production, surface erosion, and the effects of atmospheric drag and breakup on incident meteors in the Venus atmosphere. If the atmosphere is old, we may also be able to determine the importance of breakup as a mechanism for destroying incident meteors in a dense fluid. In particular, if the atmosphere is young, the old (uneroded) surfaces will have crater densities upward of 10^{-4} km^{-2} and a ratio of small (4 km) craters to large (128 km) craters near 10^3 . If the atmosphere is old and the breakup mechanism is dominant, absolute crater densities on Venus surfaces will be diminished by several orders of magnitude relative to the young atmosphere case. If atmospheric drag is dominant and the atmosphere is old, the absolute crater density will be lowered by perhaps an order of magnitude relative to the young atmosphere case, and the ratio of small to large craters will be reduced to a value near $10^{1.5}$ according to the models. The comparison of crater populations on young, as well as old, surfaces on Venus can help in distinguishing the young and old atmosphere scenarios, especially since the situation may be complicated by currently undetermined erosional and tectonic processes. Once a large fraction of Venus surface has been imaged at kilometer resolution, as the VOIR project promises to do, it could be possible to make an early determination of the age of the Venus atmosphere.

Knollenberg, R. G. (Particle Measuring Systems, Inc., 1855 South 57th Court, Boulder, CO 80301): 'Clouds and Hazes', *Nature* 296, 18 (1982)

The Pioneer observations of Venus and its cloud system is summarised in this report of papers presented at the International Conference on the Venus Environment (Palo Alto, California, 1-6 November 1981).

Knudsen, W. C., Banks, P. M., and Miller, K. L. (Lockheed Palo Alto Research Labs., 3251 Hanover St., Palo Alto, CA 94304): 'A New Concept of Plasma Motion and Planetary Magnetic Field for Venus', *Geophys. Res. Lett.* 9, 765-768 (1982)

It is shown that the magnetohydrodynamic conditions of the Venus ionosphere near the terminator favor convection of magnetic field rather than diffusion. Consequently, any planetary magnetic field which Venus may possess will be strongly affected by the global antisunward flow of the ionosphere which has been revealed by the Pioneer-Venus retarding potential analyzer. The magnetic flux from an internal magnetic field will accumulate in the night hemisphere. Details of the structure and dynamics of such accumulations depend on particular details of the magnetic field source and the time-dependent plasma flow pattern, but a simple interpretation of observational data yields a magnetic dipole moment of $7 \times 10^{20} \text{ G cm}^3$ directed along the planet spin vector.

Knudsen, W. C., Miller, K. L., and Spenner, K. (Lockheed Palo Alto Research Lab., Palo Alto, CA 94304): 'Improved Venus Ionopause Altitude Calculation and Comparison with Measurement', *J. Geophys. Res.* **87**, 2246–2254 (1982)

We calculate the altitude of the Venus ionopause following the inviscid fluid approach initially introduced by Spreiter *et al.* and later modified by Spretier and Stahara but incorporate several improved approximations. The calculated altitude is compared with median altitudes measured by the Pioneer Venus retarding potential analyzer. The calculated ionopause shape approximates the measured median shape closely in the solar zenith angle (SZA) range 0–135° and is a definite improvement over previous calculations. Improved approximations include use of an ionospheric pressure field which varies with SZA in a manner consistent with measurements, use of the modified Newtonian approximation for the pressure exerted on the ionosphere by the ionosheath, use of the Prandtl-Meyer expansion approximation for a short distance downstream from the terminator, and separation of the solar wind terminator from the solar extreme ultraviolet radiation terminator. The calculation is not expected to be accurate for solar zenith angles in excess of approximately 135°. Use of the improved approximations lowers the terminator ionopause altitude to approximately half that obtained with use of the usual Spreiter approximations. The calculated dawn ionopause is approximately 300 km higher in altitude than the dusk ionopause. Both ionopauses are close to their respective measured median values. The value of the upstream solar wind momentum flux required to fit the measured median ionopause altitudes is within 15% of the measured median solar wind momentum flux. We conclude that the median altitude of the ionopause between 0° and approximately 135° SZA may be adequately calculated without including a viscous interaction in the theory.

Kumar, S. (Center for Space Sciences, Univ. of Southern California, Los Angeles, CA 90007): 'Venus nightside Ionosphere: A Model with keV Electron Impact Ionization', *Geophys. Res. Lett.* **9**, 595–598 (1982)

A model of the 'full up' nightside ionosphere of Venus is presented for the equatorial midnight region. We propose keV electron impact as the strongest source of ionization leading to peak ion density of $\sim 10^5 \text{ cm}^{-3}$ which was observed by the PV-OIMS experiment on several occasions. The observed altitude profiles of CO_2^+ , O^+ , O_2^+ , H^+ and H_2^+ (or D^+) can be reproduced with this model if available keV electron flux is approximated by $\phi_e(E) \sim 100 E e^{-E/1000}$ in 0.3–3.0 keV range. This is a reasonable extrapolation of fluxes observed at lower energies.

Lewis, J. S. and Fegley, B. Jr. (Dept. of Earth and Planetary Sciences, MIT, Cambridge, MA 02139): 'Venus: Halide Cloud Condensation and Volatile Element Inventories', *Science* **216**, 1223–1225 (1982)

Several recently suggested Venus cloud condensates including aluminum chloride and halides, oxides, and sulfides of arsenic and antimony, are assessed for their thermodynamic and geochemical plausibility. Aluminum chloride can confidently be ruled out, and condensation of arsenic sulfides on the surface will cause arsenic compounds to be too rare to produce the observed clouds. Antimony may be sufficiently volatile, but the expected molecular form is gaseous antimony sulfide, not the chloride. Arsenic and antimony compounds in the atmosphere will be regulated at very low levels of sulfide precipitation, irrespective of the planetary inventory of arsenic and antimony. Thus arguments for a volatile-deficient origin for Venus based on depletion of water and mercury (relative to the earth) cannot be tested by a search for atmospheric arsenic or antimony.

McElroy, M. B., Prather, M. J., and Rodriguez, J. M. (Center for Earth and Planetary Physics, Harvard Univ., Cambridge, MA 02138): 'Escape of Hydrogen from Venus', *Science* **215**, 1614–1615 (1982)

Recombination of O_2^+ represents a source of fast oxygen atoms in Venus' exosphere, and subsequent collisions of oxygen atoms with hydrogen atoms lead to escape of about 10^7 hydrogen atoms per square centimeter per second. Escape of deuterium atoms is negligible, and the ratio of deuterium to hydrogen should increase with time. It is suggested that the mass-2 ion observed by Pioneer Venus is D^+ , which implies a ratio of deuterium to hydrogen in the contemporary atmosphere of about 10^{-2} , an initial ratio of 5×10^{-5} , and an original H_2O abundance not less than 800 grams per square centimeter.

McElroy, M. B., Prather, M. J., and Rodriguez, J. M. (Center for Earth and Planetary Physics, Harvard Univ., Cambridge, MA 02138): 'Loss of Oxygen from Venus', *Geophys. Res. Lett.* **9**, 649-651 (1982)

Ionization of thermal and non-thermal oxygen atoms above the plasmopause on Venus supplies an escape flux for O averaging 6×10^6 atoms $\text{cm}^{-2} \text{sec}^{-1}$. Hydrogen and oxygen atoms escape with stoichiometry characteristic of water. It is argued that escape of H is controlled by the oxidation state of the atmosphere, regulated by escape of O.

McGill, G. E. (Dept of Geology and Geography, Univ. of Massachusetts, Amherst, MA 01002): 'Geology and Geophysics', *Nature* **296**, 14-15 (1982)

Recent Pioneer Mission results, presented at the International Conference on the Venus Environment (Palo Alto, California, 1-6 November 1981), are summarised.

Mims, S. S. (Louisiana Arts and Science Center Planetarium, Baton Rouge, LA 70803): 'Revealing the Venesian Secrets', *Astronomy* **10**(7), 66-70 (1982)

V. L. Barsukov's presentation to the 13th Lunar and Planetary Science Conference is reported.

Nagy, A. F. and Brace, L. H.: 'Structure and Dynamics of the Ionosphere', *Nature* **296**, 19 (1982)

Pioneer Mission results, presented at the International Conference on the Venus Environment (Palo Alto, California, 1-6 November 1981), are summarised.

No Author Cited: 'The Other Side of Venera 14: Capturing Venesian Evolution?' *Science News* **121**, 245 (1982)

The possibility of basaltic lava flows on Venus has been anticipated from studies of radar data, gravity maps, radionuclide measurements and other analyses, and additional evidence for basalt has come from the major-element chemistry provided by X-ray fluorescence spectroscopy data from the recent Soviet Venera 13 and 14 landing craft (SN: 3/27/82, p. 214). In addition, however, the landers took four pictures of the surface (one of which has since been processed in color - see p. 248) - a feat accomplished only twice before, by Veneras 9 and 10 in 1975. And among the tiny gallery of half a dozen photos, perhaps the classic example of a familiar, flow-layered basaltic lava terrain is shown in the Venera 14 image above.

The lander reached the surface of the planet on March 5, carrying a pair of cameras angled down on opposite sides of the craft's bulbous body. (One of its photos, together with both black-and-whites from Venera 13, appeared in the March 20 SN.) The conspicuous fine material evident in the Venera 13 images is almost absent here, leaving a clean view of smooth-but-fractured, layered plates. A glance might suggest mere flat bedrock, but details such as the hole in the slab just above the landing-ring's left end strongly point to a layered evolution of the terrain. Is Venus still adding new layers?

Nozette, S. and Lewis, J. S. (Dept. of Earth and Planetary Sciences, MIT, Cambridge, MA 02139): 'Venus: Chemical Weathering of Igneous Rocks and Buffering of Atmospheric Composition', *Science* **216**, 181-183 (1982)

Data from the Pioneer Venus radar mapper, combined with measurements of wind velocity and atmospheric composition, suggest that surface erosion on Venus varies with altitude. Calcium- and magnesium-rich weathering products are produced at high altitudes by gas-solid reactions with igneous minerals, then removed into the hotter lowlands by surface winds. These fine-grained weathering products may then re-act with the lower atmosphere and buffer the composition of the observed gases carbon dioxide, water vapor, sulfur dioxide, and hydrogen fluoride in some regions of the surface. This process is a plausible mechanism for the establishment in the lowlands of a calcium-rich mineral assemblage, which had previously been found necessary for the buffering of these species.

Reasenberg, R. I., Goldberg, Z. M., and Shapiro, I. I. (Dept. of Earth and Planetary Sciences, MIT, Cambridge, MA 02139): 'Venus: Comparison of Gravity and Topography in the Vicinity of Beta Regio', *Geophys. Res. Lett.* **9**, 637-640 (1982)

The Doppler tracking data obtained from the Pioneer Venus Orbiter when it passed near Beta Regio yielded a peak vertical anomaly of 150 mGal when analyzed by our two stage procedure. A comparison of maps of the gravity and topography at comparable resolution shows a striking correlation. A scatter plot shows that the observed gravity anomaly is approximately 0.4 of that expected from uncompensated topography of half the mean density of Venus. However, the spectral admittance shows that the gravity anomalies can not be explained either by Airy compensation at fixed depth or by a model comprising an elastic plate atop an inviscid fluid. The gravity and topography variations may signify deep compensation or dynamic support for Beta Regio and more shallow compensation for other features.

Schaber, G. G. (U.S. Geological Survey, 2255 N. Gemini Drive, Flagstaff, AZ 86001): 'Venus: Limited Extension and Volcanism Along Zones of Lithospheric Weakness', *Geophys. Res. Lett.* **87**, 499-502 (1982)

Three global-scale zones of possible tectonic origin are described as occurring along broad, low rises within the Equatorial Highlands on Venus (lat 50° N. to 50° S., long 60° to 310°). The two longest of these tectonic zones, the Aphrodite-Beta and Themis-Alpha zones, extend for 21 000 and 14 000 km, respectively. Several lines of evidence indicate that Beta and Alpha Regiones, located at the only two intersections of the three major tectonic zones, are dynamically supported volcanic terranes associated with currently active volcanism. Rift valleys south of Aphrodite Terra and between Beta and Phoebe Regiones are characterized by 75- to 100-km widths, raised rims, and extensions of only a few tens of kilometers, about the same magnitudes as in continental rifts on the Earth. Horizontal extension on Venus was probably restricted by an early choking-off of plate motion by high crustal and upper-mantle temperatures, and the subsequent loss of water and an asthenosphere.

Seiff, A. and Kirk, D. B., (Ames Research Center, NASA, Moffett Field, CA 94035): 'Structure of the Venus Mesosphere and Lower Thermosphere from Measurements During Entry of the Pioneer Venus Probes', *Icarus* **49**, 49-70 (1982)

Data on the thermal structure of the nightside middle atmosphere of Venus, from 84 to 137 km altitude, have been obtained from analysis of deceleration measurements from the third Pioneer Venus small probe, the night probe, which entered the atmosphere near the midnight meridian at 27° S latitude. Comparison of the midnight sounding with the morning sounding at 31° S latitude indicates that the temperature structure is essentially diurnally invariant up to 100 km, above which the nightside structure diverges sharply from the dayside toward lower temperatures. Very large diurnal pressure differences develop above 100 km with dayside pressure ten times that on the nightside at 126 km altitude. This has major implications for upper atmospheric dynamics. The data are compared with the measurements of G. M. Keating, J. Y. Nicholson, and L. R. Lake above 140 km, with theoretical thermal structure models of Dickinson, and with data obtained by Russian Venera spacecraft below 100 km. Midnight temperatures are ~ 130 K, somewhat warmer than those reported by Keating *et al.*

Taylor, F. W. (Dept. of Atmospheric Physics, Oxford Univ. Clarendon Lab., Oxford OX1 3PU, U.K.): 'Structure and Energetics of the Atmosphere', *Nature* **296**, 16-17 (1982)

Pioneer Mission results, presented at the International Conference on the Venus Environment (Palo Alto, California, 1-6 November 1981), are summarised.

Thomsen, D. E.: 'Soviet Results on Chemistry of Venus', *Science News* **121**, 358 (1982)

Preliminary results of the Venera 13 and 14 measurements of the chemical composition of the atmosphere of Venus are presented.

Tomasko, M. (Lunar and Planetary Lab., Univ. of Arizona, Tucson, AZ 85721): 'Thermal Balance of Venus', In *Vibrational-Rotational Spectroscopy for Planetary Atmospheres - Volume I*, NASA CP-2223, Report No. 82B0303. April 1982. Pp. 211-227 (1982)

The Pioneer Venus mission measured several parameters of the atmosphere of Venus which pertain to its temperature structure and thermal balance. Among them are the temperature profile, the composition of the atmosphere, the solar fluxes throughout the atmosphere, and the thermal fluxes throughout the atmosphere.

Wallis, M. K. (Dept. of Applied Mathematics and Astronomy, Univ. College, Cardiff CF1 1XL, UK): 'Comet-like Interaction of Venus with the Solar Wind III. The Atomic Oxygen Corona', *Geophys. Res. Lett.* **9**, 427-430 (1982)

Suprathermal atomic oxygen constituting an extensive exospheric corona give rise to new heavy ions within the solar plasma flowing around Venus. Because their gyro-radii are large compared with transverse scales, the O⁺ ions do not simply effect a drag due to 'mass loading' of the flow. Some precipitate into the ionosphere and provide a novel ion source. Also, the back-reaction on the flow not only decelerates it, but also deviates it laterally and essentially asymmetrically about the planet.

Williams, M. A., Thomason, L. W., and Hunten, D. M. (Dept. of Atmospheric Sciences, Univ. of Arizona, Tucson, AZ 85721): 'The Transmission to Space of the Light Produced by Lightning in the Clouds of Venus', *Icarus* **52**, 166-170 (1982)

A Monte Carlo program by Thomason and Krider has been adapted to the Venus cloud geometry and optical properties. If lightning flashes occur within or just below the clouds, the fraction of photons of visible light escaping to space is 0.1-0.4, depending on the location of the flash. For flashes near the surface, only one blue photon in 10⁴ was found to escape; about 5% of the red ones are transmitted. Failure of the Pioneer Venus Orbiter to unambiguously detect optical lightning signals from space is not due to attenuation by the atmosphere and clouds. In any case, lightning is not acceptable as an explanation for ashen light.

Wilson, L. (Dept. Geological Sciences, Brown Univ., Providence, RI 02912): 'A Soviet View of the Venusian Surface', *Nature* **296**, 607-608 (1982)

A brief account of the Venera 13 and 14 observations of the surface of Venus is presented.

Young, A. (Dept. of Physics, Texas A and M Univ., College Station, TX 77843): 'Neutral Species in the Atmosphere of Venus', In *Vibrational-Rotational Spectroscopy for Planetary Atmospheres - Volume I*, NASA CP-2223, Report No. 82B0303. April 1982. Pp. 229-242 (1982)

About 97% of the Venusian atmosphere is CO₂, with the balance comprised of various trace constituents. I will first discuss species other than CO₂ that have either been found in Venus' atmosphere or have been sought unsuccessfully, and then will return to problems connected with the spectrum of CO₂ itself.

OTHER OBJECTS

1. Asteroids

Barucci, M. A. and Fulchignoni, M. (Istituto Astrofisica Spaziale C.N.R., Reparto Planetologia, Roma, Italy): 'The Dependence of Asteroid Lightcurves on the Orientation Parameters and the Shapes of Asteroids', *The Moon and the Planets* **27**, 27-57 (1982)

The dependence of asteroidal light curves has been derived from the obliquity, aspect and phase angles. The effects of an angle variation are discussed taking into account the possible geometry of an asteroidal body.

The amplitude-aspect relation is discussed for different asteroidal shapes.

On the basis of this relation a graphical attempt to determine the value of the aspect from the light curves' amplitude is described.

Brown, R. H., Morrison, D., Telesco, C. M., and Brunk, W. E. (Inst. for Astronomy, Univ. of Hawaii, Honolulu, HI 96822): 'Calibration of the Radiometric Asteroid Scale Using Occultation Diameters', *Icarus* **52** 188-195 (1982)

We report a new approach to the calibration of the radiometric asteroid scale using the recent accurate occultation measurements of the diameters of 2 Pallas and 3 Juno, and the Voyager diameter of J4 Callisto, and new infrared photometry of these objects obtained with the NASA 3-m Infrared Telescope Facility. This calibration is internally consistent to better than 5% and probably has an absolute accuracy of $\pm 5\%$. A revision of the TRIAD radiometric diameters downward is required to bring them into agreement with the new calibration.

Debehogne, H., De Sanctis, G., and Zappala, V. (Observatoire Royal de Belgique, B-1180 Bruxelles, Belgium): 'Photoelectric Photometry of Three Dark Asteroids', *Astron. Astrophys.* **108**, 197-200 (1982)

Lightcurves of the dark and average-size asteroids 53 Kalypso, 156 Xanthippe, and 313 Chaldaea were obtained from March 11 to 17, 1981. These observations were planned to enlarge the present knowledge of average-size and small objects, for which the statistics are poor.

For Kalypso we obtained a synodic rotation period of about 27^{h} , with an amplitude $A \geq 0.09$ mag; for Xanthippe, $P_{\text{syn}} \approx 22^{\text{h}5}$ and $A \geq 0.12$ mag; for Chaldaea, $P_{\text{syn}} = 10^{\text{h}}08 \pm 0^{\text{m}}02$ and $A = 0^{\text{m}}17 \pm 0^{\text{m}}01$. The $B-V$ and $U-B$ color indices of the three asteroids are, respectively: $0^{\text{m}}71 \pm 0^{\text{m}}02$ and $0^{\text{m}}31 \pm 0^{\text{m}}02$, $0^{\text{m}}72 \pm 0^{\text{m}}02$ and $0^{\text{m}}32 \pm 0^{\text{m}}03$, $0^{\text{m}}71 \pm 0^{\text{m}}01$ and $0^{\text{m}}34 \pm 0^{\text{m}}02$. Their values are in a good agreement with those given in Bowell *et al.* (1979). Finally for 156 Xanthippe we deduced a high value of the phase coefficient $\beta_V = (0.047 \pm 0.002)$ mag/degree, leading to an absolute magnitude, at maximum of light, of $V_0(1, 0) = (8.68 \pm 0.02)$ mag.

Debehogne, H., De Sanctis, G., and Zappala, V. (Observatoire Royal de Belgique, 3 Avenue Circulaire, 1180 Bruxelles, Belgique): 'Positions of Asteroids (1981)', *Astron. Astrophys.* **48**, 449-451 (1982)

244 positions of 11 asteroids were obtained from plates taken in 1981 by means of the GPA ($f = 4$ m, $D = 40$ cm) of the European Southern Observatory at La Silla (Chile). 5 new asteroids were also discovered. The reductions were made by dependences method using 5 or 6 reference stars.

Debehogne, H., Machado, L. E., Calderia, J. F., Vieira, G. G., and Netto, E. R. (Observatoire Royal de Belgique, Avaneue Circulaire, 3B-1180 Brussels, Belgium): 'Positions of the Minor Planets 102 Miriam, 1024 Hale and 1687 Glarona Obtained in May and June 1980 With the GPO, ESO, La Silla', *Astron. Astrophys. Suppl.* **47**, 463-465 (1982)

In May and June 1980 H. Debehogne and R. R. de Freitas Mourao observed Minor Planets at the ESO, La Silla, Chile. The GPO ($D = 40$ cm, $f = 4$ m) was used. All plates obtained were measured on the Ascorecord Zeiss, Jena, measuring machine of the Observatorio do Valongo (UFRJ). The positions were computed by means of dependences and least squares with the computer Burroughs 6700 of the Nucleo de Computacao Electronica (NCE) of the Universidade Federal do Rio de Janeiro. The reference stars, corrected for proper motions, are taken from SAO Stars Catalogue (equinox 1950.0). The Ephemeridi Malik Planet-1980 was also used.

Dermott, S. F. and Murray, C. D. (Center for Radiophysics and Space Research, Space Sciences Building, Cornell Univ., Ithaca, NY 14853): 'Asteroid Rotation Rates Depend on Diameter and Type', *Nature* **296**, 418-421 (1982)

The rotational frequency of main-belt asteroids is shown here to depend on both asteroidal type and diameter. If asteroids of any one diameter are considered, then, on average, M asteroids rotate faster than S asteroids which in turn rotate faster than C asteroids. This shows that asteroids which have been classified by their surface properties along have different bulk properties. For all three types, although the dispersions of the frequencies are large, we prove that the mean frequency increases linearly with the mean diameter. In both the C and S plots of mean rotational frequency against mean diameter there are discontinuities at diameters ~ 125 km and ~ 105 km, respectively, which may differentiate primordial asteroids from their collisional products.

Drake, M. J. (Dept. of Planetary Sciences, Univ. of Arizona, Tucson, AZ 85721): 'Igneous Rocks from Asteroids (and Mars?)', *Geotimes* 27(6), 27 (1982)

Drummond, J. D. (Physical Science Lab., New Mexico State Univ., Box 3-PSL, Las Cruces, NM 88003): 'Theoretical Meteor Radiants of Apollo, Amor, and Aten Asteroids', *Icarus* 49, 143-153 (1982)

A compilation of theoretical meteor radiants is presented for all numbered (through 2525) asteroids which approach the Earth's orbit to within 0.20 AU. On the basis of orbital similarity, asteroids associated with current meteor streams and Prairie Network fireballs are listed; plausible associations with medieval fireball radiants are also given. The best definite comet candidates in terms of meteoric evidence appear to be 2101 Adonis and 2201 1947XC. Asteroids which may be either extinct comets or perturbed main belt asteroids accompanied by collisional debris (represented by fireballs) are 1917 Cuyo, 2202 Pele, 2061 Anza, and 2340 Hathor. 1566 Icarus and 1981 Midas are the only asteroids whose orbits approach to less than 0.07 AU of the Earth's orbit, have a northern radiant, and still show no certain meteoric activity. The majority of Atens, Apollos, and Amors do not pass sufficiently close (< 0.07 AU) to the Earth's orbit for a reasonable expectation of meteoric activity, or have radiants south of -20° declination, requiring southern hemisphere observations.

Duncombe, R. L. and Hemenway, P. D. (Dept. of Aerospace Engineering/Engineering Mechanics, Univ. of Texas, Austin, TX 78712): 'A Comparison of Astrometric Measurement Techniques as Applied to Minor Planets', *Celest. Mech.* 26, 207-212 (1982)

Differential and absolute minor planet positions previously applied to the study of a Fundamental Reference System have had accuracies of the order of $\pm 2''$. Relative positions have been obtained to much higher accuracy, but that accuracy has not been applied directly to the formation of a celestial coordinate system. The regular motions of minor planets along long arcs in the sky are more accurately known than any single observed position. Thus, the dynamics of minor planets, coupled with new techniques of observation and reduction, will bring an independent component to bear on the problem of testing the Fundamental Reference System. Preliminary results based on measurements of Hypatia (238) are presented.

Fabré, R.: 'Roid Fever', *Astronomy* 10(8), 48-50 (1982)

Basic instructions for asteroid observations are given.

Gradie, J. and Tedesco, E. (Lab. for Planetary Studies, Cornell Univ., Ithaca, NY 14853): 'Compositional Structure of the Asteroid Belt', *Science* 216, 1405-1407 (1982)

The distribution of compositional types among the asteroids is found to vary systematically with heliocentric distance. Seven distinct peaks in the relative proportion of the compositional types E, R, S, M, F, C, P, and D are found from 1.8 to 5.2 astronomical units. The inferred composition of the asteroids in each semimajor axis region is consistent with the theory that the asteroids accreted from the solar nebula at or near their present locations.

Jurgens, R. F. (Communications Systems Research Section, Jet Propulsion Lab., 4800 Oak Grove Drive, Pasadena, CA 91109): 'Radar Backscattering From a Rough Rotating Triaxial Ellipsoid with Applications to the Geodesy of Small Asteroids', *Icarus* 49, 97-108 (1982)

Radar geodesy of the asteroid 433 Eros was reported by R. F. Jurgens and R. M. Goldstein. Their measurements were based on the spectral properties of a rough rotating triaxial ellipsoid. This paper presents the theory by which theoretical spectra based on a backscattering model of the form $\cos^n \theta$, or any reasonable backscattering model, can be computed. Some general properties of these spectra are demonstrated, and simple measurements of the apparent radar cross-section, center frequency, and effective bandwidth as a function of time are shown to be useful in determining the sizes of the semi-major axes, the exponent n in the scattering model, the backscatter efficiency of the surface material, the rotation period, and the declination of the observer above or below the rotation equator. Some of these parameters are correlated, and multiple estimation may be difficult unless the observations span a period sufficiently long so as to present a wide range of declinations to the observer. However, the departure from a spherical shape aids in separating the scattering properties from the target dimensions and facilitates the simultaneous estimation of all free parameters.

Lagerkvist, C. -I. (Astronomiska Observatoriet, Box 515, 751 20 Uppsala, Sweden): 'Studies of Small Asteroids. II. Positions of Asteroids Obtained During 1980 With the ESO Schmidt Telescope', *Astron. Astrophys. Suppl.* **47**, 513-521 (1982)

Positions of asteroids, mostly faint unnumbered ones, obtained during March 1980 with the ESO Schmidt telescope are presented.

Lagerkvist, C. -I. and Rickman, H. (Astronomiska Observatoriet, Uppsala, Sweden): 'Physical Studies of Asteroids IX: The Light Curve of the M Asteroid 77 Frigga', *The Moon and the Planets* **27**, 107-110 (1982)

The results of photoelectric *UBV* observations of asteroid 77 Frigga during the 1982 opposition are presented. From eight nights of observations at phase angles smaller than $2^\circ 8'$ a synodic period of $0^d 3755 \pm 0^d 0006$ is derived. The light curve appears very symmetric with two maxima per period and an amplitude of $0^m 19$. The primary maximum corresponds to $V(\alpha^\circ) = 8^m 58$, and the colour indices are: $B-V = 0^m 738 \pm 0^m 003$ and $U-B = 0^m 200 \pm 0^m 002$.

Pettersson, B., Hahn, G., and Lagerkvist, C. -I. (Astronomiska Observatoriet, Box 515, 751 20 Uppsala, Sweden): 'Positions of Asteroids Obtained During 1976-1979 With the Uppsala Astrograph and With the Kvistaberg Schmidt Telescope', *Astron. Astrophys. Suppl.* **47**, 533-534 (1982)

Precise positions are presented for 36 asteroids observed during 1976-1979 with the 20 cm astrograph at the Uppsala Observatory and with the 1 m Schmidt telescope at the Kvistaberg Station.

Schober, H. J. (Institut für Astronomie, Universitätsplatz 5, A-8010 Graz, Austria): 'A Revised Rotation Period for the Asteroid 164 Eva', *Astron. Astrophys.* **48**, 57-62 (1982)

The asteroid 164 Eva was observed photoelectrically at CTIO, Chile, during its September 1979 opposition. A new rotation period of $P = 13^h 66 \pm 0^h 01$ ($= 0^d 569 \pm 0^d 001$) was derived with a completely observed double wave lightcurve and a maximum light variation of $\Delta m = 0^m 36$. This is exactly half of the period obtained by Schober *et al.* with $P = 27^h 32?$ and $\Delta m \geq 0^m 07$ from earlier observations in 1975, when a more pole-on view to the rotational pole of 164 Eva was evident.

Using a phase coefficient of 0.039 mag/deg absolute magnitudes $\bar{V}(1, 0) = 9.06$ and $V_0(1, 0) = 8.88$ were computed; the colors $B-V = 0.69$ and $U-B = 0.35$ are in agreement with those listed in Bowell *et al.*

Schober, H. J. (Institut für Astronomie, Universitätsplatz 5, A-8010 Graz, Austria): 'Quadruple Extrema in the Complex Lightcurve of the Asteroid 37 Fides?', *Astron. Astrophys.* **105**, 419-421 (1982)

The asteroid 37 Fides was reobserved at ESO in Aug. 1979 and a period of rotation $P = 14^h 66 \pm 0^h 03$ ($0^d 611 \pm 0^d 001$) was deduced, which rules out the published value of $P = 4^h 0?$ by Scaltriti and Zapala. The lightcurve amplitude is now $0^m 16$. The new period is also supported by recent observations reported from Scaltriti and Zapala and Harris. As no fit for the lightcurve with $P = 7^h 33$ was

possible, 37 Fides shows a complicated lightcurve with four distinct and different maxima and four minima, which is unique among the asteroids until now. There is also some evidence that the period could be longer and the lightcurve even more complex than presented now.

Absolute magnitudes $\bar{V}(1, 0) = 7.42$ and $V_0(1, 0) = 7.36$ were derived, the colors are $B-V = 0.84$ and $U-B = 0.40$ with no variation during all rotational phases exceeding the scatter of 0.02.

Schober, H. J. and Schroll, A. (Institut für Astronomie, Universitätsplatz 5, A-8010 Graz, Austria): 'The Asteroids 36 Atalante and 48 Doris: Rotation, URV-Photometry, and Lightcurves, *Astron. Astrophys.* **107**, 402-405 (1982)

The asteroids 36 Atalante and 48 Doris were observed during their opposition in 1978, using the ESO-0.5 m telescope at the European Souther Observatory, Chile. Both asteroids were investigated in the same season by Harris and Young.

For 36 Atalante a period of rotation was derived with $P = 9^{\text{h}}93 \pm 0^{\text{h}}01$ ($0^{\text{d}}4137 \pm 0^{\text{d}}0005$). The maximum amplitude of the double mode lightcurve was found to be $0^{\text{m}}15$. Frequent color measurements in UBV do not show any variation during the rotation, exceeding the scatter; mean colors are $B-V = 0.70 \pm 0.01$ and $U-B = 0.37 \pm 0.01$.

48 Doris shows a rotation rate of $P = 11^{\text{h}}900 \pm 0^{\text{h}}005$ ($0^{\text{d}}4958 \pm 0^{\text{d}}0002$). Considering observations by Harris and Young we state a double mode lightcurve, too, with a maximum amplitude of at least $0^{\text{m}}30$. The lightcurve is not completely covered by observation. For 48 Doris a color variation on its surface is indicated in $B-V$, the side causing the secondary extreme being at about $0^{\text{m}}02$ redder than that causing the primary ones; mean colors are $B-V = 0.71 \pm 0.01$ and $U-B = 0.45 \pm 0.02$.

Absolute magnitudes were computed for both asteroids using the mean phase coefficient $\varphi = 0.39$ mag/deg and considering that 48 Doris was observed at small phase angles.

Soderhjelm, S. and Lindegren, L. (Lund Observatory, Box 1107, S-221 04 Lund, Sweden): 'Inertial Frame Determination using Minor Planets. A Simulation of HIPPARCOS - Observations', *Astron. Astrophys.* **110**, 156-162 (1982)

The space astrometry project HIPPARCOS will measure positions, proper motions, and parallaxes for about 100 000 stars to an accuracy of a few milliarcsec (mas). One way to define an inertial reference system is by observing minor planets, some 50 of which are bright enough to be observed by HIPPARCOS. Such observations, about 20 per year and planet, were simulated for the 4-year interval 1987-90. Each observation, with mean error 10-20 mas, gives a linear observation equation for corrections to the assumed orbital elements for the planet and the earth, and for the three components of a uniform rotation of the coordinate system. For N observed planets, a total of $6N + 9$ unknowns were determined by least squares. The most interesting parameters are those defining the ecliptical plane and the system rotation. The weight of their solution increases with the mission duration and (almost linearly with N). For a 2.5 year mission with 25 planets observed, the plane of the ecliptic is determined to within about 2 mas, and the absolute rotation of the coordinate system to about 1 mas yr^{-1} around axes in the ecliptic, 4 mas yr^{-1} around the perpendicular axis. An increase of the mission length to 3 years reduces these mean errors by about 25%. When at least 10 planets are observed, phase effects were found to cancel to a great extent, thus the non-sphericity of typical asteroids should not be a serious problem.

Soulié, G. (Observatoire de l'Université de Bordeaux I, 33270 Floirac, France): 'Positions of Minor Planets', *Astron. Astrophys. Suppl.* **47**, 611-613 (1982) (in French)

Bordeaux Observatory is sharing in photographic observations of asteroids, the purpose being to point out systematic errors in equatorial coordinates of stars. The asteroids belong to the Selected Minor Planets list. The rectilinear coordinates of both asteroids and reference stars are sent to the Leningrad Theoretical Astronomy Institute. We publish here the equatorial coordinates of the observed minor planets.

Taylor, D. B. (Royal Greenwich Observatory, Herstmonceux Castle, Hailsham, East Sussex, BN27 1RP, England): 'The Secular Motion of Pallas', *Monthly Notices Roy. Astron. Soc.* **199**, 255–265 (1982)

The secular motion of Pallas has been studied by numerically integrating the Lagrange planetary equations for 700 000 yr. Two terms with periods of approximately 15 000 yr and 190 000 yr dominate the secular elements. The former corresponds to a perturbation with argument 2ω and the latter to a perturbation with argument $\omega - \omega_J$, where ω and ω_J are the arguments of perihelion of Pallas and Jupiter respectively, defined with Jupiter's plane as the reference plane. In the 15 000 yr periodic term, which has the greater amplitude, the maximum value of the eccentricity and the minimum value of i , the inclination, occur when $\omega = 90^\circ$ and 270° and the minimum value of e and maximum value of i when $\omega = 0^\circ$ and 180° . This decreases the possibility of close approaches to Mars and Jupiter and increases the stability of the orbit. The inclination of Pallas at its minimum values over the 15 000 yr period shows remarkably little change at 28.2 ± 0.3 . Pallas is found to have a slow retrograde motion for the longitude of perihelion and this is unusual for asteroids. It circulates with a period of 544 600 yr.

A numerical integration over 100 000 yr showed that the perturbations arising from the 18:7 commensurability with Jupiter are not significant in the secular motion of Pallas.

Veeder, G. J., Matson, D. L., and Kowal, C. (Jet Propulsion Lab., California Inst. of Tech., Pasadena, CA 91109): 'Infrared (JHK) Photometry of Asteroids', *Astron. J.* **87**, 834–839 (1972)

We report *JHK* (1.2, 1.6, and 2.2 μ) photometry for several asteroids of various spectral types. All of the TRIAD asteroid classes were sampled. The C and S classes have distinct, infrared color domains. Most R-class asteroids fall within the S-color domain and the observed M asteroids fall within the C-color domain. The E asteroids have neutral colors. Asteroid 446 Aeternitas was discovered to have an unusual $-H$ color (0.88 mag).

Waldrop, M. M.: 'Operation Spacewatch', *Science* **216**, 42 (1982)

The development of a facility devoted to the search for asteroids crossing the Earth's orbit is reported.

Willis, J. and Goldstein, J. I. (Dept. of Metallurgy and Materials Engineering, Lehigh Univ., Bethlehem, PA 18015): 'The Effects of C, P, and S on Trace Element Partitioning During Solidification in Fe–Ni Alloys', Proceedings of the Thirteenth Lunar and Planetary Science Conference, Part 1, *J. Geophys. Res.* **87**, Suppl. A435–A445, November 15, 1982 (1982)

The effect of the minor elements P, S and C on the distribution coefficients of Ir, Ge, Ga, Au, Cu, and Cr between the solid and liquid phases in Fe–Ni alloys was measured experimentally. Distribution coefficients for Ir, Ga, and Au increase with increasing P content while the distribution coefficients for Ir, Ge, and Ni increase with increasing C and S contents. For Ge, the distribution coefficient exceeds 1.0 when the P or C content of the solid exceeds 0.4 or 0.9 wt% respectively, or the S content of the liquid exceeds 7 wt%. The measured distribution coefficients were used in a solidification model of a parent body core. The model assumes fractional crystallization in which the distribution coefficients vary with composition and predicts the trace element distributions in the major iron meteorite groups. The model correctly predicts the observed trends for P vs. Ni and Au vs. Ni in the iron meteorite groups considered. Although the calculated trends for Ir vs. Ni and for Ge vs. Ni are relatively satisfactory for groups IVA and IVB, they fail to produce the observed trends for groups IIAB and IIIAB. Interelement effects of S and C on the distribution coefficients may explain these inconsistencies.

Wisdom, J. (California Inst. of Tech., Pasadena, CA 91109): 'The Origin of the Kirkwood Gaps: A Mapping for Asteroidal Motion Near the 3/1 Commensurability', *Astron. J.* **87**, 577–593 (1982)

A mapping of the phase space onto itself with the same low-order resonance structure as the 3/1 commensurability in the planar-elliptic restricted three-body problem is derived. This mapping is approximately 1000 times faster than the usual method of numerically integrating the averaged equations of

motion (as used by Schubart, Froeschlé, and Scholl in their studies of the asteroid belt). This mapping exhibits some surprising behaviour that might provide a key to the origin of the Kirkwood gaps. A test asteroid placed in the gap may evolve for a million years with low eccentricity (< 0.05) and then suddenly jump to large eccentricity (> 0.3), becoming a Mars crosser. It is possible that the asteroid could then be removed by a close encounter with Mars. As a first test of this hypothesis a distribution of 300 test asteroids in the neighborhood of the 3/1 commensurability was evolved for two million years. When the Mars crossers are removed, the distribution of initial conditions displays a gap at the location of the 3/1 Kirkwood gap. While this is the first demonstration of the formation of a gap, the gap is too narrow. The planar-elliptic mapping is then extended to include the inclinations and the secular perturbations of Jupiter's orbit. The two-million-year evolution of the 300 test asteroids is repeated using the full mapping. The resulting gap is somewhat larger yet still too small. Finally the possibility that over longer times more asteroids will become Mars crossers is tested by studying the evolution of one test asteroid near the border of the gap for a much longer time. A jump in its eccentricity occurs after 18 million years, indicating that indeed it may simply be a matter of time for the full width of the gap to open.

Zappala, V., Lagerkvist, C. -I., and De Sanctis, G. (Osservatorio Astronomico di Torino, 10025 Pino Torinese, Italy): 'Positions of Asteroids Obtained During 1978', *Astron. Astrophys. Suppl.* **47**, 447-450 (1982)

Precise positions are presented for 78 asteroids observed during 1978 and the Uppsala Southern Station.

Zappala, V., Scaltriti, F., Lagerkvist, C. -I., Rickman, H., and Harris, A. W. (Osservatorio Astronomico di Torino, 10025 Pino Torinese, Torino, Italy): 'Photoelectric Photometry of Asteroids 33 Polyhymnia and 386 Siegena', *Icarus* **52**, 196-201 (1982)

Photometric parameters of the asteroids 33 Polyhymnia and 386 Siegena were obtained during an international campaign performed at three observatories: Table Mountain Observatory (A. W. Harris), European Southern Observatory (ESO; C. -I. Lagerkvist), and Catania Astrophysical Observatory (V. Zappala and F. Scaltriti). The photoelectric observations were carried out in the period August 15-September 14, 1980.

The rotational periods and amplitudes observed are: $P_{\text{syn}} = 9^{\text{h}}763 \pm 0^{\text{h}}002$, $\text{Ampl.} = 0^{\text{m}}11 \pm 0^{\text{m}}01$ for Siegena and $P_{\text{syn}} = 18^{\text{h}}601 \pm 0^{\text{h}}004$, $\text{Ampl.} = 0^{\text{m}}14 \pm 0^{\text{m}}01$ (near opposition) and $\text{Ampl.} = 0^{\text{m}}17 \pm 0^{\text{m}}01$ (at $\sim 10^\circ$ phase angle) for 33 Polyhymnia.

The multiple-scattering factor Q (as defined by K. Lumme and E. Bowell) is found to be 0.15 ± 0.06 for 386 and 0.26 ± 0.03 for 33, implying higher albedos in each case than expected according to their taxonomic classes, C and S, respectively.

The color indices $B-V$ and $U-B$, were measured and found to differ significantly from those given by Bowell *et al.* Our values are, for 386, $B-V = 0.71$ and $U-B = 0.36$; and for 33, $B-V = 0.81$ and $U-B = 0.39$.

2. Comets

Biermann, L., Giguere, P. T., and Huebner, W. F. (Los Alamos National Lab., NM 87545): 'A Model of a Comet Coma with Interstellar Molecules in the Nucleus', *Astron. Astrophys.* **108**, 221-226 (1982)

The coma of a comet is modeled assuming the icy nucleus contains interstellar molecules. This composition overcomes discrepancies between observation and earlier model predictions for CN, C_2 , C_3 , and NH_2 abundances. It is found that the abundances of CN, C_2 , and C_3 -bearing compounds in the nucleus must be constrained to trace amounts in order to account for the observed column densities. NH_3 also cannot be abundant by more than about 1%. The model gives good agreement with observed relative ranges of neutral species in the coma as well as with their observed relative intensity dependence on heliocentric distance. The size of the nucleus and the heliocentric ranges considered are relevant to comet Halley.

Bogart, R. S. and Noerdlinger, P. D. (NASA/Ames Research Center, Moffett Field, CA 94035): 'On the Distribution of Orbits Among Long-Period Comets', *Astron. J.* **87**, 911-917 (1982)

The distribution of the axes defining the planes and orientations of the orbits of 542 long-period comets are analyzed. The directions of the perihelia and of the oriented plane normals show significant nonuniformity in their distributions. The preferred direction of perihelia near the apex of solar motion is refined to an (1σ) error circle of $20^{\circ}6$, and possible concentrations of the plane normals and the directions of perihelion velocity along roughly orthogonal directions are noted, although the error circles extend to nearly full hemispheres. Planes of preference (and avoidance) are found from the distribution ellipsoids of the three orbital axes, with the perihelion directions lying preferentially along the galactic plane. The distribution ellipsoids of all three sets of orbital axes exhibit anisotropies roughly twice those expected for random distributions.

Buffoni, L., Manara, A., and Scardia, M. (Osservatorio Astronomico di Brera, Via Brera 28, I-20121 Milano, Italy): 'Halley's Comet: Energy and Perturbations', *Astron. Astrophys.* **108**, 141-142 (1982)

Mechanical energy and the planetary perturbations (always very weak) of Halley's comet are provided. In the next passage there will be a slight decrease in the mechanical energy of the comet with a corresponding decrease of the period. The main perturbation is that of Jupiter, except for two periods in which the greatest action will be exerted by Venus and by Earth.

Buti, B. (Physical Research Lab., Ahmedabad, India): 'Role of High Frequency Turbulence in Cometary Plasma Tails', *Astrophys. J.* **252**, L43-L47 (1982)

The problem of solar wind/cometary tail interaction is reinvestigated by appropriately accounting for the presence of the high frequency electrostatic turbulence observed in interplanetary space. The turbulence has a drastic stabilizing effect on the hydromagnetic waves and permits the wavy structure in the tail only beyond some critical distance from the head of the comet; this is completely in agreement with the observations.

Clube, S. V. M. and Napier, W. M. (Royal Observatory, Blackford Hill, Edinburgh, EH9 3HJ): 'Spiral Arms, Comets and Terrestrial Catastrophism', *Quarterly J. Roy. Astron. Soc.* **23**, 45-66 (1982)

We review a hypothesis of terrestrial catastrophism in which comets grow in molecular clouds and are captured by the Sun as it passes through the spiral arms of the Galaxy. Assuming that comets are a major supplier of the Earth-crossing (Apollo) asteroid population, the latter fluctuates correspondingly and leads to episodes of terrestrial bombardment. Changes in the rotational momentum of core and mantle, generated by impacts, lead to episodes of magnetic field reversal and tectonic activity, while surface phenomena lead to ice-ages and mass extinctions. An episodic geophysical history with an interstellar connection is thus implied. If comets in spiral arms are necessary intermediaries in the process of star formation, the theory also has implications relating to early solar system history and galactic chemistry. These aspects are briefly discussed with special reference to the nature of spiral arms.

Cochran, A. L., Cochran, W. D., and Barker, E. S. (McDonald Observatory, Univ. of Texas at Austin, TX 78712): 'Spectrophotometry of Comet Schwassmann-Wachmann I. II. Its Color and CO⁺ Emission', *Astrophys. J.* **254**, 816-822 (1982)

We obtained spectra of Comet Schwassmann-Wachmann I during the winter 1980-1981. On 1981 February 7 UT the comet was in outburst and had a one-armed spiral shape. On that night, spectra of the "nucleus" and of several locations along the arm were obtained. All of the spectra were reduced to relative reflectances. The quiescent state of the comet may be modeled, using Mie scattering theory, by a distribution of relatively large particles with a small variance in particle size. One of the positions observed during outburst showed a spectrum similar to the quiescent state, but the other positions required the addition of a distribution of smaller size particles. As the outburst progressed, more and more of the smaller particles were required. We see no evidence for the particles growing smaller by

sublimation as they move outward. The data may be fitted equally well by either H₂O or CO₂ ice particles.

Our data plus those of S. Larson and H. Spinrad, also show that the CO⁺ emission turns on or off on a rapid time scale. We have been able to eliminate the following mechanisms as being correlated with the CO⁺ or outburst activity: solar phase angle, rotational phase angle, comet–Sun distance, comet–Jupiter distance, and solar activity.

Clube, V. and Napier, B. (Royal Observatory, Edinburgh, UK): ‘Close Encounters With a Million Comets’, *New Scientist* **95**, 148–151 (1982)

Every few thousand years the Earth may have to buffet its way through streams of dust and meteors. The resulting explosion may account for many oddities in the fossil record – and in human history.

Covault, C.: ‘NASA to Study Diverting Satellite to Meet Comet’, *Aviation Week and Space Technology* **116**(12), 22–24 (1982)

Plans to divert the ISEE-3 spacecraft, so that it can intercept the Giacobini–Zinner comet in 1985, are reported.

Donn, B. (NASA/Goddard Space Flight Center, Lab. for Extraterrestrial Physics, Greenbelt, MD 20771): ‘Comets: Chemistry and Chemical Evolution’, *Journal of Molecular Evolution* **18**, 157–160 (1982)

Lasting commitment to cosmic chemistry and an awareness of the fascinating role of comets in that study was a consequence of an association with Harold Urey early in my astronomical career. Urey’s influence on cometary research spread as colleagues with whom I was associated, in turn, developed their own programs in cometary chemistry. One phase of the Chicago research shows that Whipple’s icy nucleus would be below about 250 K. This property, combined with their small internal pressure, means cometary interior remain essentially unchanged during their lifetime. Observations of cometary spectra indicate that they are rich in simple organic species. Experiments on comet-like ice mixture suggests that the extensive array of interstellar molecules also may be found in comets. The capture of cometary debris by the earth or the impact of comets would have been an early source of biochemically significant molecules. Recent hypotheses on radiogenic heating and melting of water ice in the central zone of nuclei do not seem consistent with recent observations or ideas of structure. Thus comets are not a likely place for life to develop.

Ershkovich, A. I. (Lab. for Astronomy and Solar Physics, NASA Goddard Space Flight Center, Greenbelt, MD 20771): ‘On the Folding Phenomenon of Comet Tail Rays’, *Monthly Notices Roy. Astron. Soc.* **198**, 297–302 (1982)

The folding phenomenon of the comet tail rays is shown to be compatible with the Ferraro isorotation law if the comet tail magnetic field has no azimuthal component: $B_\phi = 0$. Considering electric drift due to convective electric fields one obtains a formula for the angular rate of a ray closure which reduces to that of Ness and Donn if the velocity profile across the tail is linear. The magnetic field B of about 20–40 γ in the coma and $B \lesssim 10\gamma$ in the distant tail is estimated under typical solar wind conditions at 1 AU.

Ferrin, I. (Departamento de Física, Universidad de Los Andes, Merida, Venezuela, 5101): ‘On the Brightness of Halley’s Comet’, *Astron. Astrophys.* **107**, L7–L9 (1982)

Periodic comet Halley was not a “well behaved” comet photometrically in its apparition of 1910. Its light curve shows fluctuations of long and short duration that suggest that this comet has a surface with uneven distribution of volatiles. Moreover the comet shows a brightness decrease after perihelion and a sharp increase at 1.0 AU from the sun. Our reduction of the available data shows that this anomaly is significant, since four independent data sets show it. We give an explanation for it, in terms of a break up of the nucleus. As a by product, the influence of twilight on visual observations of this comet is derived. This will again be a troublesome effect, in the apparition of the comet in 1986.

Festou, M. C., Feldman, P. D., and Weaver, H. A. (Service d'Aeronomie de Centre National de la Recherche Scientifique, Verrières-le-Buisson, France): 'The Ultraviolet Bands of the CO_2^+ Ion in Comets', *Astrophys. J.* **256**, 331–338 (1982)

Eight comets have been studied with the *International Ultraviolet Explorer* spectrographs. The existence of the CO_2^+ ion in a comet is confirmed by the presence of the 2980 Å doublet in at least three of these objects. Spatial and spectral resolution obtained in comets Bradfield (1979 X) and Sargent (1978 XV) allow us to discuss the production mechanisms of this ion. The spectra show new ionic features in the 3100–3400 Å range, which are attributed to resonance fluorescence of the Fox–Duffenack–Barker system of the CO_2^+ ion and, near 3350 Å, to the OH^+ ion.

Formisano, V., Galeev, A. A., and Sagdeev, R. Z. (Space Science Dept. of ESA-Estec, Noordwijk, Netherlands): 'The Role of the Critical Ionization Velocity Phenomena in the Production of Inner Coma Cometary Plasma', *Planet. Space Sci.* **30**, 491–497 (1982)

The critical velocity triggering anomalous ionization of the neutral gas by plasma flow is calculated for the model based on the lower hybrid instability. It depends strongly on the plasma and gas parameters, defining the instability development of the ionized atoms beam in the counter-streaming plasma.

In particular, the possible role of the critical ionization mechanism for Halley's comet is examined. The fulfillment of both Townsend's condition for the self-sustained beam plasma discharge and Alfvén's condition for the critical velocity mechanism indicates that this mechanism may operate only within 10^4 km from the cometary nucleus and give an ion production rate close to that observed for Kohoutek's comet.

Goraya, P. S., Sinha, B. K., Chaubey, U. S., and Sanwal, B. B. (Uttar Pradesh State Observatory, Naini Tal, India): 'Spectrophotometry of Comet Bradfield (1980t) During Post-Perihelion Period', *The Moon and the Planets* **26**, 3–9 (1982)

Spectrum scans of the head of Comet Bradfield (1980t) covering the wavelength range $\lambda\lambda 365$ –640 nm were made on two nights when the heliocentric distance of the comet varied from 0.55 to 0.58 Au. The emission features of the CN band at $\lambda 388$ nm and Swan band sequence of C_2 at $\lambda 474$ nm, and $\lambda 563$ nm are identified and absolute fluxes in these bands as well as in the continuum are derived. The continuum energy distribution curves of the comet have been compared with those of the Sun and the star β Crv (G5 III). An estimate of the number of C_2 and CN molecules in the head of the comet has been made through the measured intensities of their respective bands lying in this region.

Hendrie, M. J.: 'The Return of Halley's Comet', *Spaceflight* **24**, 242–248 (1982)

In the past, comets were often considered as bringers of bad tidings, plague and misfortune. Even in this century some strange ideas about them and their possible influence on our lives and destiny have persisted.

Halley's Comet is accessible to scrutiny about every 75 years. No-one can hope to see it on more than two occasions, and some will not live long enough to see it even once. Between apparitions great advances have taken place in science and astronomy, so that each return yields not only fresh information but observations of a completely new kind. This will be especially so during the coming return in 1986.

Hills, J. G. (Theoretical Div., T-6, Los Alamos National Lab, NM 87545): 'The Formation of Comets by Radiation Pressure in the Outer Protosun', *Astron. J.* **87**, 906–910 (1982)

The pressure due to the radiation from the Sun and neighboring protostars may have forced the coagulation into comets of the dust grains in the collapsing layers of the protosun at $r = (1 - 5) \times 10^3$ AU. The grains were forced together by their self-shielding, which results in the radiation pressure due to photons coming from the direction of strong concentrations of dust being less than the pressure due to photons coming from a direction having a low concentration of dust. This causes the dust to drift toward regions of already strong dust concentration. The formation of comets under these

conditions is consistent with the low rotation period of new comets and their extremely volatile chemical constituents.

Hughes, D. W. (Dept. of Physics, The University, Sheffield, S3 7RH, UK): 'Finding Comets', *J. Brit. Astron. Assoc.* **92**, 61-65 (1982)

This paper investigates the statistics of cometary discovery and concludes that the discovery rate is increasing, not because more comets are coming close to the Earth, or because more people are actively seeking comets as time passes, but simply because more and more faint comets are being found. At this present time about 45 comets are being discovered per decade, there being about four long-period comets found for every short period one. If it were possible to discover all comets brighter than 11th magnitude, the discovery rate would be about 290 per decade. Change the limit to 16^m and the rate goes up to 8700.

Hughes, D. W.: 'The Recovery of Halley's Comet', *Nature* **300**, 318 (1982)

The recovery of Halley's comet on 16 October 1982 with the Hale telescope of Palomar observatory is reported.

Jackson, W. M., Halpern, J. B., Feldman, P. D., and Rahe, J. (Dept. of Chemistry, Howard Univ., Washington, DC 20059): 'Production of CS and S in Comet Bradfield (1979 X)', *Astron. Astrophys.* **107**, 385-389 (1982)

High and low resolution ultraviolet spectra of carbon monosulfide (CS) in Comet Bradfield (1979 X) were obtained with the IUE satellite. The high resolution rotational profile of the (0, 0) band at 257.5 nm can be fitted with a theoretical profile derived assuming a Boltzmann temperature of 70 K. Spatial plots of the low resolution data for both S and CS show that these emissions are concentrated toward the cometary nucleus. The results that have been obtained are consistent with a Haser model for CS and S where the parent molecule is CS_2 . A very rapid variation of CS brightness with heliocentric distance is found.

Kamoun, P. G., Campbell, D. B., Ostro, S. J., Pettengill, G. H., and Shapiro, I. I. (Dept. of Earth and Planetary Sciences, MIT, (Cambridge, MA 02139): 'Comet Encke: Radar Detection of Nucleus', *Science* **216**, 293-295 (1982)

The nucleus of the periodic comet Encke was detected in November 1980 with the Arecibo Observatory's radar system (wavelength, 12.6 centimeters). The echoes in the one sense of circular polarization received imply a radar cross section of 1.1 ± 1.07 square kilometers. The estimated bandwidth of these echoes combined with an estimate of the rotation vector of Encke yields a radius for the nucleus of $1.5^{+2.3}_{-1.0}$ kilometers. The uncertainties given are dependent primarily on the range of models considered for the comet and for the manner in which its nucleus backscatters radio waves. Should this range prove inadequate, the true value of the radius of the nucleus might lie outside the limits given.

Krishan, V. and Sivaraman, K. R. (Indian Inst. of Astrophysics, Bangalore, India): 'Peculiarities in the Ionic Tail of Comet Ikeya-Seki', *The Moon and the Planets* **26**, 209-215 (1982)

Direct photographs of Comet Ikeya-Seki obtained on four consecutive days from October 29 to November 1, 1965, are used for an analysis of the multiple helical structures in the ionised tail. The formation of these structures is explained on the basis of plasma instabilities excited in the tail containing twisted magnetic fields. The growth rate of the modes excited at the mode rational surface agrees well with the observed results. This model also accounts for the presence of harmonic structures seen in the tail of the comet.

Marconi, M. L. and Mendis, D. A. (Center for Astrophysics and Space Science, Univ. of California, San Diego, La Jolla, CA 92093): 'The Photochemistry and Dynamics of a Dusty Cometary Atmosphere', *The Moon and the Planets* **27**, 27-46 (1982)

A self-consistent solution of the dynamical and thermal structure of an H_2O -dominated, two-phase, dusty-gas cometary atmosphere has been obtained by solving the simultaneous set of differential equations representing conservation of number density, momentum and energy together with the transfer of solar radiation in the streams responsible for the major photolytic processes and the heating of the nucleus. The validity of the model is restricted to the collision-dominated region where all the gas species are assumed to attain a common velocity and common temperature. Two models are considered for the transfer of solar radiation through the circum-nuclear dust halo. In the first only the direct extinction by the dust is considered. In the second, the finding of some recent models, that the diffuse radiation field due to multiple scattering by the dust halo more or less compensates for radiation removed by direct absorption when the optical depth is near unity, is approximated by neglecting the attenuation of the radiation by the dust altogether.

As has been shown earlier, the presence of dust results in a transonic solution, and it is obtained by a two-step iterative procedure which makes use of the asymptotic behaviour of the radiation fields sufficiently far from the nucleus and a regularity condition at the sonic point.

The calculations were performed for a medium sized comet ($R_n = 2.5$ km) having a dust to gas production rate ratio of unity, at a heliocentric distance of 1 AU. The dust grains were assumed to be of the same radius (1μ), of low density ($\rho \approx 1 \text{ g cm}^{-3}$) and be strongly absorbing (having the optical properties of magnetite).

The main effect of the dust on the cometary atmosphere is dynamic. While the dust-gas coupling persists to about $20R_n$, the strong 'throat effect' of the dust friction on the gas causes the latter to go supersonic quite rapidly. Consequently the sub-sonic region around the nucleus is very thin, varying between 45 and 85 m in the two models considered. On the other hand, while this highly absorbing dust has a temperature substantially above that of the gas in the inner coma, heat exchange between them does not significantly change the temperature profile of the gas. This is because of the predominance of the expansion cooling, and even more importantly, the IR-cooling by H_2O , in the inner coma. Consequently, the gas temperature goes through a strong inversion, as in the dust-free case, achieving a temperature as low as about 6 K within about 50 km of the nucleus, before increasing to about 700 K at $r = 10^4$ km, due to the high efficiency of photolytic heating over the cooling process in the outer coma. The Mach number achieves a maximum value of about 10 at the distance of the temperature minimum, thereafter steadily decreasing to a value of about 2.5 at $r \approx 10^4$ km.

It is shown that while the dust attenuation has a strong effect on the production rate of H_2O , it also has an interesting effect on the electron density profile. It increases the electron density in the inner coma over the unattenuated case, while at the same time, decreasing it in the outer coma. In conclusion, the limitations of the present model and the necessity to extend it using a multi-fluid approach are discussed.

Michels, D. J., Sheeley, N. R. Jr., Howard, R. A., and Koomen, M. J. (E. O. Hulburt Center for Space Research, Naval Research Lab., Washington, DC 20375): 'Observations of a Comet on Collision Course With the Sun', *Science* **215**, 1097-1102 (1982)

A brilliant new comet (1979 XI: Howard-Koomen-Michels) was discovered in data from the Naval Research Laboratory's orbiting SOLWIND coronagraph. An extensive sequence of pictures, tele-metered from the P78-1 satellite, shows the coma, accompanied by a bright and well-developed tail, passing through the coronagraph's field of view at a few million kilometers from the sun. Preliminary orbital calculations based on the observed motion of the comet's head and morphology of the tail indicate that this previously unreported object is a sungrazing comet and may be one of the group of Kreutz sungrazers. It appears from the data that the perihelion distance was less than 1 solar radius, so that the cometary nucleus encountered dense regions of the sun's atmosphere, was completely vaporized, and did not reappear after the time of closest approach to the Sun. After this time, however, cometary debris, scattered into the ambient solar wind, caused a brightening of the corona over one solar hemisphere and to heliocentric distances of 5 to 10 solar radii.

Morris, C. S. and Green, D. W. E. (Prospect Hill Observatory, Harvard, MA 01451): 'The Light Curve of Periodic Comet Halley 1910 II', *Astron. J.* **87**, 918-923 (1982)

Photometric parameters for periodic comet Halley 1910II have been derived from 144 total visual magnitude estimates. The pre-perihelion data are best represented by an absolute magnitude of 5.47 and a power-law exponent of 4.44; post-perihelion results show that the absolute magnitude brightened to 4.94, and the exponent decreased to 3.07. Only small fluctuations in brightness about the power-law solutions are noted. Based on these results, a forecast of the visual brightness of periodic comet Halley's 1985-1987 apparition is presented.

Mumma, M. J. (NASA/Goddard Space Flight Center, Greenbelt, MD 20771): 'Speculations on the Infrared Molecular Spectra of Comets', In *Vibrational-Rotational Spectroscopy for Planetary Atmosphere - Volume II*, NASA CP-2223, Report No. 82B0303. April 1982. Pp. 714-744 (1982)

No infrared vibration-rotation spectra have yet been seen for any comet, even though molecular emission features in the ultraviolet and visual regions are common, and gaseous matter is the dominant constituent of the coma. This is in part due to instrumental and atmospheric limitations, but also because non-LTE conditions prevail nearly everywhere throughout the coma and tails, leading to unusual spectra. Non-LTE calculations have been applied to ultraviolet (e.g., OH) and to visual (e.g., CN) bands of comets where solar pumping and radiative decay are the dominant excitation and relaxation processes. However, similar attempts to predict the infrared molecular spectra of comets have not been made. Previous talks at this workshop have addressed stable planetary atmospheres, principally those regions where collisional rates are sufficiently high to ensure local thermodynamic equilibrium (LTE). Comets however are radically different, and might be classed as giant planetary exospheres. I will consider certain aspects of cometary physics and non-LTE spectroscopy, and attempt to predict some aspects of the infrared signatures of cometary molecules.

Murty, P. S. (Indian Inst. of Astrophysics, Kodaikana, India): 'CO in the IUE Spectrum of Comet Bradfield (1979L)', *The Moon and the Planets* **26**, 101-104 (1982)

New identifications are reported of the fourth positive bands and Cameron bands of CO in the IUE satellite spectrum of Comet Bradfield (1979L). Although the predicted band intensities as well as the band identifications in Comet West (1976 VI) support the proposed assignments. VUV cometary spectra of higher resolution are necessary for confirmation.

Napier, W. M. and Staniucha, M. (Royal Observatory, Blackford Hill, Edinburgh EH9 3HJ, Scotland): 'Interstellar Planetesimals - I. Dissipation of a Primordial Cloud of Comets by Tidal Encounters With Massive Nebulae', *Monthly Notices Roy. Astron. Soc.* **198**, 723-735 (1982)

The Oort cometary cloud is subject to tidal disruption during close encounters with massive nebulae. The process is studied by numerical integration of $\sim 33\,000$ comet orbits, using realistic models of the Oort cloud and the interstellar medium. It is found that the cloud is rapidly cleared of long period comets, and it is concluded that such comets are probably interstellar in origin. A capture event or tidal disturbance may have taken place \lesssim a few 10^7 yr ago.

Parkinson, R. C.: 'Prospects for Interplanetary Exploration', *Spaceflight* **24**, 98-102 (1982)

A personal speculation on some of the proposals and some of the possibilities for future planetary missions are presented.

Podgorny, I. M., Dubinin, E. M., and Israelevich, P. L. (Space Research Inst., USSR Academy of Sciences, Moscow, USSR): 'The Estimates of the Magnetic Field in Halley's Comet', *The Moon and the Planets* **27**, 135-138 (1982)

The estimates of the magnetic field in the Halley's comet tail based on the observed acceleration of the matter and the pressure balance are discussed.

Reddy, F.: 'Backtracking the Comets', *Astronomy* **10**(8), 6-17 (1982)

A simple review on the nature of comets is presented.

Sekanina, Z. (Jet Propulsion Lab., California Int. of Tech., Pasadena, CA 91109): 'Comet Bowell (1980B): An Active-Looking Dormant Object?', *Astron. J.* **87**, 161–169 (1982)

It is argued that solid particles in the coma and tail of the distant Comet Bowell are not recent ejecta and that the comet has probably been dormant. These conclusions are extensively documented by the circumstantial evidence which, as of early 1981, includes; the absence of molecular emissions in the spectrum of the comet; a nearly constant amount of dust in the coma, suggested by the photometric data; a slow expansion rate of the coma and implied low particle velocities, inconsistent with the theory of dust ejection instigated by expanding gas; a tail width that does not increase with increasing distance from the nucleus, also in defiance of the ejection theory; the absence in the tail of all particles $\lesssim 0.5$ mm in diameter, the dominant component of ejecta in comets at small heliocentric distances; and the development of an elongated coma that appears to be a signature of the comet's angular momentum. It is speculated that an estimated mass of more than 10^{13} g of particles observed in the coma and tail of the comet is either a leftover pristine material that has never been in contact with the nucleus surface or a product of the comet's erratic activity associated with its chemical instability at temperatures below ~ 40 K that could be stimulated by cosmic ray and/or ultraviolet light irradiation of the surface layer during the comet's long stay in the Oort cloud. Predicted variations with time in the apparent coma diameter and in the projected direction of its elongation are based on a model of continuous escape of particles from the comet's gravity field due to the Sun's gravitational perturbations, effected at heliocentric distances less than ~ 12 AU on the incoming leg of the orbit. As a by-product, the position of the spin axis of Comet Bowell – the first among "new" comets – is determined. It is not ruled out that the comet may temporarily become active near perihelion.

Singh, P. D. (Dept. of Astronomy, Inst. of Astronomy and Geophysics, Univ. of Sao Paulo, Brazil): 'Tentative Identification of CS^+ in Comets', *Astron. Astrophys.* **108**, 369–372 (1982).

Energetic solar photons and solar-wind protons may lead to the formation of the CS^+ ions in comets, respectively $\text{CS} + h\nu \rightarrow \text{CS}^+ + e^-$, and by the charge-transfer process: $\text{H}^+ + \text{CS} \rightarrow \text{CS}^+ + \text{H}$. Weak discrete emission features in $\lambda\lambda 2400\text{--}2800$ wavelength range observed in several comets are tentatively assigned as due to electronic bands of $\text{CS}^+(\text{B}^2\Sigma^+ - \text{X}^2\Sigma^+)$ system. Using the recently determined lifetime of the CS^+ molecule in the $\text{B}^2\Sigma^+$ ($v' = 0$) state, absolute transition probabilities and oscillator strengths for the electronic bands of the $\text{CS}^+(\text{B}^2\Sigma^+ - \text{X}^2\Sigma^+)$ and the $\text{CS}^+(\text{B}^2\Sigma^+ - \text{A}^2\Pi_i)$ systems are obtained.

Smoluchowski, R. (Dept of Astronomy and Physics, Univ. of Texas, Austin, TX 78712): 'Heat Transport in Porous Cometary Nuclei', Proceedings of the Thirteenth Lunar and Planetary Science Conference, Part 1, *J. Geophys. Res.* **87**, Suppl. A422–A424, November 15, 1982 (1982)

Heat transport in cometary nuclei is important because it leads to the formation of larger tails and comae after perihelia than before, to early outbursts caused by phase transitions, and to fragmentation. The role of gases in pores in icy (H_2O and $\text{H}_2\text{O} + \text{CO}_2$) nuclei in the heat transport has been investigated in the viscous and Knudsen diffusion regions. It appears that in pure H_2O -ices the heat flow is affected by the presence of pores but is affected only very close to the perihelion by water vapor contained in them. On the other hand, the presence of CO_2 vapor in the pores significantly increases the heat flow in mixed nuclei at temperatures above 140–150 K. Thus for heliocentric distances between 3 and 5 AU, the above mentioned phenomena should be considerably enhanced in proportion to the admixture of CO_2 ices. The overlap and channel formation by pores in nuclei with high porosities is discussed.

Valtonen, M. J. and Innanen, K. A. (Dept. of Physical Sciences, Turku Univ. Observatory, Univ. of Turku, Turku, Finland): 'The Capture of Interstellar Comets', *Astrophys. J.* **255**, 307–315 (1982)

A large number of numerical orbit integrations of particles interacting with the Sun–Jupiter system have been performed in order to derive for the first time, empirical, velocity-dependent expressions for the capture cross section of the system. By integrating these with appropriate velocity distribution functions, bounds can be set on whether comets can be of interstellar origin. These indicate that a

significant accumulation of interstellar comets into an "Oort cloud" could occur only with a prolonged transit of the solar system through a relatively large, dense cloud of interstellar debris (comets) having a mean internal velocity dispersion of $\sim 1.0 \text{ km s}^{-1}$ and at a relative velocity not exceeding 0.5 km s^{-1} . At these levels, a significant antisymmetry of cometary aphelia in the direction of the relative solar motion is also to be expected. Finally, it is pointed out that suitable binary stars must be exceedingly efficient traps for both protostellar and interstellar debris.

Waldrop, M. M.: 'In Quest of Comet Halley', *Science* **216**, 606 (1982)

Efforts - unsuccessful so far - at Kitt Peak for an early observation of the Halley comet, are reported.

Yamamoto, T. (Inst. of Space and Astronautical Science, Meguro-Ku, Tokyo 153, Japan): 'Evaluation of Infrared Line Emission from Constituent Molecules of Cometary Nuclei', *Astron. Astrophys.* **109**, 326-330 (1982)

Infrared fluxes of the line emission from candidate constituent molecules of a cometary nucleus are estimated for future observations with evaluations of other infrared sources such as zodiacal light, thermal emission of the nucleus, and infrared continuum from dust in a coma. It is shown that there are many detectable emission lines in the near infrared. Of these, the emissions from H_2O , CO , CO_2 , CH_4 , and OH are particularly remarkable, from which the fluxes larger than $10^{-17} \text{ W cm}^{-2}$ are expected for a comet having a standard gas production rate of $1 \times 10^{29} \text{ H}_2\text{O s}^{-1}$ at $R = \Delta = 1 \text{ AU}$, where R is heliocentric distance, and Δ is comet-observer distance. Some observational items interesting in cometary physics are presented.

3. Meteorites

Armstrong, J. T., Meeker, G. P., Huneke, J. C., and Wasserburg, G. J. (Lunatic Asylum, Div. of Geological and Planetary Science, California Inst. of Tech., Pasadena, CA 91125): 'The Blue Angel: I. The Mineralogy and Petrogenesis of a Hibonite Inclusion From the Murchison Meteorite', *Geochim. Cosmochim. Acta* **46**, 575-595 (1982)

A detailed mineralogic, chemical, and petrologic study of the Blue Angel, a relatively large ($\sim 1.5 \text{ mm}$) hibonite-containing inclusion from the Murchison meteorite, was performed in an attempt to understand the mechanisms of formation and modification of hibonite-rich inclusions. The Blue Angel inclusion is composed of roughly equal amounts of hibonite and calcite, with minor amounts of spinel, perovskite, diopside, and an Fe-rich silicate. The inclusion can be divided into three roughly concentric zones - a hibonite-rich core, a calcite-rich mantle, and a spinel-rich layered rim. The mineral chemistry and petrography of the Blue Angel are consistent with a three-stage formation history: (a) an early stage of nebular condensation which produced the hibonite, perovskite, and spinel; (2) a moderate temperature stage of aqueous alteration and metamorphism occurring on a small planetary body containing CO_2 and H_2O during which calcite was formed in the inclusion; and (3) the final emplacement of the Blue Angel into its present position in Murchison. The study of the Blue Angel indicates that extensive alteration of Ca-Al rich inclusions (CAI) may have occurred by aqueous alteration and thermal metamorphism followed by explosive mixing processes on a parent body. Such metamorphic reactions may involve formation and destruction of phases, such as melilite and diopside, which have been previously thought to be primary condensates. The mechanisms proposed for the formation and modification of the Blue Angel help to explain the secondary phases and oxygen isotope anomalies found in many CAI and eliminate the need for invoking kinetically-complicated back-reactions at very low pressures with a cool part of the solar nebula. The contribution of planetary metamorphism in the formation and alteration of CAI must be considered along with the nebular processes in order to understand the formation of carbonaceous chondrites.

Ashwal, L. D., Warner, J. L., and Wood, C. A. (Lunar and Planetary Inst., 3303 NASA Road 1, Houston, TX 77058): 'SNC Meteorites: Evidence Against an Asteroidal Origin', Proceedings of the Thirteenth Lunar and Planetary Science Conference, Part 1, *J. Geophys. Res.* **87**, Suppl. A393-A400, November 15, 1982 (1982)

The 1.3 b.y. crystallization ages and other features of the nine SNC meteorites (shergottites, nakhlites, and chassignites) distinguish them from all other meteorites which apparently formed more than 3 b.y. earlier. Proposed models for the origin of the young SNC meteorites include internal melting, either within a large planet such as Mars or within a large asteroid, and impact melting on one or more asteroids. Although an asteroidal source is dynamically more reasonable, we discuss petrologic, geochemical, and isotropic observations that strongly argue against an asteroidal origin for SNC meteorites, either as impact melts or as endogenically derived melts. Cumulate textures, as displayed by the SNC meteorites, have never been observed in terrestrial or lunar impact melts. Even the largest impact melt sheets cooled relatively quickly by thorough mixing with cool clastic debris, and the resulting rocks show obvious lithic and/or mineral clasts derived from the target materials. No clasts or remnants of clasts are present in SNC meteorites. The chemical and isotopic homogeneity of impact melt rocks is not displayed by SNC meteorites. Differences in initial $^{87}\text{Sr}/^{86}\text{Sr}$ among some of the shergottites, which are otherwise chemically similar, preclude an origin in the same impact melt sheet. These relationships indicate that the SNC meteorites did not form within an impact melt sheet, either on an asteroid or anywhere else. Instead, their parental magmas probably formed by internal melting within their parent body. Although thermal models of large asteroids (> 800 km diameter) can be devised to allow endogenic melting as young as 1.5 b.y. ago, isotopic and geochemical data for SNC meteorites preclude them from having formed in this way. Specifically, the isotopic signature of the ancient (~ 4.6 b.y.) large-scale heating event which established the shergottite sources is inconsistent with such asteroidal thermal models which require cold accretion of materials with initially low thermal conductivities. The thermal models further require that the young melts were restricted to the asteroid's core; total fragmentation of such asteroids would be required to liberate these rocks into Earth-crossing orbits. Destruction of an 800 km asteroid would have produced an immense swarm of asteroids with similar orbits. No Hiryama family with sufficient mass has been identified in the asteroidal belt. If retention of residual garnet in the shergottite sources is a requirement, as indicated by geochemical modeling, this would directly imply a parent body larger than the largest asteroid (Ceres, diameter = 1020 km). A planet-sized parent body such as Mars still remains the most likely candidate for the SNC meteorites.

Axon, H. J. and Grokhovsky, V. J. (Metallurgy Dept., Univ. of Manchester, UK): 'Discontinuous Precipitation Reaction in the Metal of Richardton Chondrite', *Nature* **296**, 835–836 (1982)

A metallographic and microprobe study was conducted on the H5 chondritic meteorite Richardton, using material that was free of terrestrial corrosion and ablation heating effects. Our observations indicate that initially well annealed and slowly cooled metal experienced an incomplete episode of discontinuous precipitation in the temperature range 350–400°C, perhaps after mild deformation at some of the metal-silicate interfaces. There were no indications of externally imposed deformation after the 350°C episode. The mechanism of discontinuous precipitation rather than plane interface growth has implications for the rate of formation of the metallographic structures, and the apparent temperature of this final heat treatment has implications for proposed reheating events identified by isotopic measurements of the silicate minerals that accompany the metal in this meteorite.

Berkley, J. L. and Jone, J. H. (Lunar and Planetary Lab., Univ. of Arizona, Tucson, AZ 85721): 'Primary Igneous Carbon in Ureilites: Petrological Implications', Proceedings of the Thirteenth Lunar and Planetary Science Conference, Part 1, *J. Geophys. Res.* **87**, Suppl. A353–A364, November 15, 1982 (1982)

The ureilite meteorites are carbonaceous olivine-pyroxene achondrites. They typically contain up to 4 wt.% carbon (carbonaceous matrix) as graphite, diamond, and lonsdaleite. Shock degradation has effectively obliterated primary textures in the carbonaceous matrix of previously described ureilites, a factor that has hampered efforts to explain the origin of this material. In contrast, the Antarctic ureilite ALHA78019 displays perfectly preserved primary textures in the carbonaceous matrix characterized by euhedral graphite blades intergrown with Fe-Ni metal and sulfide (diamonds are absent). This petrographic feature suggests that most graphite in ureilites originated by crystallization from a C-rich metallic phase. Assuming that $f\text{O}_2$ is controlled by C-Co-CO₂ reaction, the compositions of silicates

and metals in ureilites imply a two-stage redox history. The noble gases and rare earths of ureilites are discussed in light of this model.

Bhandari, N. and Potdar, M. B. (Physical Research Lab., Ahmedabad 380 009, India): 'Cosmogenic ^{21}Ne and ^{22}Ne Depth Profiles in Chondrites', *Earth Planet. Sci. Lett.* **58**, 116–128 (1982)

The production rate profiles of ^{21}Ne and ^{22}Ne as a function of depth in meteoroids due to spallation by solar flare cosmic rays (SCR) and galactic cosmic rays (GCR) are calculated and their dependence on size and composition of meteoroids has been evaluated. The GCR production rate at a given depth increases with size for radii $\lesssim 25$ cm and then decreases whereas the $^{22}\text{Ne}/^{21}\text{Ne}$ ratio (NeR) generally decreases with size and depth. The calculated GCR production rates and NeR are consistent with the measurements in several chondrites. A plot of track production rate vs. NeR shows that some chondrites have NeR values smaller than those expected for their sizes. This observation suggests *at least* a two-stage irradiation for such meteorites; the meteoroid exposure as a small body in the interplanetary space must have been preceded by exposure under deep shielding, possibly in its parent body.

Bogard, D. D. and Annexstad, J. O. (NASA/Johnson Space Center, Houston, TX 77058): 'Antarctic Meteorites: Their Curation and Study', *Antarctic Journal* **16**(5), 62–64 (1982)

A brief report on the study of Antarctic meteorites is presented.

Caffee, M. W., Hohenberg, C. M., Horz, F., Hudson, B., Kennedy, B. M., Podosek, F. A., and Swindle, T. D. (McDonnell Center for the Space Sciences, Washington Univ., St. Louis, MO 63130): 'Shock Disturbance of the I–Xe System', Proceedings of the Thirteenth Lunar and Planetary Science Conference, Part 1, *J. Geophys. Res.* **87**, Suppl. A318–A330, November 15, 1982 (1982)

Three separate samples of the meteorite Bjurbole were artificially shocked at pressures of 70 kb, 200 kb, and 400 kb. Analysis of xenon released in stepwise heating shows that the I–Xe system of the 400 kb sample is substantially altered by the shock loading and it is no longer possible to infer an age or trapped xenon composition for that sample. The 200 kb and 70 kb samples display isotopic structures progressively less altered demonstrating the graduations in shock disturbance likely to be found in natural systems. Interpretations of the I–Xe and ^{40}Ar – ^{39}Ar systems for several naturally shocked meteorites are also presented. New data for Arapahoe do not confirm the preciously reported age and trapped xenon composition, demonstrating instead that its I–Xe structure has been strongly disturbed by shock.

Caffee, M. W., Hohenberg, C. M., Swindle, T. D., and Hudson, B. (McDonnell Center for the Space Sciences, Washington Univ., St. Louis, MO 63130): 'I–Xe Ages of Individual Bjurbole Chondrules', Proceedings of the Thirteenth Lunar and Planetary Science Conference, Part 1, *J. Geophys. Res.* **87**, Suppl. A303–A317, November 15, 1982 (1982)

We have obtained initial iodine isotopic compositions for 10 individual chondrules from the meteorite Bjurbole, with a total range in well-determined values of 6.5%, which would correspond to an age difference of 1.6 m.y. These results can be interpreted as distinct formation ages, metamorphic ages or isotopic inhomogeneities in the early solar system, and can serve to constrain models for chondrule formation. Two of the chondrules show evidence of either isotopic inhomogeneities or disturbances of their I–Xe systems.

Cassidy, W. A. and Annexstad, J. O. (Dept. of Geology and Planetary Science, Univ. of Pittsburgh, Pittsburgh, PA 15260): 'Antarctic Search for Meteorites, 1980–1981', *Antarctic Journal* **16**(5), 61–62 (1982)

A brief report on the search for meteorites in the Antarctic during the 1980–81 austral summer season is given.

Cassidy, W. A. and Rancitelli, L. A. (Dept. of Geology and Planetary Science, Univ. of Pittsburgh, PA 15260): 'Antarctic Meteorites', *American Scientist* **70**, 156–164 (1982)

Climatic conditions in Antarctica have made a great number of specimens accessible.

Clarke, R. S. Jr. (Dept. of Mineral Sciences, Smithsonian Institution, Washington, DC 20560): 'Meteoritic Metal from Antarctica', *Antarctic Journal* **16**(5), 64-65 (1982)

Preliminary studies of Allan Hills and Purgatory Peak iron meteorites are reported.

Crozaz, G., Sibley, S. F., and Tasker, D. R. (Dept. of Earth and Planetary Sciences, Washington Univ., St. Louis, MO 63130): 'Uranium in the Silicate Inclusions of Stony-Iron and Iron Meteorites', *Geochim. Cosmochim. Acta* **46**, 749-754 (1982)

The microdistribution of U has been studied, using fission track techniques, in eleven mesosiderites, seven pallasites and four iron meteorites with silicate inclusions. When concentrated, U is usually found in phosphates: Merrillite and/or chlorapatite. As in stony meteorites, the U concentrations in a given phosphate phase are highly variable from meteorite to meteorite and sometimes also exhibit variations in same meteorite. Uranium is found to be concentrated in merrillite (0.25 to 1.43 ppm) in all the mesosiderites except Bondoc where none was observed. No U-rich phase was identified in six of the seven pallasites. In the seventh, Marjalahti, there are merrillite grains with concentrations ranging from 0.06 to 0.14 ppm. Where observed, the phosphates from silicate inclusion in the irons appear to have U concentrations similar to the mesosiderites.

Delaney, J. S., Prinz, M., Nehru, C. E., and O'Neill, C. (Dept. of Mineral Sciences, American Museum of Natural History, New York, NY 10024): 'The Polymict Eucrites Elephant Moraine A79004 and A79011 and the Regolith History of a Basaltic Achondrite Parent Body', Proceedings of the Thirteenth Lunar and Planetary Science Conference, Part 1, *J. Geophys. Res.* **87**, Suppl. A339-A352, November 15, 1982 (1982)

The achondrites Elephant Moraine A79004 and A79011 are closely related polymict eucrites of a type previously unrecognized in Antarctica. They contain an early, metamorphically homogenized breccia containing clasts of great textural diversity very similar to those in howardites, and a late injected mafic clast component that contains a suite of basalts that may, in part, be the result of impact melting rather than internal igneous processes. The basaltic achondrite parent body (BAP), of which they are regolith samples, had a complex igneous history of (1) early igneous activity, (2) brecciation to form polymict breccias, (3) localized metamorphism resulting in partial homogenization of areas of the regolith, (4) late igneous activity resulting from internal igneous or impact melting processes, and (5) further brecciation and mixing of late formed mafic rocks with early breccias.

Desnoyers, C. (Laboratoire de Mineralogie-Cristallographie, Associé au C.N.R.S., Université Pierre et Marie Curie, 4 Place Jussieu, 75230 Paris Cedex 05, France): 'Olivine dans les Howardites: Origine, et Implications pour Le Corps Parent de Ces Meteorites Achondritiques', *Geochim. Cosmochim. Acta* **46**, 667-680 (1982)

Electron microprobe analyses have been performed on 300 olivine grains found in 11 howardites. The olivine compositions almost continuously range from Fa 8 to Fa 89 with two prominent populations at Fa 13 and Fa 30. The tail of the fayalite content distribution may correspond to the succession of several small clusters of Fe-rich olivine grains. Most howardites have olivine populations in common that would result from the fragmentation of different rock of the howardites parent body. The distribution of the olivine grains between several groups of different FeO/MnO ratios indicates olivine crystallization from distinct magmas. The chemical characteristics of the olivines of the pallasites, diogenites and mesosiderites are found among the olivines of the howardites and suggests a common parent body for these different types of meteorites. The differentiation model of the eucrites parent body proposed by Stolper is extended to the partial fusion of distinct assemblages silicates + metal which could proceed from recrystallizations, under different oxidation-reduction conditions, or a primordial chondritic material depleted in volatile elements.

Eberhart, J.: 'A Meteorite Messenger from the Moon', *Science News* **122**, 341 (1982)

The suggestion that ALHA 81005 has come from the Moon is discussed.

Engel, M. H. and Nagy, B. (Geophysical Lab., Carnegie Institution of Washington, 2801 Upton St. N.W., Washington, DC 20008): 'Distribution and Enantiomeric Composition of Amino Acids in the Murchison Meteorite', *Nature* 296, 387-840 (1982)

Early determinations of the amino acid distribution in water extracts of the Murchison meteorite revealed unusual amino acids, including isovaline (Ival), α -aminoisobutyric acid (α -Aiba) and pseudo-leucine (Ple), as well as common ones such as glycine (Gly), alanine (Ala) and glutamic acid (Glu). Amino acids that could be resolved into their respective D- and L-enantiomers were reported to be racemic although small sample size might have hindered the precise determination of D/L values. Using improved chromatographic and mass spectrometric procedures we have now been able to amplify and resolve the partially racemized amino acids, Glu, aspartic acid (Asl), proline (Pro), leucine (Leu) and Ala, in an interior sample of a Murchison meteorite stone. Water-extractable amino acids were more racemized than those recovered by digesting the water-extracted meteorite in 6 M HCl. The amino acid composition of this stone was similar to previous reports, including the absence of tyrosine (Tyr), methionine (Met), phenylalanine (Phe) and only minor traces of serine (Ser) and threonine (Thr). Serine and Thr are usually considered to be terrestrial contaminations. This is the first report of amino acids in a carbonaceous meteorite which, based on currently accepted criteria, appear to be indigenous but for unknown reasons are not racemic. Confirmation of these findings by other investigators suggests that further examination of amino acids in clean carbonaceous meteorites could be beneficial.

Fitzgerald, M. J. and Jaques, A. L. (Centre for Precambrian Research, Univ. of Adelaide, G.P.O. Box 498, Adelaide, South Australia, 5001): 'Tibooburra, a New Australian Meteorite Find, and Other Carbonaceous Chondrites of High Petrologic Grade', *Meteoritics* 17, 9-26 (1982)

Tibooburra, a new meteorite find from western New South Wales, belongs to the Vigarano subgroup of the carbonaceous chondrites and, on the basis of its opaque mineralogy, appears to be oxidised. Petrological evidence suggests that, like the Allende meteorite, Tibooburra is a CV3 chondrite which has experienced greater metamorphic effects than other CV3 meteorites. Tibooburra has a bulk composition intermediate between the CO and less altered CV chondrites. This transitional nature is exhibited by several elements and is convincingly displayed by the multivariate techniques of cluster analysis and principal component analysis. Tibooburra thus resembles several other CV chondrites, such as Coolidge and Karoonda, which have been strongly metamorphosed. This group of meteorites is believed to have accreted early in the history of the Vigarano parent body and, as a result, contain greater quantities of high temperature Ca-Al rich inclusions but less low temperature matrix and volatile phases than other CV chondrites. Furthermore, in these meteorites both the matrix and magnesium silicate phases appear to be more iron rich than those in later accreted meteorites. Subsequently, these deeper seated meteorites have undergone more pronounced thermal metamorphism than those located in shallower portions of the parent body.

Grady, M. M., Swart, P. K., and Pillinger, C. T. (Planetary Sciences Unit, Dept. of Earth Sciences, Univ. of Cambridge, Cambridge CB2 3EQ, England): 'The Variable Carbon Isotopic Composition of Type 3 Ordinary Chondrites', Proceedings of the Thirteenth Lunar and Planetary Science Conference, Part 1, *J. Geophys. Res.* 87, Suppl. A289-A296, November 15, 1982 (1982)

A survey of bulk carbon isotopic compositions has been carried out for a suite of H, L, and LL ordinary chondrites, from the most unequilibrated type 3 to the metamorphosed type 6. The isotopic composition of the higher petrologic types 4-6 is lighter (in the range -25 to -30‰) and less variable than specimens of type 3 (-11 to -28‰). There is no simple relationship between bulk carbon and its isotopic composition; several carbon phases of different $\delta^{13}\text{C}$ may be present in the meteorites in variable proportions. To characterize the variability of type 3 chondrites, a selection has been treated with orthophosphoric acid to test for the presence of terrestrial weathering products of high $\delta^{13}\text{C}$. Some contamination and weathering products seem to be present, but such an interpretation is less than straightforward. The heavier isotopic composition and variability of type 3 meteorites may also be due, in part, to the presence of a component of graphite-magnetite matrix in the H and L group samples.

Gradie, J. and Veverka, J. (Lab. for Planetary Studies, Cornell Univ., Ithaca, NY 14853): 'When are Spectral Reflectance Curves Comparable?', *Icarus* **49**, 109-119 (1982)

Spectral reflectance curves of flat laboratory samples of the carbonaceous chondrite Allende, a basalt, and the ordinary chondrite Buderheim measured in a bidirectional geometry are shown to differ from those measured using an integrating sphere. In general, reflectance curves obtained by the bidirectional method are redder than those obtained with an integrating sphere. The degree of difference increases with increasing absolute reflectance. When spectral reflectance curves obtained by the two methods are compared to the reflectance curves expected for spherical and aspherical planets covered with the same materials, it is found that in general the integrating sphere measurements provide a better match to a planet at small phase angles. As the phase angle increases, bidirectional reflectance curves provide a closer match.

Grieve, R. A. F. (Earth Physics Branch, Dept. of Energy, Mines and Resources, Ottawa, Canada): 'The Vredefort Structure Still Not Understood', *Nature* **295**, 644-645 (1982)

The geology and geochemistry of the Vredefort "Dome", which is considered to be one of the largest terrestrial impact structures, is discussed.

Grimm, R. E. and McSween, H. Y. Jr. (Dept. of Geological Sciences, Univ. of Tennessee, Knoxville, TN 37996): 'Numerical Simulation of Crystal Fractionation in Shergottite Meteorites', Proceedings of the Thirteenth Lunar and Planetary Science Conference, Part 1, *J. Geophys. Res.* **87**, Suppl. A385-A392, November 15, 1982 (1982)

Cumulus clinopyroxenes in the Shergotty and Zagami meteorites suggest crystal fractionation occurred, possibly by gravitative settling. Numerical models of this process in a nonconvecting environment argue that the small phenocrysts can segregate only under extreme conditions of cooling time or gravitational field strength. Since textures indicate that cooling time was not excessive, a large (planetary) g is required by these models, in agreement with other suggestions that the shergottite parent body may be Mars. Other calculations indicate that it is extremely difficult to produce the observed textures in a convecting environment, unless crystal setting occurred in a quiescent zone at the bottom of the magma chamber.

Grossman, J. N. and Wasson, J. T. (Inst. of Geophysics and Planetary Physics, Univ. of California, Los Angeles, CA 90024): 'Evidence for Primitive Nebular Components in Chondrules From the Chainpur Chondrite', *Geochim. Cosmochim. Acta* **46**, 1081-1099 (1982)

The least equilibrated ordinary chondrites contain chondrules which have experienced little change since the time of their formation in the early solar system. These chondrules are excellent indicators of the physical and chemical nature of the solar nebula. We separated 36 chondrules from the Chainpur (LL3.4) chondrite and analyzed each for 20 elements and petrographic properties. Sampling biases were minimized as far as possible.

Chondrules seem to have formed through the melting of random mixtures of grains comprising a limited number of nebular components. The identity of these components can be deduced from chondrule compositions. The dominant components appear to be: (1) a mixture of metal and sulfide with composition similar to whole-rock metal and sulfide; (2) refractory (Ir-rich) metal; (3) refractory, olivine-rich silicates; (4) low-temperature, pyroxene-rich silicates, and, possibly, (5) a component containing the more volatile lithophiles.

Most of the textural types of chondrules formed from the same set of precursor components. In some cases chondrules having different textures are almost identical in composition. A few, unusual chondrule types seem to mainly consist of uncommon nebular components, possibly indicating different modes of formation.

Etching experiments confirm that chondrule rims are enriched in metal, troilite and moderately volatile elements relative to the bulk chondrules. However, a large fraction of the volatiles remains in the unetched interior.

Haliday, I. and Griffin, A. A. (Herzberg Inst. of Astrophysics, National Research Council of Canada, Ottawa, Canada K1A 0R6): 'A Study of the Relative Rates of Meteorite Falls on the Earth's Surface', *Meteoritics* 17, 31-46 (1982)

Meteorite camera networks have provided reliable data on typical orbits for meteorites. Using an adopted distribution of 20 orbits we determine the relative rates of meteorite falls over the surface of the earth taking account of the important effects due to the earth's gravity. The data are then used to study the expected variation in rates as a function of daylight, twilight or night conditions; time of day; and geographical latitude.

The rates of meteorite falls have a deep minimum near the area of the earth facing the earth's apex but a surprisingly broad maximum on the opposite side, facing the antapex. Twilight rates are lower than average and nighttime rates 3% higher than daytime rates. Minimum rates occur near 6^h local time and there is a broad maximum from noon to midnight. Rates are highest near the beginning of spring for either hemisphere and lowest near the beginning of autumn. The decline in rates with increasing latitude is quite moderate. The existing camera networks observe average fall rates at night which are very close to the average rate over the whole earth for the whole year.

Heide, K., Volksch, G., and Florenski, P. W. (Otto-Schott-Institut, Sektion Chemie, Friedrich-Schiller-Universität, 6900 Jena, GDR): 'Comparing Investigations of the Surface Structures of Irghizites and Pyroclastics by SEM', *Meteoritics* 17, 1-7 (1982)

The surface structures of irghizites from the Zhamanshin crater in Kazakhstan, USSR, play an important role in the discussion of their genesis. These surface structures were compared with those of typical tektites (australites) and pyroclastics (obsidians, lapilli) based on investigation by electron microscope. The results of these investigations indicate that there are no unambiguous genetical relationships between the morphology of irghizites and the surface features of tektites and pyroclastics. The surface shapes of irghizites result from several simultaneous or successive processes, in the course of which globules of different size melted, stuck together and were eaten into by corrosive gases after their solidification. The assumption that the verrucose swellings were caused by expanding gas bubbles immediately below the surface of the glass bulk can be excluded. The verrucose glass globules are identical in chemical composition to the glass bulk of the irghizites.

Honda, M., Nishiizumi, K., Imamura, M., Takaoka, N., Nitoh, O., Horie, K., and Komura, K. (Inst. for Solid State Physics, Univ. of Tokyo, Roppongi, Minato-Ku, Tokyo, Japan): 'Cosmogenic Nuclides in the Kirin Chondrite', *Earth Planet. Sci. Lett.* 57, 101-109 (1982)

Radioactive and stable cosmogenic nuclides have been determined in the various fragments of the Kirin chondrite (H5). Experimental results obtained from our samples are described and compared with similar data obtained in other laboratories. Cosmogenic ⁵⁴Mn, ²²Na, ⁶⁰Co, ²⁶Al, ⁵³Mn, ⁴⁰K (in the metal phase), and light noble gases were measured. Based on these data, the irradiation history of this meteorite can be explained in terms of (1) a multi-stage exposure which involves a first-stage irradiation for 10⁷ years and a second stage for about 4 × 10⁵ years, and (2) depth effects in the productions of the nuclides in 4π (second stage) and 2π (first stage) geometries. These conclusions are consistent with those of our previous work which was based on a limited number of samples.

Huntchison, R. (British Museum (Natural History), Cromwell Road, London SW7 5BD, England): 'Meteoritics: Evidence for Chemical Fractionation in the Early Solar System', *Nature* 297, 20-21 (1982)

Suggestions on the formation of chondrites, which, in turn, place constraints on theories of the planetary formation, are discussed.

Jaques, A. L. and Fitzgerald, M. J. (Bureau of Mineral Resources, Box 378, Canberra City, Act 2601, Australia): 'The Nilpena Ureilite, an Unusual Polymict Breccia: Implications for Origin', *Geochim. Cosmochim. Acta* 46, 893-900 (1982)

Nilpena (173 g), a new ureilite find from the Parachilna area of South Australia, is an unusual polymict breccia containing polymineralic aggregates, mineral fragments and achondritic and chondritic lithic enclaves in a dark, C-rich matrix. The polymineralic aggregates consist of equigranular-textured olivine Fa_{20} and pigeonite $En_{75}Wo_9Fs_{16}$, and exhibit evidence of shock in the form of undulose extinction and king-banding. Monomineralic fragments consist of olivine Fa_{19-24} (with highly forsteritic rims up to Fa_3) and pigeonite, and appear to be derived by brecciation of the polymineralic aggregates. The enclave material consists of lithic granular olivine fragments, porphyritic enstatite fragments (either enstatite chondrite or aubrite), olivine-clinobronzite fragments resembling and H3 chondrite, and eucrite-like lithic fragments composed of plagioclase An_{98} , salitic clinopyroxene $Wo_{48.5}En_{31.4}Fs_{20.1}$ and olivine Fa_{49-53} . The matrix contains kamacite (generally rich in P), schreibersite and troilite. The texture of Nilpena suggests formation by disruption of an olivine-pigeonite granular aggregate while the presence of the diverse chondritic and achondritic enclave material suggests an origin as a surface or near-surface breccia.

Like other ureilites Nilpena is strongly differentiated with respect to cosmic abundances but is significantly enriched in Ba and LREE. A lack of correlation of lithophile elements with $Fe/(Fe + Mg)$ ratio among ureilites suggests that the differentiation was not caused by varying degrees of partial melting of a homogeneous source. A cumulate origin therefore seems more plausible.

King, E. A. (Dept. of Geosciences, Univ. of Houston, Texas 77004): 'Refractory Residues, Condensates and Chondrules From Solar Furnace Experiments', Proceedings of the Thirteenth Lunar and Planetary Science Conference, Part 1, *J. Geophys. Res.* 87, Suppl. A429-A434, November 15, 1982 (1982)

Vertical access solar furnace experiments have produced refractory residues, condensates and chondrules that are similar to components of chondritic meteorites. In particular, Ca-Al rich refractory residues similar in chemistry to inclusions in carbonaceous chondrites have been produced by partial evaporation of basaltic bulk rock samples. Fe-Mg-Si-rich condensates with distinctive microbotryoidal morphology have been collected from the same sample runs. Particle coatings and aggregates with virtually identical microbotryoidal morphology and major element chemistry have been identified in both the Allende and Murchison meteorites. Spattered drops from melt beads undergoing heating and partial evaporation resemble some meteoritic chondrules in their mineralogies, textures, grain size, and sorting. The spatter mechanism is highly efficient in the production of chondrules. If any of the refractory inclusions in chondrites are, in fact, partial evaporation residues, many meteoritic fluid drop chondrules must have been formed by this process. The hot central portion of the solar nebula, acting on a cloud of dust and gas, is the probable source of heat required to produce the fractionated chemistry and physical state of many of the components of chondritic meteorites.

Kracher, A. (Naturhistorisches Museum, P. O. Box 417, A-1014, Wien, Austria): 'Crystallization of a S-Saturated Fe, Ni-Melt, and the Origin of Iron Meteorite Groups IAB and IIICD', *Geophys. Res. Lett.* 9, 412-415 (1982)

New data on trace element partitioning in the Fe-Ni-S-P system suggest that iron meteorites of groups IAB and IIICD come from one or more S-rich parent bodies. Heating of the IAB parent bodies. Heating of the IAB parent body melted all troilite, but caused only very minor partial melting of silicates. Cocrystallization of metal and troilite produced the high-Ni "tail" of group IAB. The trace element patterns are consistent with a parent body with CI sulfur and siderophile abundances. Compositionally the parent body was intermediate between ordinary and E4 chondrites, its thermal history was in between ordinary chondrite and fully differentiated (achondrite, group IIIAB iron) parent bodies.

IAB and IIICD may be complementary fractional crystallization/partial melting suites from the same parent body. Since the model also explains some unusual irons, it seems for the first time possible to understand the genesis of almost all irons, and link them to the major groups of primitive and differentiated meteorites.

Mackinnon, I. D. R. (Lockheed, C23, Johnson Space Center, Houston, TX 77058): 'Ordered Mixed-Layer Structures in the Mighei Carbonaceous Chondrite Matrix', *Geochim. Cosmochim. Acta* **46**, 479-489 (1982)

High resolution transmission electron microscopy of the Mighei carbonaceous chondrite matrix has revealed the presence of a new mixed layer structure material. This mixed-layer material consists of an ordered arrangement of serpentine-type (S) and brucite-type (B) layers in the sequence . . SBBSBB . . . Electron diffraction and imaging techniques show that the basal periodicity is ~ 17 Å. Discrete crystals of SBB-type material are typically curved, of small size ($< 1 \mu\text{m}$) and show structural variations similar to the serpentine group minerals. Mixed-layer material also occurs in association with planar serpentine. Characteristics of SBB-type material are not consistent with known terrestrial mixed-layer clay minerals. Evidence for formation by a condensation event or by subsequent alteration of preexisting material is not yet apparent.

Marvin, U. B.: 'Meteorite Placer Deposits of Antarctica', *Episodes* **1982**(3), 10-15 (1982)

The change discovery in 1969 of several dark rocks on a patch of bare ice in Antarctica has led to an extensive international program of meteorite recovery and research. More than 5000 specimens have been collected, probably representing several hundred meteorites including some rare and previously unknown varieties. Isotopic determinations of terrestrial residence times indicate that many Antarctic meteorites fell to Earth several hundred thousand years ago. They apparently represent a population of Earth-crossing planetary fragments older than meteorites found on other continents, where few survive weathering for more than 10 000 years. These deposits of extraterrestrial samples are yielding fresh clues to the earliest history of the solar system and generating new lines of research on the dynamics of large ice sheets.

Mason, B. and Taylor, S. R. (Smithsonian Institution Press, Washington, DC 20560): 'Inclusions in the Allende Meteorite', *Smithsonian Contributions to the Earth Sciences*, Number 25, 1982, Pp. 30 (1982)

Six discrete groups of inclusions have been distinguished in the Allende meteorite. Groups I, V, and VI are mostly melilite-rich chondrules, although some have been extensively altered to fine-grained aggregates; Groups II and III are mostly fine-grained aggregates made up largely of spine and fassaite; Group IV are olivine-rich aggregates and chondrules. Each group has a distinctive trace-element pattern, most clearly shown by the rare-earth (RE) distribution pattern. Group I has an unfractionated pattern (except for a small positive Eu anomaly) at about 10-15 times chondrites; Group II has a highly fractionated pattern with depletion of the heavier lanthanides (Gd-Er) and negative Eu and positive Tm and Yb anomalies; Group III has an unfractionated pattern at about 20 times chondrites, except for negative Eu and Yb anomalies; Group IV has a relatively unfractionated pattern at 2-4 times chondrites; Group V has an unfractionated pattern at 10-20 times chondrites; Group VI has an unfractionated pattern at 10-20 times chondrites, except for positive Eu and Yb anomalies (i.e., complementary to Group III). The complex patterns of trace element distribution in these Allende inclusions indicate a complex history of formation of this meteorite from the solar nebula.

McKeever, S. W. S. (Dept. of Physics, Univ. of Birmingham, B15 2TT, UK): 'Dating of Meteorite Falls Using Thermoluminescence: Application to Antarctic Meteorites', *Earth Planet. Sci. Lett.* **58**, 419-429 (1982)

The date of fall of a meteorite may be estimated from its thermoluminescence (TL) and in this paper the principle of a method of utilising TL to determine the terrestrial ages of eight Antarctic meteorites (Allan Hills-77) is described. The TL in a meteorite is primarily induced by cosmic ray irradiation in space and once the meteorite is on the Earth's surface, it is shielded from further cosmic ray irradiation. Under these conditions the TL will decay at a rate governed by the thermal stability of the TL and by the environmental temperature.

An estimate of the decay rate may be arrived at by using recently calculated data for the trapping parameters associated with meteorite TL. A major problem is the environmental storage temperature.

The "effective" storage temperature of the Antarctic meteorites is unknown, but appears to be greater than the mean annual temperature of the region of the meteorite find.

Only upper limits to the terrestrial ages can be calculated because the TL at the time of the fall to Earth is highly variable from sample to sample.

McNaughton, N. J., Fallick, A. E., and Pillinger, C. T. (Planetary Sciences Unit, Dept. of Earth Sciences, Univ. of Cambridge, Cambridge CB2 3EQ, England): 'Deuterium Enrichments in Type 3 Ordinary Chondrites', Proceedings of the Thirteenth Lunar and Planetary Science Conference, Part 1, *J. Geophys. Res.* 87, Suppl. A297-A302, November 15, 1982 (1982)

The majority of sixteen type 3 ordinary chondrites studied contain D/H ratios above the typical terrestrial range. We observe the most extreme deuterium enrichments in the least metamorphosed samples, and a trend of decreasing D/H with increasing metamorphism as measured by thermoluminescence sensitivity. Stepwise pyrolysis of bulk meteorite samples demonstrates that the amount of water released decreases rapidly with increasing temperature, and that the 450-750°C heating step releases the most deuterium enriched water. More detailed stepwise pyrolysis of one of the least metamorphosed ordinary chondrites, Semarkona, produces water from the 550-650°C heating step which has a δD of +5740‰ (SMOW). Although this is the most deuterium-rich composition yet encountered in a solar system material, it may not represent a limiting value. It is suggested that a deuterium enrichment of this magnitude may only be produced by ion-molecule reactions in interstellar clouds.

McNaughton, N. J. and Swart, P. K. (Planetary Sciences Unit, Dept. of Earth Sciences, Univ. of Cambridge, CB2 3EQ, UK): 'In, Out and About Meteorites', *Nature* 297, 453-454 (1982)

A brief account of the papers related to meteorites, which were presented during the 13th Lunar and Planetary Conference at Houston, is given.

McSween, H. Y. Jr. (Dept. of Geological Sciences, Univ. of Tennessee, Knoxville, TN 37996): 'Chondrites Chronicle Solar System', *Geotimes* 27(6), 20-21 (1982)

A summary of papers related to chondritic meteorites, which were presented during the 13th Lunar and Planetary Science Conference, is given.

Michel, R., Brinkmann, G., and Stuck, R. (Institut für Kernchemie der Universität zu Köln, D5000 Köln-1, FRG): 'Solar Cosmic-Ray-Produced Radionuclides in Meteorites', *Earth Planet. Sci. Lett.* 59, 33-48 (1982)

Model calculations were performed for the production of cosmogenic nuclides by solar protons in meteorites. Depth-dependent proton spectra are derived via energy loss calculations for a simple irradiation geometry (vertical incidence on a half plane). In a second step, solar proton fluxes in arbitrarily shaped meteorites can be derived from these spectra by numerical methods or, for ellipsoidal geometry, by closed form expressions.

Based on these proton spectra, depth profiles of cosmogenic radionuclides in meteorites were evaluated by a system of excitation functions for the production of radionuclides ($44 \leq A \leq 59$) from target elements ($22 \leq Z \leq 28$). Moreover, production rates for ^{26}Al and ^{22}Na were calculated. The new excitation functions were also used to derive production rates for ^{26}Al , ^{53}Mn and ^{59}Ni in cosmic dust. Our data differ considerably from earlier predictions and indicate that the interactions of solar protons in meteorites should be of greater importance than supposed earlier. Exemplarily ^{53}Mn is used for a detailed discussion of the role of various target elements, the influence of meteoritic shape, and the contributions by solar and galactic cosmic rays. Theoretical production rates for ^{53}Mn are compared with depth profiles measured in St. Severin and Madhipura. Evidence is supported that for a successful interpretation of cosmic ray interaction especially in small meteorites and/or in surface samples with minor ablation it is necessary to consider interactions of both solar and galactic cosmic rays.

Narayan, C. and Goldstein, J. I. (Dept. of Metallurgy and Materials Engineering, Lehigh Univ., Bethlehem, PA 18015): 'A Dendritic Solidification Model to Explain Ge-Ni Variations in Iron Meteorite Chemical Groups', *Geochim. Cosmochim. Acta* **46**, 259-268 (1982)

Segregation during solidification is responsible for the secondary fractionation of trace elements in iron meteorite chemical groups. This study examines the consequences of dendritic segregation on the Ge-Ni fractionation in iron meteorite chemical groups. Solidification experiments and computer simulations of the dendritic solidification process indicate that the effect of P on the partitioning behaviour of Ge and the effect of solid state diffusion on segregation are both important in understanding the observed Ge-Ni correlations. The Ge-Ni concentration trends predicted by the dendritic solidification model agree well with the observed variations.

Nehru, C. E., Prinz, M., and Delaney, J. S. (Dept. of Mineral Sciences, American Museum of Natural History, New York, NY 10024): 'The Tucson Iron and its Relationship to Enstatite Meteorites', Proceedings of the Thirteenth Lunar and Planetary Science Conference, Part 1, *J. Geophys. Res.* **87**, Suppl. A365-A374, November 15, 1982 (1982)

Tucson is a unique iron meteorite with Si-Cr bearing metal and about 8 vol.% of silicates that are almost free of Fe, Cr, Mn, and alkalis. The silicates are mainly forsterite (66.4%) and enstatite (30.2%) with minor diopside (2.7%), anorthite plus feldspathic glass (0.7%), and traces of Mg-Al spine and brezniaite. 'Enstatite' contains 0.5 to 21% Al_2O_3 and 'diopside' from 5 to 18%. Al_2O_3 generally increases away from early formed forsterite. The pyroxene is the most aluminous known in nature and contains close to the theoretical limit of Mg-Tschermaks solution. These compositions crystallized metastably because of the difficulty of nucleating feldspar in the rapidly cooled assemblage. The preferred hypothesis is that the present forsterite-enstatite silicate assemblage is similar to the precursor silicate assemblage, with little or no high temperature metal-silicate interaction. The metal and silicates were turbulently impact mixed at temperatures high enough to produce melt and forsterite (about 1500°C), with volatilization of Ga, Ge, and As from the metal and Na, K, and Mn from the silicates, and then rapidly cooled so that silicates formed metastable aluminous pyroxenes and anorthitic glass. The precursor forsterite-enstatite assemblage is a previously unrecognized new type of chondritic or achondritic highly reduced assemblage related to the enstatite meteorites.

Nozette, S. and Wilkening, L. L. (Dept. of Earth and Planetary Sciences, MIT, Cambridge, MA 02139): 'Evidence for Aqueous Alteration in a Carbonaceous Xenolith From the Plainview (H5) Chondrite', *Geochim. Cosmochim. Acta* **46**, 557-563 (1982)

Within a CM-like clast in the Plainview (H5) chondrite are two inclusions which have the distinctive morphologies of an Allende-like, coarse-grained CAI and an amoeboid olivine inclusion respectively. The compositions of the mineral components within the inclusions were ascertained in this microprobe study. The major constituents of the altered inclusions are calcite, Mg-Fe-rich phyllosilicates, Fe-Ti oxides, and an unusually Al-rich (21-32 wt% Al_2O_3) phyllosilicate. Assuming the starting compositions for these inclusions suggested by their morphologies, namely, Ca-Al refractory-rich oxides and silicates, the alteration process would have required transport of Na, Cl, H_2O , " CO_2 " and "FeO". Because significant quantities of iron are required to produce the mineral assemblages now present from the inferred starting materials, and because of the presence of hydrous phases, it seems that liquid water was probably the medium in which the alteration reactions took place. The two possible sources of liquid water in meteorite parent bodies are primordially formed clay minerals and water ice. As yet neither source can be ruled out.

Pillinger, C. T. (Dept. of Earth Sciences, Univ. of Cambridge, Cambridge CB2 3EQ, England): 'Not Quite Full Circle? - Non-Racemic Amino-Acids in the Murchison Meteorite', *Nature* **296**, 820 (1982)

The discovery of partially racemized glutamic acid, aspartic acid, proline, leucine and alanine in the Murchison meteorite by Engel and Nagy is discussed.

Planner, H. N. and Keil, K. (Dept. of Geology, Univ. of New Mexico, Albuquerque, NM 87131): 'Evidence For the Three-Stage Cooling History of Olivine-Porphyrific Fluid Droplet Chondrules', *Geochim. Cosmochim. Acta* **46**, 317-330 (1982)

Three haplochondritic melts were experimentally examined to investigate thermal parameters in the pre-accretionary chondrule environment. The melts, in the form of 2-mm-diameter spherules, were subjected to cooling rates of 220-460 or 1300-3700°C hr⁻¹ and either held at ~1460°C for up to 90 minutes or continuously cooled to ~600°C. A fractional crystallization model, designed to incorporate the effects of lattice diffusion in olivine but not volume diffusion of magnesium or iron in the melt was found to yield results in excellent agreement with olivine formed in experimental charges having a melt composition most similar to chondrules. Application of this numerical model to three olivine-porphyrific chondrules from the Tieschitz (H3) chondrite indicates that their mean olivine phenocryst compositions are too fayalitic to have been derived from a continuous cooling event. Partial equilibration of the phenocrysts with the melt in a high-temperature isothermal environment is postulated to explain the measured mean values.

From this investigation, the following three-stage model for the cooling of olivine-porphyrific fluid droplet chondrules found in ordinary chondrites is proposed: (a) initial continuous cooling from at least liquidus temperatures, at rates of 300 to 4000°C hr⁻¹, to about 1300°C, a process that may have taken ~5-60 minutes; (b) interruption of the initial cooling by a "short" duration isothermal event at ~1300°C, and (c) quenching. Thus, the entire cooling history of fluid droplet chondrules is but a brief process in the early history of the solar system. This thermal model suggests a rather specific and restricted physical setting for the origin of chondrules. It is unlikely that such a severely constrained physical setting could have been achieved by repetitive, small-scale events such as impact splattering on planetary surfaces or volcanism. Rather, a single, large-scale event is suggested.

Rajan, R. S. and Tamhane, A. S. (Dept. of Terrestrial Magnetism, Carnegie Institution of Washington, 5241 Broad Branch Road, N.W., Washington, DC 20015): 'Evidence For 244 Pu Fission Tracks in Hibonites from Murchison Carbonaceous Chondrite', *Earth Planet. Sci. Lett.* **58**, 129-135 (1982)

We have developed a technique for revealing nuclear tracks in the mineral hibonite (CaAl₁₂O₁₉), found in the refractory inclusions from carbonaceous chondrites. The tracks in hibonites from Murchison carbonaceous chondrite are dominated by fission tracks from ²⁴⁴Pu (constituting more than 90% of the total). The measured uranium contents in these crystal range from 1.2 to 62 ppb. We deduce that the average value for the ²⁴⁴Pu/²³⁸U ratio in most of the Murchison hibonites at the time of track retention is 0.022 ± 0.011.

Rambaldi, E. R. and Wasson, J. T. (Inst. of Geophysics and Planetary Physics, Univ. of California, Los Angeles, CA 90024): 'Fine, Nickel-Poor Fe-Ni Grains in the Olivine of Unequilibrated Ordinary Chondrites', *Geochim. Cosmochim. Acta* **46**, 929-939 (1982)

Fine (≲ 2 μm), Ni-poor (≲ 10 mg/g) Fe-Ni grains are common inclusions in the olivine in porphyritic chondrules in unequilibrated ordinary chondrites. The olivine grains appear to be relicts that survived chondrule formation without melting. The most common occurrence of this "dusty" metal is in the core of olivine grains having clear Fe-poor rims and surrounded either by small euhedral clear olivine grains zoned with FeO increasing toward the border of the grains or by large elongated Fe-poor orthopyroxenes oriented parallel to the chondrule surface and enclosing small round olivine grains. Various amounts of Ca, Al-rich glass are always present. The dusty metal is occasionally found in the rims of olivine grains either isolated in the matrix or included in chondrules. A rare occurrence is as bands in highly deformed olivines.

This dusty metal appears to be the product of *in situ* reduction of FeO from the host olivine. Among the possible reductants H₂ or carbonaceous matter (CH₂)_n seem the most likely. Hydrogen may have been implanted by solar-wind or solar-flare irradiation, but this requires that dissipation of nebular gas occurred before the end of the chondrule formation process. Carbonaceous matter may have been implanted by shock. Less likely reductants are nebular CO or C dissolved in the olivine lattice. The large relict olivine grains may be nebular condensates or, more likely, fragments broken off earlier generations of chondrules.

Reid, A. M. (Dept. of Geology, Univ. of Cape Town, Cape Town, South Africa): 'Basaltic Achondrite Meteorites From the Antarctic', *Antarctic Journal* 16(5), 65 (1982)

Preliminary studies of the 20 achondrite meteorites collected in the Antarctic between 1976 and 1979 are reported.

Reid, C. G. R. and Fredriksson, K. (Dept. of Mineral Sciences, Smithsonian Institution, Washington, DC 20560): 'The Madiun, Indonesia, Chondrite', *Meteoritics* 17, 27-30 (1982)

Madiun is a white, veined olivine-hypersthene, L6 chondrite. It can be classed as such on the basis of its petrography and chemistry, uniform olivine ($Fa_{24.2}$) and pyroxene ($Fs_{21.2}$) and total iron content of 23.7 wt.% Fe.

Reimold, W. U. (Inst. for Mineralogy, Univ. of Münster, D-4400 Münster, FRG): 'The Lappajarvi Meteorite Crater, Finland: Petrography, Rb-Sr, Major and Trace Element Geochemistry of the Impact Melt and Basement Rocks', *Geochim. Cosmochim. Acta* 46, 1203-1225 (1982)

Impact melt lithologies of the 77 m.y. old Finnish meteorite crater Lappajarvi as well as the Precambrian target rocks have been studied in detail, to identify and characterize different impact melt types (clast-poor, clast-rich, suevitic melt) and to study their chemical (major and trace elements) and isotopic (Rb-Sr) compositions in comparison to the composition of the target rocks.

The Rb-Sr system of the whole melt body - including the suevitic melt - is shown to have been re-equilibrated by the impact by extensive turbulent mixing of the various melted or vaporized target rocks. Chemical interactions (exchange of alkali elements, ^{87}Sr -redistribution) between feldspar clasts and impact melt surrounding them are the result of thermal metamorphism following the incorporation of target rock fragments of various degrees of shock metamorphism into the superheated melt. Exchange reactions between clasts and melt are determined by thermal activation, but the degree of shock metamorphism in the clasts plays an important role, too.

Major and trace element distributions in impact melt and basement rocks indicate that the Lappajarvi melt body chemically is extremely homogeneous. Even volatile elements (such as Zn and Cu) were not strongly fractionated. Comparison of the abundances of siderophile elements in the impact melt (e.g., 118-117 ppm Cr, 195-340 ppm Ni, 6-12 ppb Ir and calculated target rock mixture (79% mica schist, 1% granite-pegmatite, 10% amphibolite) (e.g., 85.6 ppm Cr, 54.8 ppm Ni, 0.5 ppb Ir) revealed the chondritic nature (C or H chondritic) of the meteorite projectile. Less than 2% of the meteorite can be detected in the coherent melt, whereas the suevitic melt is uncontaminated by the projectile.

Ryder, G. (Lunar Curatorial Lab., Northrup Services, Inc., P.O. Box 34116, Houston, TX 77234): 'A Note Against a Small-Body Origin for Shergottites, Nakhilites, and Chassignites', Proceedings of the Thirteenth Lunar and Planetary Science Conference, Part 1, *J. Geophys. Res.* 87, Suppl. A401-A402, November 15, 1982 (1982)

With the possible exception of Brachina, shergottites, nakhilites, and chassignites all crystallized about 1.3 b.y. ago on the same planet, and they were probably ejected from it together about 180 m.y. ago. No breccias from the parent planet have yet been identified, thus a dominantly impact-processed surface or a small body internal melt scenario is virtually untenable. These meteorites must have formed in a magmatic complex, and on a planet from which it was difficult to remove material: as far as we know, it only happened once. Everything we know about shergottites, nakhilites, and Chassigny is consistent with an igneous origin on Mars.

Scott, E. R. D. (Inst. of Meteoritics, Univ. of New Mexico, Albuquerque, NM 87131): 'Origin of Rapidly Solidified Metal-Troilite Grains in Chondrites and Iron Meteorites', *Geochim. Cosmochim. Acta* 46, 813-823 (1982)

Inclusions of troilite and metallic Fe, Ni 0.24-4 mm in size with a dendritic or cellular texture were observed in 12 ordinary chondrites. Cooling rates in the interval 1400-950°C calculated from the spacing of secondary dendrite arms or cell widths and published experimental data range from 10^{-7} to

10^4 °Csec⁻¹. In eight of these chondrites, which are breccias containing some normal slow-cooled metal grains, the inclusions solidified before they were incorporated into the breccias. Their cooling rates of 1–300°Cs⁻¹ indicate cooling by radiation, or by conduction in contact with cold silicate or hot silicate volumes only 6–40 mm in size. This is quantitative evidence that these inclusions and their associated clasts were melted on the surface of a parent body (by impact), and were not formed at depth from an internally derived melt. In Ramsdorf, Rose City and Shaw, which show extensive reheating to ≥ 1000 °C, Fe–FeS textures in melted areas are coarser and indicate cooling rates of 10^{-1} to 10^{-4} °Cs⁻¹ during solidification. This metal may have solidified inside hot silicate volumes that were 10–300 cm in size. As Shaw and Rose City are breccias of unmelted and melted material, their melted metal did not necessarily cool through 1000°C within a few m of the surface. Shock-melted, fine-grained, irregular intergrowths of metal and troilite formed *in situ* in many irons and some chondrites by rapid solidification at cooling rates of $\geq 10^5$ °Cs⁻¹. Their kamacite and taenite compositions may result from annealing at ~ 250 °C of metallic glass or exceedingly fine-grained quench products.

Sears, D. W., Kallemeyn, G. W., and Wasson, J. T. (Inst. of Geophysics and Planetary Physics, Univ. of California, Los Angeles, CA 90024): 'The Compositional Classification of Chondrites: II, The Enstatite Chondrite Groups', *Geochim. Cosmochim. Acta* **46**, 597–608 (1982)

We present new data from a neutron activation analysis of four enstatite chondrites including the taxonomically important St. Sauveur, and discuss the classification of enstatite chondrites. The enstatite chondrites can be divided into two compositionally distinct sets; in one set abundances of nonrefractory siderophiles and moderately volatile chalcophiles and alkalis are 1.5–2.0× higher than in the other. A well-resolved compositional hiatus separates these two sets. The differences in composition are as great as those between the groups of ordinary chondrites, and therefore it appears best to treat these sets as separate groups. By analogy with the symbols used for ordinary chondrites we propose to designate the high-Fe, high siderophile group EH and the low-Fe, low-siderophile group EL. Known members of the EH group belong to petrologic types 4 and 5, whereas all EL members are petrologic type 6. Within the EH group no correlation is observed between petrologic type and abundance of non-refractory siderophiles or moderately volatiles or alkalis.

Two physical properties show only modest overlap between the EH and EL groups. Cosmic-ray ages for EH chondrites are 0.5–7 Ma, while those for EL chondrites are 4–18 Ma. Relative to Bjurböle, I–Xe formation intervals are -1.3 ± 0.6 Ma for EH chondrites and 2.0 ± 0.5 Ma for EL chondrites. The weight of the chemical and physical evidence indicates that the EH and EL groups formed separate bodies at similar distances from the Sun.

The available evidence for Shallowater and Happy Canyon, two strongly recrystallized silicate-rich meteorites containing > 40 mg/g Fe–Ni, indicates that the former is an enstatite-clan chondrite altered by loss of sulfide- and plagioclase-rich melts, whereas the latter is intermediate in composition between EL chondrites and the chondritic silicates in the Pine River IAB-anomalous meteorite.

Simon, C.: 'Amino Acids: Fixed in Space?', *Science News* **121**, 310 (1982)

The discovery of aminoacids rotating light in both directions is discussed.

Smith, M. R. and Schmitt, R. A. (Dept. of Chemistry and the Radiation Center, Oregon State Univ., Corvallis, OR 97331): 'Chemical Composition of the Howardite Parent Body Deduced from Kapoeta Primary "Mafic" Magmas', Proceedings of the Thirteenth Lunar and Planetary Science Conference, Part 1, *J. Geophys. Res.* **87**, Suppl. A331–A338, November 15, 1982 (1982)

Chemical data are presented for three 'mafic' clasts extracted from the Kapoeta howardite. Bulk compositions and petrologic observations suggest that two of these lithic clasts represent olivine-plagioclase bearing orthopyroxenites. Chondrite-relative refractory LIL abundances of two of the clasts are inferred to represent primary Mg-rich magmas produced by extensive ($\geq 70\%$) partial melting of a source composition indistinguishable from the silicate fraction of average CH–CL ordinary chondrites, with the exception of the depletion of the alkalis Na and K by a factor of 13 ± 1 in the source composition. A metal-free and volatile deplete Kapoeta Parent Body (KPB) is subsequently deduced and is shown to compare very well with other similarly derived Achondrite Parent Body (APB) and

Howardite Parent Body (HPB) estimates but not to parent body estimates derived from inferences based on eucrite phase equilibrium studies. Other implications suggest that the KPB is heterogeneous with respect to Fe/Mg ratios.

Steele, I. M. and Smith, J. V. (Dept of the Geophysical Sciences, Univ. of Chicago, Chicago, IL 60637): 'Petrography and Mineralogy of Two Basalts and Olivine-Pyroxene-Spinel Fragments in Achondrite EETA79001', Proceedings of the Thirteenth Lunar and Planetary Science Conference, Part 1, *J. Geophys. Res.* 87, Suppl. A375-A384, November 15, 1982 (1982)

Three lithologies occur in shocked achondrite EETA79001: A1, exotic irregular crystals and clusters of coarse-grained olivine (Fo₈₁₋₅₅: CaO 0.2, Cr₂O₃ 0.06, NiO 0.5 wt.%), low-Ca pyroxene (En₈₂Wo₂-En₅₈Wo₁₂), and low-Ti chromite (Cr₂O₃ 59, FeO 27, TiO₂ 0.7 wt.%); A2 basaltic host to A1 containing pyroxene (mainly pigeonite En₆₇Wo₁₂-En₅₂Wo₁₃), maskelynite (An₆₁₋₅₅Or_{0,7}), high-Ti chromite (some rimming low-Ti chromite), whitlockite, minor Cl-apatite, ilmenite, pyrrhotite, and mesostasis; and B, a homogeneous basalt containing augite laths (~En₄₀₋₅₀Wo₂₅₋₃₅) in a matrix of pigeonite-augite, maskelynite (An₆₂₋₅₆Or_{1,2}), ulvöspinel-ilmenite intergrowth, whitlockite, Cl-apatite, and mesostasis. Mineral compositions indicate an oxidation state similar to that of shergottites. Lithology A1 represents an unmetamorphosed cumulate that was disrupted and partly resorbed by a basaltic magma. Incorporation of low-Ca magnesian pyroxens and olivine increased the Mg/Fe ratio of the basaltic magma responsible for A2, and resulted in abundant crystallization of pigeonite. Lithology B was generated from a distinct magma lacking fragments of A1. The parental spinel harzburgite of A1 was not annealed, and is probably a near-surface igneous cumulate from a shergottite-type basalt. Ringwood (?) and majorite (?) were found in shock veins.

Stoks, P. G. and Schwartz, A. W. (Lab. of Exobiology, The University, Nijmegen, Netherlands): 'Basic Nitrogen-Heterocyclic Compounds in the Murchison Meteorite', *Geochim. Cosmochim. Acta* 46, 309-315 (1982)

A fragment of the Murchison (C2) carbonaceous meteorite was analyzed for basic, *N*-heterocyclic compounds, by dual detector capillary gas chromatography as well as capillary gas chromatography/mass spectrometry, using two columns of different polarity. In the formic acid extract 2,4,6-trimethylpyridine, quinoline, isoquinoline, 2-methylquinoline and 4-methylquinoline were positively identified. In addition, a suite of alkylpyridines and quinolines and/or isoquinolines was tentatively identified from their mass spectra. The (iso)quinolines were found to contain methyl substituents exclusively. The distribution of the pyridines observed reveals a similarity to that observed from catalytic reactions of ammonia and simple aldehydes under conditions similar to those applied in Fischer-Tropsch type reactions.

Swart, P. K., Grady, M. M., and Pillinger, C. T. (Planetary Sciences Unit, Dept. of Earth Sciences, Univ. of Cambridge, Cambridge, CB2 3EQ, UK): 'Isotopically Distinguishable Carbon Phases in the Allende Meteorite', *Nature* 297, 381-383 (1982)

The stepwise oxidation of the Allende meteorite reported here has shown that there are at least three isotopically distinct carbon phases, each combustible over different temperature ranges. The temperature of combustion is dependent both on grain size of the fragments studied and/or on the nature of the carbonaceous material and its availability to the oxygen. Thus we attempt here to correlate the isotopic signatures recognized with phases whose existence has been postulated to explain noble gas systematics and to provide some insight into the nature and location of these phases. Most of the carbon ($\delta^{13}\text{C} = -20\text{‰}$), possibly a highly cross-linked polymer, exists predominantly in the matrix and has been reported by others to be the host of most of the normal planetary noble gases. Carbon protected in mineral grains may be isotopically heavier at -13 to -7‰ , but is still more easily oxidized than graphite when exposed by HF/HCl demineralization. A very easily oxidized phase, as yet unidentified, has a $\delta^{13}\text{C}$ value typically ~ -23 to -27‰ .

Swart, P. K., Grady, M. M., Wright, I. P., Pillinger, C. T. (Planetary Sciences Unit, Dept. of Earth Sciences, Univ. of Cambridge, Cambridge CB2 3EQ, England): 'Carbon Components and Their Isotopic Compositions in the Allende Meteorite', Proceedings of the Thirteenth Lunar and Planetary Science Conference, Part 1, *J. Geophys. Res.* **87**, Suppl. A283-A288, November 15, 1982 (1982)

High resolution stepwise oxidations have been undertaken on two bulk fractions and on an acid residue of the Allende meteorite. The results show the existence of at least three carbon phases and suggest the possible presence of two more. The bulk of the carbon has a temperature of peak release closely corresponding to amorphous (free) carbon and an isotopic composition of approximately -20‰ . At a slightly lower temperature of release we believe there to be carbon depleted in ^{13}C . As far as variations in experimental technique allow a decision to be made, combustion of this component appears to take place under conditions which previous workers have shown to liberate exotic compositions of nitrogen and xenon.

Unruh, D. M. (U.S. Geological Survey, M.S. 963, Box 25046, Federal Center, Denver, CO 80225): 'The U-Th-Pb Age of Equilibrated L Chondrites and a Solution to the Excess Radiogenic Pb Problem in Chondrites', *Earth Planet. Sci. Lett.* **58**, 75-94 (1982)

U, Th, and Pb analyses of whole-rock and troilite separates from seven L chondrites suggest that the excess radiogenic Pb relative to U and the large variations in Pb-Pb model ages commonly observed in chondritic meteorites are largely due to terrestrial Pb contamination induced prior to analyses. Using the Pb isotopic composition of troilite separates to calculate the isotopic composition of the Pb contaminants, the whole-rock data have been corrected for pre-analysis terrestrial Pb contamination. Two approaches have been used: (1) the chondrite-troilite apparent initial Pb isotopic compositions were used to approximate the mixture of indigenous initial Pb and terrestrial Pb in the whole-rock sample, and (2) a single-stage (concordant) model was applied using the assumption that the excess radiogenic Pb in these samples was terrestrial. Data for L5 and L6 chondrites yield a 4551 ± 7 My age using the former correction and a 4550 ± 5 My age using the latter one.

Corrected data for one L4 chondrite, Tennesilm, yield a 4552 ± 13 My age which is indistinguishable from that of the L5-L6 chondrites. However, the other L4 chondrite, Bjurböle, yields a 4590 ± 6 My age. Th-U-Pb data suggest that this older age may be an artifact of the correction procedure, and that some of the discordancy of the Bjurböle data is the result of either a recent geologic disturbance to the U-Th-Pb system or to terrestrial U loss. Some aliquots of the L5-L6 chondrites also show small amounts of discordancy ($\sim 10\%$) which are not easily attributable to terrestrial Pb contamination.

The data from the L5-L6 chondrites and Tennesilm suggest that there are not more than ~ 15 My differences in the ages of L4-L6 chondrites.

Waldrop, M. M.: 'Dreams of Planetary Fire', *Science* **216**, 607 (1982)

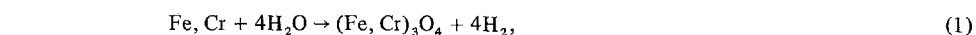
There are indications that the Allende meteorite has been subject to a high temperature variation early in its history.

Wood, C. A. and Lee-Berman, R.: 'Houston Chondrite Register; H Chondrites', March 1982, Pp. 14, NASA Johnson Space Center, Houston, TX 77058 (1982)

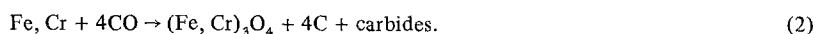
A listing of 577 H chondrites, based on various catalogues, is presented.

Yang, J. and Anders, E. (Enrico Fermi Inst., Univ. of Chicago, IL 60637): 'Sorption of Noble Gases by Solids, With Reference to Meteorites. II. Chromite and Carbon', *Geochim. Cosmochim. Acta* **46**, 861-875 (1982)

We studied trapping of noble-gases by chromite and carbon: two putative carriers of primordial noble gases in meteorites. Nineteen samples were synthesized in a Ne-Ar-Kr-Xe atmosphere at 440 K to 720 K, by the following reactions:



or



The reactant metal films were prepared either by vacuum evaporation of alloy or by thermal decomposition of Fe- and Cr-carbonyls. The products – including Fe_3O_4 , Cr_2O_3 , carbides, and unreacted metal – were partially separated by selective solvents, such as HCl, H_2SO_4 - H_3PO_4 , or HClO_4 . Samples were characterized by XRD, SEM, and atomic absorption; noble gases were measured by mass spectrometry. Surface areas, as measured by the BET method, were 2 to $100\text{ m}^2\text{ g}^{-1}$.

All samples are dominated by an adsorbed noble gas component that is largely released upon heating at $\leq 400^\circ\text{C}$ or slight etching. Elemental abundance patterns show that this component is derived from the highest-pressure noble gas reservoir seen by the sample – atmosphere or synthesis vessel – indicating the desorption or exchange rates at room T are slow on the time scale of our experiments (up to 1 year). Adsorptive capacity is reduced by up to 2 orders of magnitude upon light etching with HClO_4 (though the surface area actually doubles in this treatment) and, less drastically, by heating. Apparently some active adsorption sites are destroyed by these treatments. A trapped component (typically 30% of the total) is readily detectable only in samples synthesized at partial pressures close to or greater than atmospheric.

Noble gas contents roughly obey Henry's Law, but show only slight, if any, correlations with composition, surface area, or adsorption temperature. (Geometric) mean distribution coefficients for bulk samples and HCl-residues are, in $10^{-3}\text{ cc STP/g atm}$: Xe(100), Kr(15), Ar(3.5), Ne(0.62). Elemental fractionations are large and variable, but are essentially similar for the adsorbed and trapped components, or for chromite and carbon. They bracket the values for the corresponding meteoritic minerals.

	Ne/Xe	Ar/Xe	Kr/Xe
Geom. mean	0.006	0.035	0.15
Range	0.0004–0.03	0.01–0.2	0.06–0.4

These data largely support the suggestion of Lewis *et al.* that chromite and carbon in C2 and C3 chondrites were formed by reaction (2) in the solar nebula. Reaction (2) indeed is somewhat faster than (1); it yields ferrichromite (with part of the Cr replaced by Fe^{3+}); part of the carbon apparently is carbyne, judging from the thermal release of C_2 - C_3 chains at 320 to 600°C ; chromite and carbon trap substantial and essentially similar amounts of noble gases; and the gases show an elemental fractionation pattern resembling that for meteoritic chromite and carbon. However, in contrast to the meteoritic minerals, the synthetic materials show no isotopic fractionation of noble gases ($\leq 1\%$ /dalton).

Yang, J. and Anders, E. (Enrico Fermi Inst., Univ. of Chicago, IL 60637): 'Sorption of Noble Gases by Solids, With Reference to Meteorites. III. Sulfides, Spinels, and Other Substances; on the Origin of Planetary Gases', *Geochim. Cosmochim. Acta* **46**, 877–892 (1982)

To simulate trapping of noble gases by meteorites, we reacted 15 FeCr or FeCrNi alloy samples with CO, H_2O or H_2S at 350 – 720 K , in the presence of noble gases. The reaction products, including $(\text{Fe, Cr})_3\text{O}_4$, FeCr_2S_4 , FeS, C, and Fe_3C , were analyzed by mass spectrometry, usually after chemical separation by selective solvents. Three carbon samples were prepared by catalytic decomposition of CO or by dehydration of carbohydrates with H_2SO_4 .

The spinel and carbon samples were similar to those of earlier studies with only minor effects attributable to the presence of Ni. All samples sorbed substantial amounts of noble gases, with distribution coefficients of 10^{-1} – $10^{-2}\text{ cm}^3\text{ STP/g atm}$ for Xe. On the basis of release temperature three gas components were distinguished: a generally dominant physisorbed component (20–80% of total), and two more strongly bound, chemisorbed and trapped components. Judging from the elemental pattern, the adsorbed components were acquired at the highest noble gas partial pressure encountered by the sample – atmosphere or synthesis vessel.

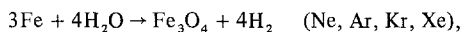
Sulfides, particularly daubréelite, showed three distinctive trends relative to chromite or magnetite: the high- T component was larger, 30–70% of the total; Ne/Xe ratios were higher, by up to 10^2 , possibly due to preferential diffusion of Ne during synthesis. In one synthesis, at relatively high P , the gases were sorbed with only minimal elemental fractionation, presumably by occlusion.

Most of the features of primordial noble gases can be explained in terms of the data and concepts presented in the three papers of this series. The elemental fractionation pattern of Ar, Kr, Xe in

meteorites, terrestrial rocks, and planets resembles the adsorption pattern on the solids studied: carbon, spinels, sulfides, etc. The variation in Ne/Ar ratio may be explained by preferential diffusion of Ne. The high release temperature of meteoritic noble gases may be explained by transformation of physisorbed to chemisorbed gas, as observed in some experiments. The ready loss of meteoritic heavy gases on surficial oxidation ("Phase Q") is consistent with adsorption, as is the high abundance. Extrapolation of the limited laboratory data suggests that the observed amounts of noble gases could have been adsorbed from a solar gas at 160–170 K and 10^{-6} – 10^{-5} atm, i.e., in the early contraction stages of the solar nebula. The principal unsolved problem is the origin of isotopically anomalous, apparently mass-fractionated noble gases in the Earth's atmosphere and in meteoritic carbon and chromite.

Yang, J., Lewis, R. S., and Anders, E. (Enrico Fermi Inst., Univ. of Chicago, IL 60637): 'Sorption of Noble Gases by Solids, With Reference to Meteorites. I. Magnetite and Carbon', *Geochim. Cosmochim. Acta* **46**, 841–860 (1982)

To simulate trapping of meteoritic noble gases by solids, 18 samples of Fe_3O_4 were synthesized in a noble gas atmosphere at 350–720 K by the reactions:



Phases were separated by selective solvents (HgCl_2 , HCl). Noble gas contents were analyzed by mass spectrometry, or, in runs where 36 d Xe^{227} tracer was used, by γ -counting. Surface areas, as measured by the BET method, ranged from 1 to $400\text{ m}^2\text{ g}^{-1}$. Isotopic fractionations were below the detection limit of 0.5%/m.u.

Sorption of Xe on Fe_3O_4 and C obeys Henry's Law between 1×10^{-8} and 4×10^{-5} atm, but shows only a slight temperature dependence between 650 and 720 K ($\Delta H_{\text{sol}} = -4 \pm 2$ kcal/mole). The mean distribution coefficient K_{Xe} is 0.28 ± 0.09 cc STP/g atm for Fe_3O_4 and only a factor of 1.2 ± 0.4 greater for C; such similarity for two cogenetic phases was predicted by Lewis *et al.* (1977). Stepped heating and etching experiments show that 20–50% of the total Xe is physically adsorbed and about 20% is trapped in the solid. The rest is chemisorbed with $\Delta H_s \approx -13$ kcal/mole. The desorption or exchange half-time for the last two components is $> 10^2$ yr at room temperature.

Etching experiments showed a possible analogy to "Phase Q" in meteorites. A typical carbon + carbide sample, when etched with HNO_3 lost 47% of its Xe but only 0.9% of its mass, corresponding to a ~ 0.6 Å layer. Though this etchable, surficial gas component was more thermolabile than Q (releas T below 1000°C , compared to 1200 – 1600°C), another experiment shows that the proportion of chemisorbed Xe increases upon moderate heating (1 hr at 450°C). Apparently adsorbed gases can become "fixed" to the crystal, by processes not involving volume diffusion (recrystallization, chemical reaction, migration to traps, etc.). Such mechanisms may have acted in the solar nebula, to strengthen the binding of adsorbed gases.

Adsorbed atmospheric noble gases are present in all samples, and dominate whenever the noble gas partial pressure in the atmosphere is greater than that in the synthesis. Many of the results of Lancet and Anders seem to have been dominated by such an atmospheric component; other are suspect for other reasons, whereas still others seem reliable. When the doubtful samples of Lancet and Anders are eliminated or corrected, the fractionation pattern – as in our samples – no longer peaks at Ar, but rises monotonically from Ne to Xe. No clear evidence remains for the strong temperature dependence claimed by these authors.

4. Cosmic Dust, Other Particles etc.

Alvarez, W., Asaro, F., Michel, H. V. and Alvarez, L. W. (Dept. of Geology and Geophysics, Univ. of California, Berkeley, CA 94720): 'Iridium Anomaly Approximately Synchronous With Terminal Eocene Extinctions', *Science* **216**, 886–888 (1982)

An iridium anomaly has been found in coincidence with the known microtektite level in cores from Deep Sea Drilling Project site 149 in the Caribbean Sea. The iridium was probably not in the

microtektites but deposited simultaneously with them; this could occur if the iridium was deposited from a dust cloud resulting from a bolide impact, as suggested for the anomaly associated with the Cretaceous-Tertiary boundary. Other workers have deduced that the microtektites are part of the North American strewn tektite field, which is dated at about 34 million years before present, and that the microtektite horizon in deep-sea cores is synchronous with the extinction of five radiolarian species. Mass extinctions also occur in terrestrial mammals within 4 million years of this time. The iridium anomaly and the tektites and microtektites are supportive of a major bolide impact about 34 million years ago.

Archibald, J. D. and Clemens, W. A. (Peabody Museum of Natural History, Yale Univ., New Haven, CT 06520): 'Late Cretaceous Extinctions', *American Scientist* **70**, 377-385 (1982)

The fossil evidence currently available suggests that changes across the Cretaceous-Tertiary boundary were the result of gradual processes and not of a single catastrophic event.

Drummond, J. D. (Physical Science Lab., New Mexico State Univ., Box 3-PSL, Las Cruces, NM 88-3): 'Theoretical Twin Meteor Showers', *Icarus* **49**, 135-142 (1982)

Attention is drawn to, and theoretical radiants calculated for, 27 hypothetical twin showers to Cook's (1973, in *Evolutionary and Physical Properties of Meteoroids*, NASA SP-319, U.S. Govt. Printing Office, Washington, D.C.) working list of meteor streams. Of these twin showers, 7 are previously known, 1 is a night-time twin to the ϵ Geminids, 9 are found to be contained among Sekanina's radar streams, and the remaining 10 are undetected daytime showers. Minimum radii are computed for all of Cook's streams and are used to assess the possibility of detecting the twin showers.

Fraundorf, P., Lyons, T., Schubert, P. (McDonnell Center for the Space Sciences, Washington Univ., St. Louis, MO 63130): 'The Survival of Solar Flare Tracks in Interplanetary Dust Silicates on Deceleration in the Earth's Atmosphere', Proceedings of the Thirteenth Lunar and Planetary Science Conference, Part 1, *J. Geophys. Res.* **87**, Suppl. A409-A412, November 15, 1982 (1982)

Pulse heating experiments on magnesium-rich olivine and pyroxene, two silicates often found in micrometeorites collected in the stratosphere, show that iron ion tracks remain detectable in the transmission electron microscope for temperature maxima up to $\sim 600^{\circ}\text{C}$. Assuming thermal emissivities near unity, this implies that micrometeorites with surface densities above 1 mg cm^{-2} are likely to have their track record erased, and that tracks in reentrant or low-density micrometeorites smaller than $7 \mu\text{m}$ in size are likely to survive atmospheric entry.

Fraundorf, P., McKeegan, K. D., Sandford, S. A., Swan, P., and Walker, R. M. (McDonnell Center for the Space Sciences, Washington Univ., St. Louis, MO 63130): 'An Inventory of Particles From Stratospheric Collectors: Extraterrestrial and Otherwise', Proceedings of the Thirteenth Lunar and Planetary Science Conference, Part 1, *J. Geophys. Res.* **87**, Suppl. A403-A408, November 15, 1982 (1982)

Examination of 526 particles in the $2\text{-}50 \mu\text{m}$ size range obtained from stratospheric impactation collectors has shown that most of them fit into one of three groups on a simple plot of Mg/Si vs. Al/Si energy dispersive X-ray peak ratios. The particles within a given group exhibit strong correlations in composition and mineralogy to one another, and the groups appear to largely consist either of earth crustal, manmade, or extraterrestrial materials. The temporal variability and relatively flat size distribution of material in the earth crustal group, in particular, suggests an aircraft-related, as opposed to stratospheric, source for these particles.

Ganapathy, R. (Research Lab., J.T. Baker Chemical Co., Phillipsburg, NJ 08865): 'Evidence For a Major Meteorite Impact on the Earth 34 Million Years Ago: Implications For Eocene Extinctions', *Science* **216**, 885-886 (1982)

A deep-sea core from the Caribbean contains a layer of sediment highly enriched in meteoritic iridium. This layer underlies a layer of North American microtektites dated at 34.4 million years ago and

coincides with the extinction of five major species of Radiolaria. It is suggested that a massive, chemically undifferentiated meteorite collided with the earth, producing the tektites and leading to extinctions 34 million years ago.

Glass, B. P., Dubois, D. L., and Ganapathy, R. (Dept. of Geology, Univ. of Delaware, Newark, DE 19711): 'Relationship Between an Iridium Anomaly and the North American Microtektite Layer in Core RC9-58 From the Caribbean Sea', Proceedings of the Thirteenth Lunar and Planetary Science Conference, Part 1, *J. Geophys. Res.* 87, Suppl. A425-A428, November 15, 1982 (1982)

In a previous publication, an iridium anomaly was reported in core RC9-58 from the Caribbean Sea, about 30 cm below the peak abundance of North American microtektites. In order to determine more precisely the relationship between the iridium anomaly and the North American microtektite layer, we searched for microtektites in the samples that were used for the iridium studies. We found that the North American microtektite layer is actually two layers, with the peak abundances separated by 25 cm. The upper layer consists of 'normal' North American microtektites and the lower layer consists of previously described clinopyroxene-bearing spherules. The iridium anomaly was found to correlate with the lower layer. Although the two layers appear to be the result of two separate events, several lines of evidence suggest that they were produced by a single event. The separation into two layers may have been produced by differential settling in the sediment due to density variations. The correlation between the iridium anomaly and the North American microtektite layer supports the terrestrial impact origin for tektites.

Grieve, R. A. F. (Earth Physics Branch, Dept. of Energy, Mines and Resources, Ottawa, Canada K1A 0Y3): 'Cosmic Dust and Impact Events', *Geotimes* 27(6), 23-24 (1982)

Papers presented to the 13th Lunar and Planetary Science Conference and dealing with cosmic dust and impact events are summarised. It is concluded that studies of cosmic dust and the Cretaceous-Tertiary boundary represent challenges in terms of sampling, data acquisition and interpretation.

Lequeux, J. (Observatoire de Meudon, 92190 Meudon, France): 'Chemical Composition of Gas and Grains in Dense Interstellar Clouds', *Geochim. Cosmochim. Acta* 46, 777-782 (1982)

This paper is a short review of the present knowledge on the composition of dense clouds where stars form, with extensions to the less dense interstellar medium and to the most likely sites of grain formation. The problem is complex and intricate, and it is still difficult to answer such fundamental questions as the lifetime of the dense clouds or the lifetime of the interstellar grains.

MacKinnon, I. D. R., McKay, D. S., Nace, G., and Isaacs, A. M. (NASA Johnson Space Center, Houston, TX 77058): 'Classification of the Johnson, Space Center Stratospheric Dust Collection', Proceedings of the Thirteenth Lunar and Planetary Science Conference, Part 1, *J. Geophys. Res.* 87, Suppl. A413-A421, November 15, 1982 (1982)

The NASA Johnson Space Center stratospheric dust collection program has made available to the scientific community a rate set of materials for studies of (1) extraterrestrial materials germane to the early history of the solar system and (2) natural and man-made terrestrial materials in the stratosphere. A review of the first 291 cataloged particles provides a basis for a reliable taxonomy of all stratospheric particles. Data used in this review include particle shape, size, bulk chemistry, and texture. Extraterrestrial materials occur in all three defined categories: spheres, aggregates, and fragments. Approximately 76% of aggregates are of probably extraterrestrial origin. Spheres contain the least amount of extraterrestrial material (~43%). A number of new groups of stratospheric particles have been identified. These include aluminium and silicate aggregates, aluminium fragments, and aluminium prime spheres and fragments. Limitations to the use of this classification scheme are based primarily upon the lack of additional data to unambiguously define particle origin.

Mendis, D. A., Houppis, H. L. F., and Hill, J. R. (Dept. of Electrical Engineering and Computer Sciences, Univ. of California, San Diego, La Jolla, CA 92093): 'The Gravitro-Electrodynamics of Charged Dust in Planetary Magnetospheres', *J. Geophys. Res.* **87**, 3449-3455 (1982)

The dynamics of small electrically charged dust grains within the rigidly corotating regions of planetary magnetospheres such as those of Jupiter and Saturn is considered. Depending on whether one is inside or outside the synchronous orbit, it is possible to have different populations of both positively and negatively charged particles moving in equilibrium circular orbits either in the prograde or retrograde sense. Not all these are stable, however, to small perturbations, such as would be produced by the gravitational tug of a neighboring satellite. The stable perturbed grains will perform a motion that can be described as an elliptical gyration about a guiding center which is in uniform circular motion. For different values of the specific charge, the ratio of the semiaxes of this 'epicyclic' ellipse lies between 1/2 and 1, while the gyration frequency ω of the grain about the guiding center lies between the Kepler frequency Ω_K and ω_0 (which is the grain gyrofrequency in a nonrotating frame). In the environments of Jupiter and Saturn, where the grains are expected to be negatively charged both in the sunlit side and in the shadow and which move in the prograde sense, their guiding centers must have speeds intermediate to the Kepler speed and the corotation speed. Such particles with a unique specific charge (and therefore a specific size) could have a 1:1 magneto-gravitational resonance with a neighboring satellite. A dispersion relation between ω and the wavelength λ of the perturbed orbits in the frame of the perturbed satellite has been derived. This result has been used to discuss the appearance and disappearance of the waves in the F ring of Saturn elsewhere. We merely point out here that, while the existence of a single well-defined wavelength implies a dust size distribution sharply peaked at a diameter of about 1μ , the present theory also anticipates this situation. The only collisionless (and therefore nonevolving) state of small electrically charged dust grains moving in the same orbit is when they have precisely the same specific charge and therefore the same size (assuming the same density), since the electrical potential is the same for all sizes.

Minster, J. -F. and Allegre, C. J. (Laboratoire de Geochimie et Cosmochimie, Institut de Physique du Globe, Departement des Sciences de La Terre, Universit s de Paris VI et VII, 4 Place Jussieu 73230 Paris Cedex 05, France): 'The Isotopic Composition of Zirconium in Terrestrial and Extraterrestrial Samples: Implications for Extinct ^{92}Nb ', *Geochim. Cosmochim. Acta* **46**, 565-573 (1982)

Since Nb and Zr are only little fractionated during magmatic processes, the ^{92}Nb - ^{92}Zr relative chronometer has the potential of dating the formation of planetary bodies through their differentiation. Thus, we have analyzed the isotopic composition of zirconium in lunar, meteoritic and old and recent terrestrial samples.

No isotopic variation has been found. However, the $^{92}\text{Zr}/^{90}\text{Zr}$ ratio of 3.8 Ga. old zircons from the Isua acid conglomerate is on the lower limit of the range of the standard measurements. If considered an anomaly, it would correspond to a $+1.5 \times 10^{-492}$ Zr relative deficiency or to a 3.0×10^{-494} Zr relative excess.

Our data constrain the $^{92}\text{Nb}/^{93}\text{Nb}$ isotopic ratio at the time of formation of the solar system to be less than 0.007, so that the maximum sensitivity of the ^{92}Nb - ^{92}Zr relative chronometer for the formation of planetary bodies is around 10^7 a. A discussion of some possible nuclear reactions indicates that zirconium isotopic variations in zircons are not easily produced, and that the ^{92}Nb and ^{94}Nb natural activities cannot be explained by any single one of the processes proposed so far.

Mukai, T. and Yamamoto, T. (Kanazawa Inst. of Tech., Nonoichi, Ishikawa 921, Japan): 'Solar Wind Pressure on Interplanetary Dust', *Astron. Astrophys.* **107**, 97-100 (1982)

The pseudo-Poynting-Robertson effect on an interplanetary grain due to solar wind bombardments is examined with careful consideration for sputtering of a grain and for the velocity dispersion of the solar wind particles. It is found that for water-ice and obsidian grains with the radii in the range 0.01-100 μm , the retarding force due to solar wind is stronger than, and of the same order as, respectively, that due to solar radiation. On the other hand, for magnetite this drag force is always less than that due to solar radiation.

In addition, since the wind flow generally comes from the east of the sun, a grain in a prograde orbit suffers a larger retarding force compared with a grain in a retrograde orbit.

Murray, C. D. (Center for Radiophysics and Space Research, Space Sciences Building, Cornell Univ., Ithaca, NY 14853): 'Nodal Regression of the Quadrantid Meteor Stream: An Analytic Approach', *Icarus* **49**, 125-134 (1982)

The mean orbit of the Quadrantid meteor stream has a high eccentricity and inclination with an aphelion close to the orbit of Jupiter. The nodal regression rate, a quantity which has been well determined from observations, cannot be calculated with sufficient accuracy using standard low-order expansions of the disturbing function. By using a high-order expansion of the disturbing function we show how the behavior of the longitude of ascending node of the Quadrantid stream is a result of both secular and resonant effects. Our analysis illustrates how the proximity of the stream's orbit to the 2:1 commensurability with Jupiter dominates the short-term variations in orbital elements.

Simon, C., 'Impacts and Rare Metals: Searching for Evidence', *Science News* **121**, 340 (1982)

The correlation of rare-metal anomalies and possible impact phenomena is discussed.

Viggiano, A. A., Arnold, F., Fahey, D. W., Fehsenfeld, F. C., and Ferguson, E. E. (Max-Planck-Institut für Kernphysik, Heidelberg, West Germany): 'Silicon Negative Ion Chemistry in the Atmosphere - In Situ and Laboratory Measurements', *Planet. Space Sci.* **30**, 499-506 (1982)

The results of a rocket-borne mass spectrometer measurement indicate that large concentrations of negative ions exist above the bottom of the atmospheric atomic oxygen layer. A large majority of these ions have a mass greater than 100 amu. In addition, an ion at mass 76 was observed with concentrations too large to be CO_4^- . In order to explain these features, a number of reactions involving silicon oxide negative ions have been measured in a flowing afterglow system. The ion SiO_3^- is produced by reaction of O_3^- and CO_3^- with SiO. The SiO_3^- ion is extremely stable and does not react measurably with NO, NO_2 , CO, CO_2 , O_3 or O. Since meteoroid ablation produces a large silicon input into the atmosphere, it appears possible that the ions observed at mass 76 may be SiO_3^- . Possible production mechanisms for this ion as well as the heavy ions are discussed.